FOG

Freiberg Online Geoscience

FOG is an electronic journal registered under **ISSN 1434-7512**

2016, Volume 44

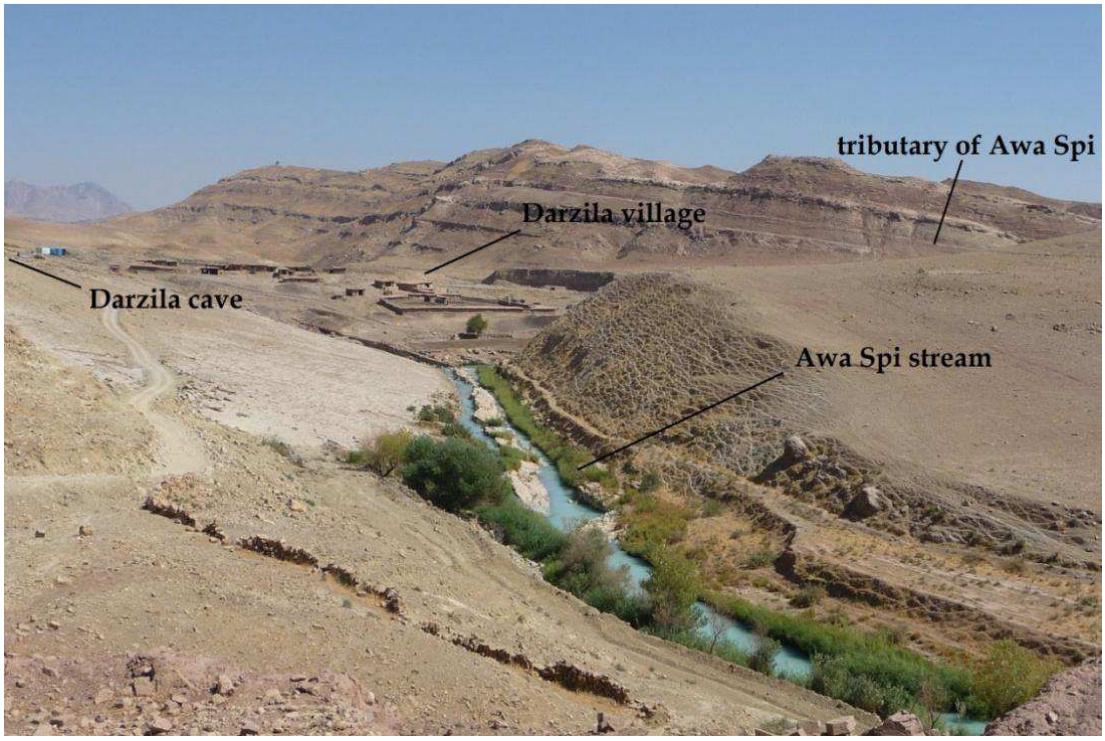

Karin Heiland

Hydrogeochemical investigation of Darzila karst cave, NE Iraq

121 pages, 43 figures, 16 tables, 79 references

Acknowledgement

First of all, I want to thank my first supervisor Prof. Merkel for realising this project and for his support and advices during the fieldwork and the writing process.

My special thank is addressed to Dr. Polla and Dr. Diary for their kind hospitality and help. Thanks for organising field trips and providing laboratory facilities. I am also very grateful for organising an accommodation for us, for their care and for giving us many opportunities to experience their fascinating country and culture.

Furthermore, I generally want to thank the team of the *Kurdistan Institution for Strategic Studies & Scientific Research* in Sulaimani for their support, hospitality and friendship.

For laboratory assistance with the water analyses in Freiberg, my thanks go to Dr. Sascha Kummer, Karina Taupadel and Dipl.-Chem. Hajo Peter.

I also want to thank my fellow student Anna Seither, who worked together with me on this research project. Thanks for your patience with me and your company during our stay in Iraq. I also thank you for our discussions and for proofreading my thesis.

Moreover, I wish to thank my sister and her husband for their support and for improving the English of my thesis.

I sincerely like to thank my parents, who not only supported me financially but also mentally over the entirety of my studies. Thanks to my dear boyfriend who always encouraged me in good and bad times.

Abstract

Darzila cave, an active sulphuric acid cave located in Sulaimani Governorate (NE Iraq), was subject to hydrogeological and hydrogeochemical investigations in September and October 2011. Several field and laboratory analyses (in-situ parameter, photometry, titration, IC, ICP-MS, GC, LiquiTOC, XRF, XRD) were accomplished on water, gas and rock samples in order to improve the general understanding of the formation of the Darzila cave by means of sulphuric acid.

The cave is embedded in limestone bedrock and is fed by several groundwater inlets, commonly present as floor feeders. A subterranean source of Awa Spi river (DR-W-1) could be identified as a main outlet of the cave. The cave water and atmosphere are both enriched in sulphides (up to 6.32 mg/L in water) deriving either from the reduction of sulphates by organic carbon or from oil-rich reservoirs directly. Maximal contents of sulphides (50 mg/L) were measured at a well nearby.

Waters flowing in Darzila cave are brackish; predominant ions in water are SO_4^{2-}, Ca^{2+} and Mg^{2+}. Redox conditions are determined by degradation of organic matter and sulphate/sulphide disequilibria. Water that rises from deep sites indicates elevated CO_2 contents, strongly reducing conditions, and the input of sulphide is supposed to be high. Under these conditions, subaqueous dissolution of the limestone bedrock by sulphuric acid (and carbonic acid) at or near the water table is enhanced. Upstream from the inlets, CO_2 and H_2S degassing and oxidation of H_2S to SO_4^{2-} takes place. Thus, the aggressiveness of the cave water diminishes. Meanwhile, subaerial dissolution by sulphuric acid and gypsum replacement reactions at the cave ceilings increases along the flow path.

Acidic, pools of (moderately) saline water are formed where gypsum coatings shield ascending water from the limestone bedrock. A potential influence of hydrocarbon-bearing layers was pointed out at these sites. Indices are significantly elevated SO_4^{2-}/Ca^{2+} ratios, increased TDS (10-31 g/L) and DOC values (14-20 mg/L), and relative enrichments of trace elements commonly present in hydrocarbon-related groundwaters.

Zusammenfassung

Gegenstand von hydrogeologischen und hydrogeochemischen Untersuchungen im September und Oktober 2011 war eine Höhle bei Darzila, Sulaimani Governorate (Irak). Diese Höhle unterliegt aktiv der Verkarstung durch Schwefelsäure. Um die Prozesse der Höhlenbildung genauer zu untersuchen, wurden verschiedene Feld- und Laboranalysen an Wasser-, Gesteins- und Gasproben durchgeführt und ausgewertet (Vorort-Parameter, Photometrie, Titration, IC, ICP-MS, GC, LiquiTOC, XRF, XRD).

Die Höhle befindet sich in einer Kalksteinformation und wird von verschiedenen Grundwasserzuflüssen gespeist, welche entlang tiefer Fließpfade aufsteigen. Ein unterirdischer Zufluss des Awa Spi (DR-W-1) konnte als ein Hauptabfluss der Höhle identifiziert werden. Höhlenwasser sowie -atmosphäre sind angereichert an Sulfid (bis zu 6.32 mg/L im Wasser), welches der Reduktion von Sulfat durch organisches Material oder direkt aus unterliegenden Erdölreservoirs entstammt. Die höchsten Gehalte (50 mg/L) wurden in einem naheliegenden Brunnen gemessen.

Fließgewässer in der Höhle sind brackisch; wobei die Ionen SO_4^{2-}, Ca^{2+} und Mg^{2+} prädominant sind. Die Redoxverhältnisse sind bestimmt durch Sauerstoffzehrung infolge des Abbaus von organischen Material und Sulfat/Sulfid Ungleichgewichten. In die Höhle aufsteigende, H_2S- und CO_2-haltige Wässer sind stark reduzierend. In diesen Bereichen ist die subaquatische Verkarstung des anliegenden Kalkgesteins durch Schwefelsäure (und Kohlensäure) nahe der Wasseroberfläche hoch. Mit zunehmendem Abstand von den Grundwasserzutritten gasen CO_2 und H_2S aus und Oxidation von H_2S zu SO_4^{2-} findet statt; die Aggressivität des Wassers nimmt ab. Gleichzeitig ist eine Zunahme an subaerischen Lösungsprozessen und Gipsbildungsreaktionen an den Höhendecken zu beobachten.

Saure, (mäßig) salzige Wasserpools bilden sich, wo langsam aufsteigendes Wasser durch Ausbildung von Gipskrusten vom Kalkgestein abgeschirmt wird. Verschiedene Indikatoren weisen darüber hinaus auf den Einfluss von Kohlenwasserstoffen an diesen Stellen hin: signifikant erhöhte SO_4^{2-}/Ca^{2+} Verhältnisse, erhöhte TDS- (10-31 g/L) und DOC-Werte (14-20 mg/L), und relative Anreicherungen an Spurenelementen, welche typischerweise in erdölnahen Grundwässern vorkommen.

List of Content

List of Figures

List of Tables

Symbols and Abbreviations

Symbol	Denotation	Unit
[C]	Organic compounds	-
AD	Absolute deviation	-
BSR	Bacterial sulphate reduction	-
c	concentration	mg/L
CCT	Collision cell technology	-
DO	Dissolved oxygen	mg/L
DOC	Dissolved organic carbon	mg/L
EC	Electrical conductivity	µS/cm
EDL	Estimated detection limit	-
$E_{25°C}$	Redox potential at 25°C referred to Ag/AgCl electrode	V
E_H	Redox potential at 25°C referred to standard hydrogen electrode	V
EMF	Electro motoric force (readings)	V
ET_o	reference evapotranspiration	mm
GC	Gas chromatography	-
GPS	Global Positioning System	-
GRI	Geoscience Resources Iraq	-
I	Ionic strength	mol/L
IAP	Ion activity product	-
IC	Ion chromatography	-
ICP-MS	Inductively coupled plasma mass spectrometry	-
IR	Infrared	-
$K_{B,8.2}$ value	Titration endpoint of CO_2-acidity	-
$K_{A,4.3}$ value	Titration endpoint HCO_3^--alkalinity	-
K_{SP}	Solubility product of a mineral phase	-
LDO	Luminescent dissolved oxygen	-

Symbol	Denotation	Unit
M	Molar mass	g/mol
m_i	Molar concentration	mol/L
n	Number of samples	-
NTU	Nephelometric turbidity units	-
PE	Polyethylene	-
PET	Polyethylene terephthalate	-
PTFE	Polytetrafluoroethylene	-
RD	Relative deviation	%
SAS	Sulphuric acid speleogenesis	-
SI	Saturation index	-
SD	Standard deviation	-
T	temperature	°C
TDS	Total dissolved solids	mg/L
TIC	Total inorganic carbon	mg/L
TSR	Thermochemical sulphate reduction	-
UIS	International Union of Speleology	-
V	Volume	m^3
v	Variance	-
XRD	X-ray diffraction	-
XRF	X-ray fluorescence spectrometry	-
z_i	charge	-
α	significance	-

Nomenclature

	Nomenclature	**Denotation**
General	D	Darzila
Location	C	Cave
	R	River
	W	Well
	S	Surrounding
Type of sample	W	Water
	GW	Gases in water
	GA	Gases in air
	P	Precipitation
	O	Oil
	K	Karst feature
	PG	Primary gypsum
	SG	Secondary gypsum
	PL	Primary limestone
	C	Clay
Location number	1, 2. 3, etc.	
Additional remarks	a, b, c, etc.	

Example: DC-W-1 = Darzila Cave-Water sample-at location 1

1. Introduction

1.1. Motivation

The number of nonconventional karst caves amounts only to about 10 to 15% of the worldwide known caves (Palmer 2007). Among them, those formed by sulphuric acid are the most interesting. However, just about 5% have been clearly attributed to dissolution by sulphuric acid (Palmer 2012). For a long time, the possibility of deep-seated karstification has been neglected. But, in the past two decades the recognition of the variety and importance of deep-seated dissolution processes has grown considerably (Klimchouk 2007). In particular, sulphuric acid caves provide evidence for a variety of deep-seated processes, which are important to petroleum geology, ore geology, tectonic history and the nascent field of karst microbiology (Palmer, Hill 2012). However, there are only very few detailed field studies available because of the small number of examples that are both actively forming and accessible (Palmer 2012).

Darzila cave meets these requirements and offers remarkable opportunities to investigate an active karst system of sulphuric acid origin. However, until now, only little research was carried out about this cave and its surroundings. Preliminary investigations were conducted by Khanaqa, P.A. & Al-Manmi, D.A. (2011). Reconnaissance studies of active sulphide springs in Sulaimani Governorate by Iurkiewicz, A.A. & Stevanovic, Z.P. (2010) provide an initial overview of the extent of sulphuric acid karstification in the region. However, knowledge about the mechanism of speleogenesis is still little with regard to Darzila cave. This work and also the collaborative work of Anna Seither shall contribute towards a better understanding of the complexity of karstification processes in Darzila cave.

1.2. GRI Project

Co-author: Anna Seither

Three decades of war have severely damaged Iraq's infrastructure and the loss of qualified personnel slows down the reconstruction of the country. In order to support the rebuilding of the Iraqi university system, the DAAD initiated cooperations

between German and Iraqi universities. In 2009, altogether five academic programs at four German universities were selected for funding.

The *Geoscience Resources Iraq* (GRI) project of the TU Bergakademie Freiberg is one of these. The project outlines were compiled by Prof. Merkel, the head of the Geology department of the TU Bergakademie Freiberg. Goal of GRI is capacity building at several Iraqi universities in Bahdad, Basrah, Erbil, and Sulaimani, establish a joint master course and foster joint research activities.

Last but not least GRI aims on initiating joint research programs, which facilitated the investigation of Darzila cave. The research was carried out as cooperation between the TU Bergakademie Freiberg, the University of Sulaimani and the *Kurdistan Institution for Strategic Studies and Scientific Research*.

1.3. Objectives

The investigation of Darzila cave was carried out in a context of a diploma thesis in collaboration with Anna Seither. The main objective of the collaborative project is to improve the general understanding of fundamental karst processes in Darzila cave. In particular, the extent of sulphuric acid speleogenesis will be investigated. Moreover, a closer study on the specific mode of cave origin shall be given and evidences for supporting or rejecting the partial or entire hydrocarbon-related origin of cave sulphur shall be carried out. Since hydrogen sulphide and its by-products are the most potent agents in producing nonconventional karst caves, the distribution of sulphur species will be regarded in detail. Furthermore, attempts are made to examine microbial effects on karst chemistry. Beyond that, the research will focus on mapping of cave pattern, speleothems and mineral types commonly associated with deep-seated cave origins.

In addition, a description of cave dimensions will be provided. The exploration of the karst system and surface karst features in the vicinity of Darzila cave is another focus of the collaborative work. Furthermore, it is aimed to discover potential hydraulic connections between Darzila cave and the nearby river Awa Spi.

1.4. Deliverables

Main deliverables of this thesis are:

- Detailed hydrogeochemical and hydrogeological investigations of Darzila cave
  - Brief description of the hydrogeological situation
  - Providing a general overview of hydrogeochemical variations
  - Investigation of a potential influence of hydrocarbon-bearing layers on the water chemistry in Darzila cave
  - Detailed investigation of the formation of acidic water bodies (modelling approach)
  - Interpretation of the occurrence of individual sulphur species in dependence on the local setting and general hydrochemistry
  - Study of dissolution and precipitation processes, enrichment and depletion of elements, elemental ratios
- Providing a map and cross sectional view of Darzila cave
- Presentation of surface karst features in the vicinity of Darzila cave
- Investigation of potential hydraulic connectivity between Darzila cave and the nearby river Awa Spi on the basis of hydrogeochemical data

In the associated work of Anna Seither, the focus will be on isotopic investigations (sulphur, oxygen and hydrogen isotopes). Moreover, microbiological effects on hydrochemistry will be studied in detail in this second thesis.

2. Study area

2.1. Location of the study area

The study area is located in the southern part of Sulaimani Governorate in Kurdistan Region, NE Iraq. Administratively, this area belongs to the Sangaw District, but is commonly also called Garmian area ("Garmian" means very hot in Kurdish) (Figure 1). Sangaw region is located to the west of the Sagirma Mountains, representing the southeastern segment of the Iraqi Zagros Mountains (Iurkiewicz, Stevanovic 2010).

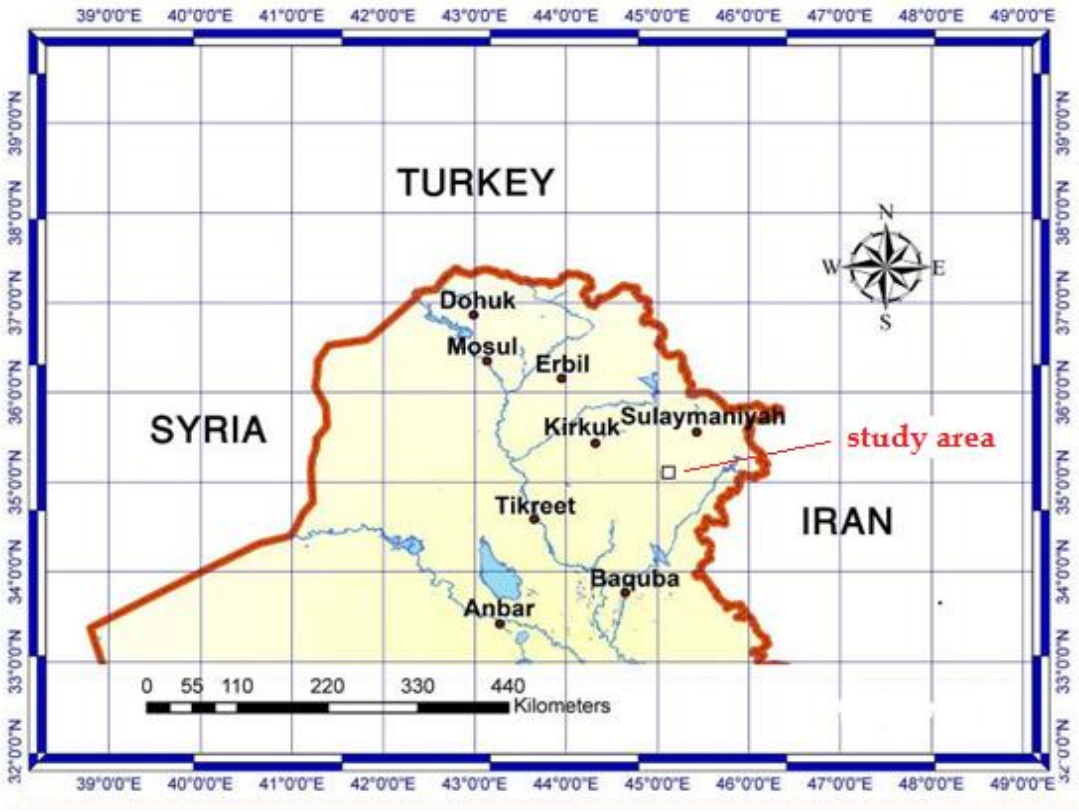

Figure 1: Location of Sangaw region (modified after Khanaqa, Al-Manmi 2011)

2.2. Geological description

Tectonically, the study area is a part of the Unstable Shelf which represents a subunit of the Arabian Shelf and is characterised by surface anticlines. In NE Iraq, the principal tectonic units generally trend NW-SE parallel to the Zagros-Taurus suture belts following the regional orogenic trend. More precisely, the area of interest is located within the Butmah-Chamchamal Subzone, which represents the structurally highest part of the Low Folded (Foothill) Zone. Prominent features of this subzone

are long, medium-sized anticline structures: mountain ridges trending NW-SE in the SE of the subzone as well as very conspicuous long, deep synclines containing thick Miocene-Quarternary molasse sediments forming intermountain valleys in between them (Jassim, Goff 2006).

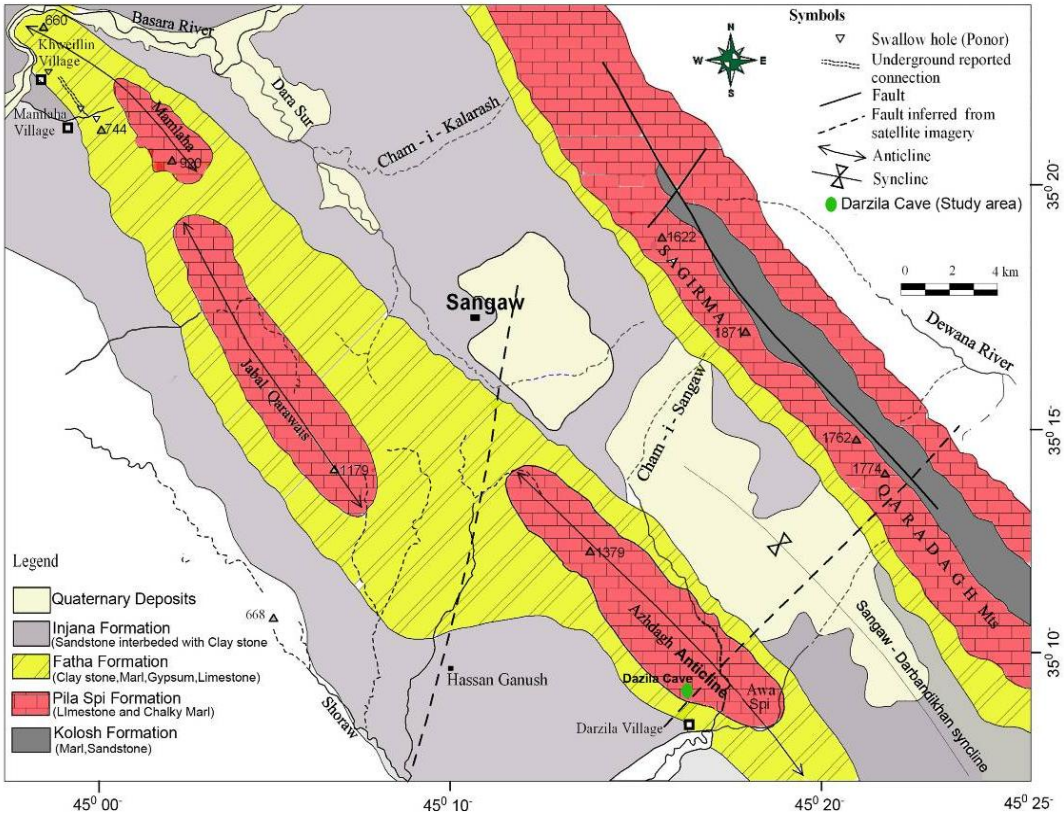

Figure 2: Geological map and location of the study area (modified after Maala 2006)

As it can be seen in Figure 2, Darzila cave is sited at the southern limb of the Azhdagh double plunging anticline consisting of Pila Spi Formation overlain by Lower Fars and Upper Fars. In addition, Iurkiewicz and Stevanovic (2010) also mention a thin Oligocene horizon allocated in between. The core of the sector is represented by the impermeable layers of Kolosh Formation. Characteristics of the relevant formations of the Azhdagh anticline are given in Table 1.

To the east, the geology is dominated by the Sagirma Qaradagh Mountains. The south eastern limb of the Sagirma anticline is composed of Kolosh, Sinjar, Gercus, Pila Spi and eventually Lower Fars Formation; within the southwestern limb, the Gercus Formation is replaced by the Sagirma Formation (Lawa 2004). Because Iurkiewicz and Stevanovic (2010) suggest a potential influence of these formations on Awa Spi springs, the main characteristics are also depicted in Table 1.

Furthermore, an important NE-SW striking lineament that crosses the SE plunge of the Azhdagh anticline has to be mentioned since the associated weakened zone is likely to have controlled the surface and the underground water flow (Figure 2). Lineaments of similar characteristics are considered as pathways for ascending bitumen in this region (Iurkiewicz, Stevanovic 2010).

Table 1: Characteristics of the main geological formations occurring in the study area (modified after Iurkiewicz, Stevanovic 2010 and Hassan et al.)

Formation	Age	Lithology	Thickness	Hydrogeological function
Fatha (Upper Fars)	Late Miocene	Massive beds of red claystone, silty & clayey sandstone	500 m	Very low productive aquifer (aquitard)
Injana (Lower Fars)	Middle Miocene	Alternation of gypsum, anhydrite, salt, green marl, limestone, sandstone, red claystone; bituminous & sulphuric components to the lower part	400-900 m	Low to medium productive aquifer to the base
Oligocene horizon	Late Oligocene	Limestone with bituminous material	20 m	
Pila Spi	Middle-Late Eocene	Lower part: dolomitic limestone; upper part: crystalline chalky limestone with thin beds of calcareous marl & chert nodules	100-200 m	Fissured-karst aquifer
Gercus		Red mudstone, sandstone, shale		Aquitard
Sagirma		Gypsum, dolomite (extents laterally over 50 km)	>100 m	Probably aquifer
Sinjar	Paleocene-Early Eocene	Limestone	100-200 m	Fissured-karst aquifer
Kolosh	Paleocene-Early Eocene	Typical flysch: shale limestone, sandstone, conglomerate	500-1000 m	Aquitard

2.3. Hydrogeological and hydrological setting

Hydrogeologically, the study area is located in the Chamchamal-Sangaw basin. The main aquifer system in the area of interest is the Pila Spi fractured karst aquifer that extents in NW-SE direction in the central and southern area of northern Iraq. Pila Spi consists of Eocene limestone, sometimes up to 200 m thick, and represents a typical heterogeneous anisotropic aquifer that is fractured and intensively karstified, though to a lesser extent than the Bekhme aquifer which covers large areas mostly in the northern and central northern part of northern Iraq (Stevanovic, Markovic 2003b).

The aquifer contains medium to large groundwater reserves strongly varying in space and time. As a result of general aquifer anisotropy and the presence of many fissures, the aquifer is generally characterised by a very high permeability (Stevanovic, Markovic 2003b). Values of transmissivity are in the range of 3.5 to 42000 m²/day (Jassim, Goff 2006).

Another characteristic of the Pila Spi aquifer is a turbulent water-flow regime. A highly fractured karst aquifer system such as Pila Spi combined with a lack of vegetation result in a highly effective infiltration capacity. According to Stevanovic, Markovic (2003b), estimated recharge coefficients of the Pila Spi aquifer amounts to about 30%, in particular cases up to 50% of the total rainfall. Compared to the Bekhma aquifer, pure limestone outcrops are present to a less extent resulting in lower values of aquifer recharge for the Pila Spi aquifer. Furthermore, sequences of marly and clayed components reduce the absorption capacity and contribute to secondary filling of existing fractures (secondary permeability).

Since Pila Spi Formation is largely overlaid by the Lower and Upper Fars Formation, which represent aquitards, confined conditions are created in the Pila Spi aquifer (see Table 1).

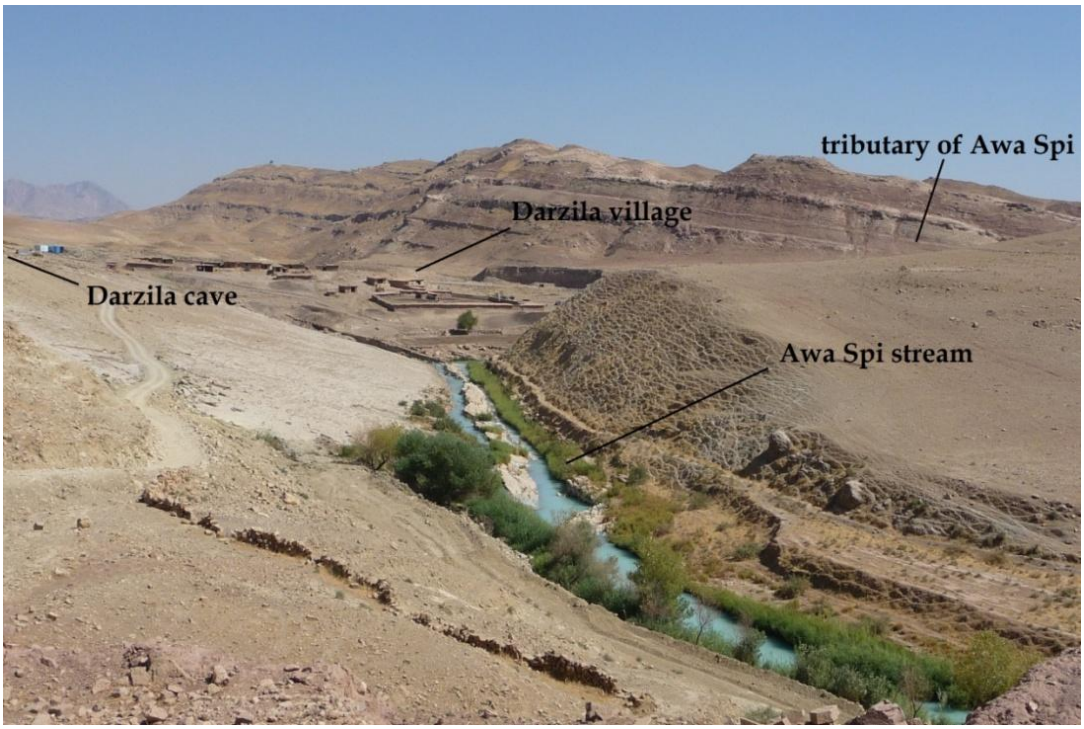

Figure 3: Awa Spi river and Darzila village

Nearby Darzila cave, the perennial river Awa Spi is located (Figure 3). The river has cut the Pila Spi limestone deeper and deeper and nowadays forms a canyon of about

50-60 m depth and 5-10 m width in the river upper course. The river initially flows parallel to the Azhdagh anticline towards SE and then changes towards SW at the anticline plunge. As sampling was carried out at the end of the dry season flow rates were low.

2.4. Climate conditions

Due to unstable political situations and periods of war in the past, the network of meteorological stations is relatively underdeveloped in northern Iraq. Long periods of rainfall observation exist only for the three stations: Sulaimani (since 1941), Dokan dam (since 1958) and Darbandikhan dam (since 1962). However, approximate rainfall analyses have been conducted by Stevanovic & Markovic (2003a) based on data from 23 meteorological stations. The distribution of rainfall varies strongly over the year. The average annual rainfall rate amounts to about 675 mm (Sulaimani station, 1941-2002) of which the highest precipitations occur in January (115 mm, Sulaimani station, 1941-2002) whereas there is a long dry period between June and September. As the topography strongly influences the rainfall distribution, precipitation rates decreases from NE to SW direction. In the Sangaw District, average annual rainfall rates amounts to about 600 mm (isohyets maps in Stevanovic, Markovic 2003a). Precipitation usually occurs in bursts and thus wadies drain quickly restricting recharge of groundwater aquifers (Jassim, Goff 2006).

The Sangaw District is one of the warmest regions of Kurdistan within the Iraq (Stevanovic, Iurkiewicz 2009). However, long-time data about monthly and annual variations of air temperatures are only rarely available. Data exist for Diana (two-hourly recorded data in the period from November 1957 to January 1959) (HAZRA Eng.Co. 1963) and for Erbil city (average monthly temperatures for the period from 1959 to 1972) (Haddad 1973). In order to give an overview of the monthly variations in air temperatures in the Sangaw District a temperature graph provided by World Weather Online (2011) is depicted in Figure 4.

Moreover, average monthly air temperatures and several other meteorological parameters were recorded during the year 2002 at the FAO stations Qaradagh, Mawat, Degala, Gopal, Qadish and Jelan, which are distributed throughout northern Iraq. According to these data, average annual relative humidity ranges from 44.5% (Jelan) up to 52% (Mawat) whereupon the monthly average minimum is in June

(Gopal, 18%) and the monthly maximum in December (Qaradagh, 84%) (Stevanovic, Markovic 2003a).

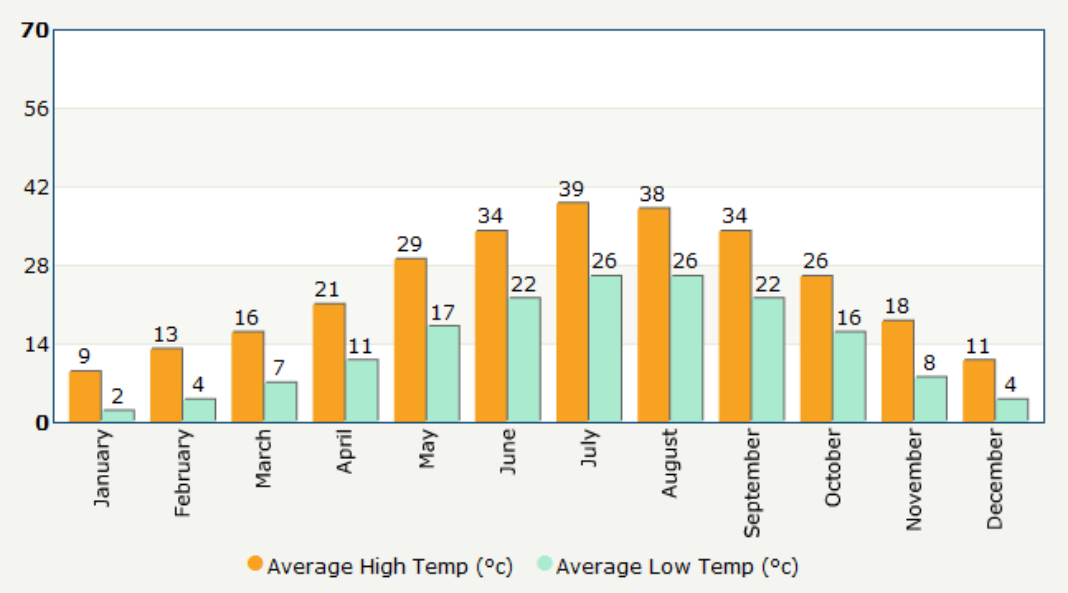

Figure 4: Average temperature graph for Sangaw District (World Weather Online 2011)[1]

In the year 2002, the rates of reference evapotranspiration (ET_o)[2] vary from 920 mm/year (Qaradagh) to 1506 mm/year (Gopal). Highest rates occur during the summer. Monthly variations range from 17 mm/month in January (Gopal) to 274 mm/month in July (Gopal) in 2002. In mountainous areas, ET_o rates are much lower (Stevanovic, Markovic 2003a).

Due to the direct influence of Zagros Mts. in the Sulaimani Governorate, northern winds are dominant throughout the year (Stevanovic, Markovic 2003a). Beyond that, Aziz (2001) mentions the influence of Mediterranean anticyclones in the summer moving from (south-) west to north and developing dust storms. Mediterranean cyclones moving from (north-) east are responsible for high rainfall rates in the winter period (Aziz 2001).

In summary, the climate of Sangaw region can be described as continental arid to semiarid climate with very hot and dry summers and cold and wet winters. Due to the given climate conditions vegetation and fertile soils are generally absent. (Iurkiewicz, Stevanovic 2010).

[1] any information about period of measurements are not provided

[2] Calculations are based on Penmen-Monteith formula (Cropwat 5.7 Programme)

3. Fundamentals

3.1. Sulphur species and the microbial sulphur cycle

Co-author: Anna Seither

Sulphur is one of the most abundant elements in nature. It is present in various minerals (e.g. elemental sulphur, gypsum, metal sulphides), gases (e.g. SO_2, H_2S), aqueous species (e.g. SO_4^{2-}, H_2S_{aq}), as well as organic compounds (e.g. humic matter, oil, coal, dimethyl sulphoxide). Furthermore, sulphur is highly redox sensitive, occurring in oxidation states from -2 in sulphides to +6 in sulphate. The latter species commonly are the dominant forms of sulphur. Species with intermediate or mixed oxidation states occur as well, though in lesser amounts (Kaasalainen, Stefánsson 2011). Transformations between different sulphur species can occur through chemical or biological pathways. However, the abiotic route usually is significantly slower (Ehrlich 2002). Table 2 lists geomicrobially important forms of sulphur and their oxidation states.

Table 2: Geomicrobially important forms of sulphur (modified after Ehrlich 2002)

Species	Formula	Oxidation state(s) of Sulphur
Sulphide	S^{2-}, HS^-, H_2S	-2
Polysulphides	S_n^{2-}	-2 and 0
Elemental sulphur	S_8 (usually written S^0)	0
Sulphite	SO_3^{2-}	+4
Thiosulphate	$S_2O_3^{2-}$	-1and +5
Polythionates	$S_nO_6^{2-}$ ($n \geq 2$)	+4 with n = 2; -2 and +6 with n > 2
Sulphate	SO_4^{2-}, HSO_4^-	+6

The microbial metabolism comprises a major portion of the global sulphur cycle (Trüper 1984). A simplified scheme of the microbial sulphur cycle is presented in Figure 5.

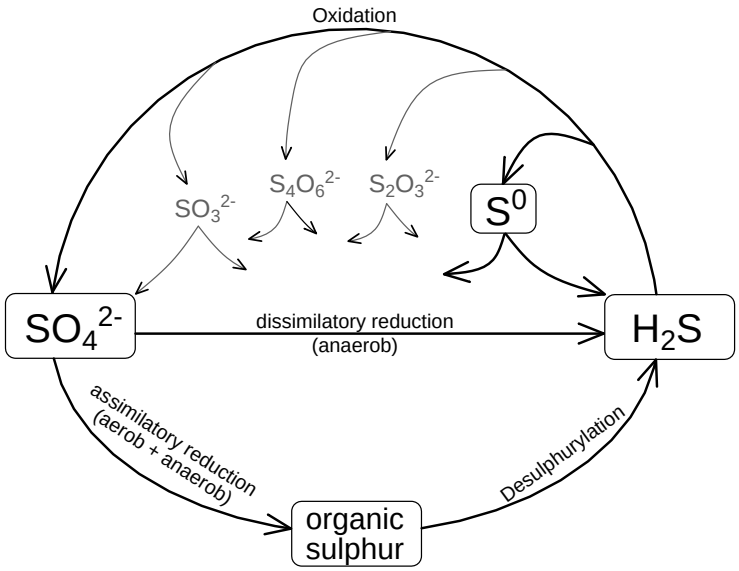

Figure 5: The microbial sulphur cycle (modified after Canfield 2001; Tang et al. 2009)

Sulphur is an essential element for living cells. Most commonly in the form of sulphate, it is assimilated and incorporated into amino acids, vitamins, and various other components of the cell (Le Faou 1990). Some prokaryotes can use sulphate or elemental sulphur as electron acceptor. For others, reduced forms of sulphur, especially sulphide, serve as sources of energy or reducing power. Sulphide oxidation may proceed by numerous different pathways and numerous intermediate compounds can arise. Each of these intermediates has a variety of possible fates, such as oxidation, reduction, or disproportionation[3] (Canfield 2001).

3.2. Sulphuric acid speleogenesis

Co-author: Anna Seither

In cave science, the term *speleogenesis* refers to the origin as well as the development of caves (Gunn 2004). Unfortunately, expressions used by cave scientists are not always consistent with the terminology of geosciences. In order to avoid confusions, cave science nomenclature was avoided in this thesis. The terms *epigene* and *hypogene* karst were replaced by *phytokarst* and *unconventional karst* or *karst of deep-seated origin*, respectively.

Most accessible karstic caves are phytokarst caves that are formed by dissolution of limestone by infiltrating shallow, meteoric water enriched in CO_2 (Palmer 2011). However, the expression karst is a much wider concept. Ford (2006) defines karst as a terrain with distinctive hydrology and landforms that is formed due to the

[3] Results in simultaneous formation of sulphate and sulphide

combination of high rock solubility and a well-developed secondary porosity underground.

The typical difference between phytokarst and unconventional karst caves is the direction of the water or gas flow, namely descending in the former and ascending in the latter (Ford 2006, Klimchouk 2007).

Like phytokarst caves, uncommon karst caves can be formed by carbonic acid dissolution. However, Klimchouk (2007) lists a variety of other processes that are relevant for the formation of the latter. Possibly the most interesting among these is the dissolution by sulphuric acid. Typically, these caves consist of a central area or passage with irregular rooms, ascending blind passages, abundant gypsum deposits and floor feeders (Palmer, Hill 2012). Egemeier (1973, 1981) was the first who systematically studied such features and proposed the sulphuric acid speleogenesis (SAS) model to explain the origin and evolution of Lower Kane Cave in Wyoming: When H_2S-bearing water enters the oxygenated, subaerial cave environment, hydrogen sulphide reacts with oxygen to produce sulphuric acid. Adjacent limestone dissolves and is replaced by gypsum precipitation.

The SAS model was later recognised to explain the development of some major cave systems, such as la Cueva de Villa Luz in Mexico (Hose, Pisarowicz 1999), Carlsbad Cavern and Lechuguilla Cave in New Mexico (Hill 1990; Hose et al. 2000; Engel et al. 2004), the Frasassi Cave System in Italy (Galdenzi 1995; Galdenzi, Maruoka 2000) and the caves in the Cerna Valley in Romania (Onac et al. 2011).

A typical setting for SAS is shown in Figure 6.

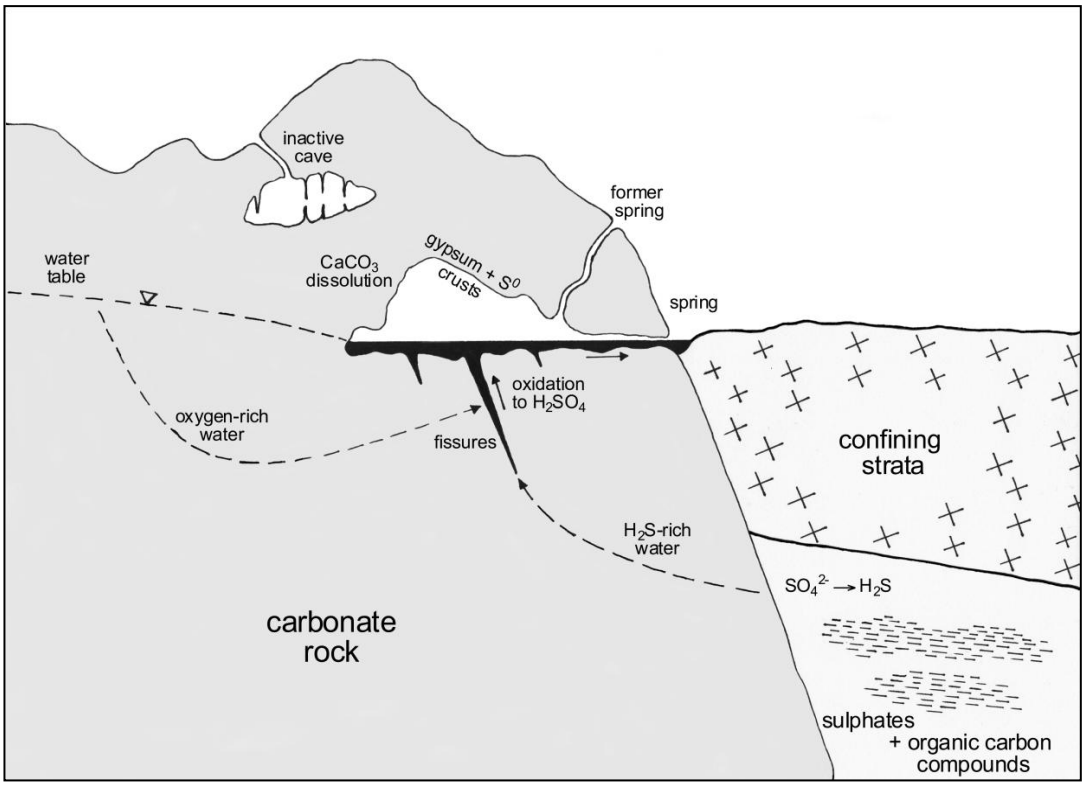

Figure 6: A typical setting for sulphuric acid caves (after Palmer, Palmer 2004)

Cave-forming hydrogen sulphide typically originates either from oil-rich reservoirs directly or from the reduction of sulphates by organic matter (Palmer, Palmer 2004), as shown in this representative but unbalanced reaction:

$$SO_4^{2-} + 2H_2O + 2[C] \rightarrow H_2S + HCO_3^- \qquad [1]$$

The expression [C] is symbolic for an organic compound. Theoretically, thermochemical sulphate reduction (TSR) without any microbiological support may occur at temperatures as low as 25 °C (Worden, Smalley 1996). However, only at temperatures above 100-140 °C reaction rates appear to be high enough to be geologically significant. At temperatures less than about 80 °C the reaction requires bacterial mediation (bacterial sulphate reduction = BSR) (Machel 2001).

When H_2S-bearing water encounters oxygenated groundwater, ascends to the water table, or volatises into the cave atmosphere and adsorbs to moist cave wall surfaces, sulphuric acid is produced; either in a single or, more commonly, in several intermediate steps (Palmer, Palmer 2004):

$$H_2S + 2O_2 \rightarrow \cdots \rightarrow 2H^+ + SO_4^{2-} \qquad [2]$$

Polysulphides (S_n^{2-}), elemental sulphur (S^0), sulphite (SO_3^{2-}), thiosulphate ($S_2O_3^{2-}$), and polythionates ($S_nO_6^{2-}$) are possible intermediate sulphur species of the reaction (Kaasalainen, Stefánsson 2011).

In the first SAS model, sulphuric acid production was completely ascribed to chemical oxidation. Later studies (especially Angert et al. 1998; Hose et al. 2000; Engel et al. 2004; Barton, Luiszer 2005) demonstrated that microbial mediation by sulphur oxidising bacteria like Thiobacillus can enhance this process substantially.
The sulphuric acid dissolves the carbonate rock of the limestone, and freed calcium ions may combine with the sulphate ions to form gypsum:

$$CaCO_3 + 2H^+_{(aq)} \rightarrow Ca^{2+} + H_2O + CO_2 \quad [3]$$

$$Ca^{2+} + SO_4^{2-} + H_2O \rightarrow CaSO_4 * 2H_2O \quad [4]$$

These secondary gypsum precipitates tend to be blistered and poorly bonded to the carbonate rock (Palmer, Palmer 2004). When they become too heavy to support their own weight, they fall to the cave floor and are carried away by cave rivers. The net result is the removal of mass from the host rock and the enlargement of void volume.
At places where thick gypsum precipitates coat adjacent carbonate rock sulphuric acid is not neutralised. As the acid concentration increases, the pH drops to fairly low levels. Below about pH 2, gypsum dissolves again and HSO_4^- becomes the dominant sulphate species. If there are also reducing conditions (Osseo-Asare, K. 1989), elemental sulphur might precipitate on the gypsum crust (Palmer, Palmer 2000).

Darzila cave has been proposed to enlarge by the same mechanisms (Iurkiewicz, Stevanovic 2010; Khanaqa, Al-Manmi 2011). Cave sulphur is thought to originate from petroleum fields, or from gypsum of Lower Fars Formation (Iurkiewicz, Stevanovic 2010). A small oil spill into Awa Spi river confirms the general presence of hydrocarbons. The occurrence of substantial oil reservoirs in the vicinity of the cave is not documented in the literature. However, only about 5 km from the cave, confidential test drillings are performed. Furthermore, the Chamchamal and the Khor Mor gas-condensate field, as well as the famous Kirkuk oil field are located within a few tens of km distance from the study area.

3.3. Characterisation of hydrocarbon-associated waters

As a possible afflux of H_2S from deep oil reservoirs is assumed and likely, a brief description of the hydrogeochemistry of hydrocarbon-associated groundwaters shall be given in this section.

Since the presence of hydrocarbons facilitates reduction processes, groundwaters associated with hydrocarbons are typically characterised by low E_H values. Common constituents of reduced groundwaters are H_2S, NH_4, Fe^{2+}, Mn^{2+} as well as elevated CO_2 contents (Matthess 1994). The most typical feature of oilfield waters is the presence of organic compounds (Chilingar et al. 2005). Moreover, large quantities of dissolved gases such as CO_2, H_2S, CH_4, N_2 etc. are common. In addition, oil field waters are commonly enriched in volatile and non-volatile phenols and fatty and naphtenic acids (Chilingar et al. 2005). Major and minor constituents in oilfield waters according to Satyanarayana (2011) are given in the following table:

Table 3: Major and minor constituents in oilfield waters (Satyanarayana 2011)

Concentration	Constituent
Per cent	Na, Cl
> 100 mg/L	Ca, Mg, Br, SO_4, K, Sr
1-100 mg/L	Al, B, Ba, Fe, Li
µg/L (most oilfields)	Cr, Cu, Mn, Ni, Sn, Ti, Zr
µg/L (some oilfields)	Be, Co, Ga, Pb, V, W, Zn

Beyond that, Chilingar et al. (2005) mentions iodine in high concentrations as a direct hydrochemical indicator of oilfield waters. According to Matthess (1994) PO_4 and Cd are also commonly present in hydrocarbon-associated waters. Furthermore, waters associated with hydrocarbons are generally characterised by a high salt concentration, mostly higher than that of seawater (Matthess 1994).

4. Methods

4.1. Sampling, storage and sample preparation

Water sampling as well as in-situ and on-site measurements were performed at 19 sampling spots in the period from September, 15th to October, 6th 2011 at the end of the dry season.

4.1.1. Water samples

Depending on later analysis preparation and storage of samples vary. The following Table 4 gives an overview of it.

Table 4: Overview of preparation and storage of samples according to the purpose of analysis

	Analysis	**Preparation**	**Storage**
Main anions & cations	IC	Filtration	50 ml PE bottles
Thiosulfate ($S_2O_3^{2-}$), Polythionate ($S_nO_6^{2-}$)	IC	Filtration, stabilisation	50 ml PE bottles*
Trace elements	ICP-MS	Filtration, acidification	30 ml PE bottles*
TIC	Elementar liquiTOC	-	50 ml PE bottles
DOC	Elementar liquiTOC	Filtration	100 ml glass flasks*
Redox-sensitive elements	Photometry	-	PET bottles*
K_S-/K_B-value	Titration	-	250 ml glass flasks*

*Filled up completely

Filtration was carried out for IC, ICP-MS and DOC samples using filter syringes and 0.2 µm cellulose acetate filters (Satorius Stedim Biotech; Macherey-Nagel). Before use, filter syringes were rinsed three times with the water to be sampled. Sampling bottles for filtered samples were previously rinsed three times with distilled water. Sampling bottles for unfiltered samples were rinsed three times with the water to be sampled before use.

For ICP-MS analysis water samples were acidified to a pH < 2 using supra-pure 65% HNO_3 (3 drops/ 30 ml sample) and stored in 30 ml PE bottles. The pH was controlled by indicator sticks (Macherey-Nagel).

For TIC determination samples were filled directly in 50 ml PE bottles. In order to avoid a gas phase above the water phase bottles were filled completely. Water

samples for analysis of DOC were filtered as described above and then stored in 100 ml glass flasks. Sampling was carried out in the same way at every sampling point.

For IC analysis samples were filtered and stored in 50 ml PE bottles. Because thiosulfates are readily generated by oxidation of sulphides, it is an accepted procedure to add a Zn^{2+} or Cd^{2+} solution upon sampling in order to precipitate sulphide (Xu et al. 1998). However, ZnS and CdS precipitates are photometrically unstable in aqueous solutions. Even weak oxidants such as CO_2 and H_2O can photo-oxidise ZnS and CdS precipitates (Reber, Meier 1984; Kanemoto et al. 1992). Detailed studies of Cunningham et al. (1996) on the effect of storage and sample preservation indicate that ZnS is a better sulphide removal agent than CdS because of its larger bandgap energy. Thus, Zn^{2+} solutions were used for preservation. According to stabilisation procedures conducted by Xu et al. (1998) and Lauerwald (2007), $ZnCl_2$ as well $Zn(CH_3COO)_2$ solutions were used in this work. An overview of the applied methods of stabilisation is provided in Table 5.
Unfortunately, a stabilisation of sulphites was not conducted.

Table 5: Methods of stabilisation and storage of samples for thiosulfate and polythionate analyses (Lauerwald 2007; Xu et al. 1998)

Sample type	Analysis	Stabilisation	Storage
First method of stabilisation			
Thiosulfate ($S_2O_3^{2-}$)	IC	Filtration + 1 ml 0.6 M $Zn(CH_3COO)_2$ + 1 ml 1 M NaOH	50 ml PE bottles
Polythionate ($S_nO_6^{2-}$)	IC	Filtration + 1ml 0.6 M $Zn(CH_3COO)_2$ + 1ml 1 M NaOH + 1ml 1 M KCN	50 ml PE bottles
Second method of stabilisation			
Thiosulfate ($S_2O_3^{2-}$)	IC	Filtration + 1 ml 1 M $ZnCl_2$ + 1 ml 1 M NaOH	50 ml PE bottles
Polythionate ($S_nO_6^{2-}$)	IC	Filtration + 1ml 0.6 M $ZnCl_2$ + 1ml 1 M NaOH + 1ml 1 M KCN	50 ml PE bottles

For the purpose of polythionate determination, KCN was added to the solution. The cyanolysis of polythionate generates thiocyanate and thiosulphate according to equation 5 (Xu et al. 1998).

$$S_nO_6^{2-} + (n-3)CN^- + H_2O \rightarrow S_2O_3^{2-} + SO_4^{2-} + (n-3)SCN^- + 2H^+ \quad [5]$$

The concentration of polythionate is then determined from the difference in thiosulfate concentration between the cyanolysed and uncyanolysed samples (Xu et al. 1998).
However, it needs to be taken in mind that the preservation of thiosulfates over extended periods of time is still a serious problem. But, unfortunately, no other convenient sulphide stabilisation method is yet available for water sampling (Xu et al. 1998).

During transport from the investigation area to the local laboratory all samples were stored in a cooling box. In the laboratory, samples were stored in the fridge at approximately 8°C until analyses were carried out.

4.1.2. Gas samples

For gas analyses of CH_4, C_2H_6, C_2H_4 and C_6H_{14} water samples were stored in 50 ml headspace glass flasks. The flasks were filled completely and closed tightly with special pliers to prevent gas exchange processes. Altogether 19 samples were taken.
To trap and transport gas samples (CH_4, C_2H_6, C_2H_4, C_6H_{14}) of the cave atmosphere 40 ml glass bulbs including PTFE stopcocks (hellbach-glas) were used. Sampling was carried out at two different sampling points within the cave. The first gas sample (DC-GA-3) was taken next to the water sampling point DC-W-3; stuffy air and walls covered by elemental sulphur were significant characteristics of that place. The second sampling (DC-GA-9) was carried out next to DC-W-9. That place was characterised by fresh air and freshly formed gypsum minerals.

4.2. In-situ parameters

The parameters pH, electrical conductivity, temperature, oxygen content and redox potential were measured in-situ. Calibration and check of functionality of the instruments were carried out on the eve of each field day.

Table 6: Overview of in-situ parameters and used measurements

In-situ parameters	Instrument	Electrode/ Sensor
pH	HQ40d multi (HACH)	PHC101 pH electrode (HACH)
EC, temperature	WinLab Data Line Conductivity-Meter (WINDAUS Labortechnik)	LVC 0.35/23 electrode (Meinsberger Elektroden), PT-100 temperature sensor
Oxygen content	HQ40d multi (HACH)	LDO sensor
Redox potential	WinLab DataLine pH-Meter (Windaus)	Ag/AgCl electrode, PCE-228 Redox
Turbidity	turbidity meter Wag-WT3020 (Waagtech International, Berkshire, U.K.)[4]	

- **pH value**

The pH value was measured by the instrument HQ40d multi (HACH) and the PHC101 pH electrode (HACH). Two-point calibration of the pH electrode was performed using standard solutions of pH 4.01 and 7. Based on experience, however, also measurements of lower pH-values of around 2 are still sufficiently accurate (Kummer 2012). The pH electrode was stored in a 3 M KCl solution.

- **Dissolved oxygen**

The content of dissolved oxygen in water was determined using the instrument HQ40d multi (HACH) and an optical sensor (LDO sensor). A calibration is not required.

- **Specific electrical conductivity and temperature**

To measure specific electrical conductivity as well as water temperature WinLab Data Line Conductivity-Meter (WINDAUS Labortechnik) and a LVC 0.35/23 electrode (Meinsberger Elektroden) including a temperature sensor were used. The electrode was checked by measuring the EC of a reference solution (1413 µS/cm at 25 °C). A reference temperature of 25°C was set and the cell constant k was adjusted to the reference value according to the instructions of the manual.

- **Redox potential and pe value**

Measuring the redox potential was carried out using the WinLab DataLine pH-Meter (Windaus) and an Ag/AgCl electrode named PCE-228 Redox. The electrode was stored in 3 M KCl. The accuracy of the measuring instrument was verified by

[4] provided by the Kurdistan Institution for Strategic Studies & Scientific Research, Sulaimani, Iraq

determining the redox potential of a standard solution of 220 mV. If it differs from 220 mV, readings were corrected according to the occurring deviations. Moreover, the readings were corrected for temperature and converted to the potential of a standard hydrogen electrode according to the following formula (Merkel et al. 2005):

$$E_{25°C} = EMF - 0.198 \times \left(\frac{T}{°C} - 25°C\right) mV \quad [6]$$

$$E_H = E_{25°C} + E_t \quad [7]$$

Where: EMF ... readings [mV]
$E_{25°C}$ ... redox potential at 25°C referred to Ag/AgCl electrode [mV]
E_H ... redox potential at 25°C referred to standard hydrogen electrode [mV]
E_t ... redox potential of the Ag/AgCl electrode (3 KCl mol/L) = 207 mV at 25°C

Since measured pH values varied over a wide range, pH corrections of the E_H values were required based on the following relationship (Merkel et al. 2005):

$$E_H[mV] = -59.1 \times pH \quad [8]$$

For thermodynamic modelling with PreeqC conversion of the E_H value to the pe value is required. Calculations are based on the following simplified formula (Merkel et al. 2005):

$$pe \approx 16.9 \times E_H\,[V] \quad [9]$$

- **Turbidity**

The portable turbidity meter Wag-WT3020 was used to measure turbidity, in nephelometric turbidity units (NTU). The instrument was calibrated on each day of measurement using the supplied control vials (0.02 NTU, 20 NTU, 100 NTU, 800 NTU).

4.3. Field analysis

4.3.1. Photometry

Photometrical measurements were done immediately after return from fieldwork. Redox-sensitive species such as ammonia (NH_4^+), nitrite (NO_2^-), iron (Fe_{total}, Fe^{2+}), phosphate (PO_4) and sulphide ($H_2S_{(aq)}$, HS^-, S^{2-}) were determined according to the

given instructions using a DR/890 Colorimeter (HACH). Important parameters as range of concentration, precision and estimated detection limit (EDL) of the conducted methods are given in Table A 1. If the detectable concentration range is exceeded, an appropriate dilution with distilled water was performed.
Table A 2 summarises common interferences in the test procedures of the photometrical determinations according to Hach Company.

4.3.2. Titration

Titration was carried out in the local laboratories of the *Kurdistan Institution For Strategic Studies and Scientific Research* on the day after fieldwork.
Alkalinity of water is its acid-neutralising capacity and was determined by titrating with HCl to pH 4.3. The acidity of water is its base-neutralising capacity and was determined by titrating with NaOH to pH 8.2. Because alkalinity as well as acidity is a property caused by several constituents, the following conventions are used for reporting it quantitatively as concentrations assuming that HCO_3^- is the main source of alkalinity and CO_2 is the main source of acidity:

- Acidity = $K_{B,8.2} \sim c[CO_2]$ $(4.3 < pH < 8.2)$
- Alkalinity = $K_{A,4.3} \sim c[HCO_3^-]$ $(4.3 < pH < 8.2)$

Concentrations of HCO_3^- and CO_2 were calculated according to:

$$c_{HCO_3^-(CO_2)} = \frac{V \times c_{HCl(NaOH)}}{V_s} \times 10^3 \, M_{HCO_3^-(CO_2)} \quad [10]$$

Where:
$c_{HCO3-(CO2)}$ ... concentration of HCO_3^- respectively CO_2 [mg/L]
V ... volume of added HCl respectively NaOH [ml]
$c_{HCl(NaOH)}$ ... concentration of added HCl respectively NaOH [mol/L]
V_s ... sample volume [ml]
M ... molar mass [g/mol]

4.4. Laboratory analysis

4.4.1. ICP-MS analysis

Element analyses were performed in the water chemistry lab of the Hydrogeology department of TUBAF by means of a Thermo Scientific X Series 2 Quadrupole ICP-MS combined with a CETAC ASX-520 Autosampler. Elements were measured either in normal (non-CCT) mode or in CCT mode. In CCT mode, an energy barrier

of 1 V, 2 V or 3 V was set and a reactive gas of 7 % H_2 in He (5 ml/min) was added. In both modes, argon served as carrier gas. Considering EC values, samples were diluted accordingly in order to keep the number of counts on the detector in a moderate level. Standards at two concentrations were run for each element determined by using the multi-element standard Merck VI Standard (30 elements), a REM multi-element standard (17 elements) and mixed standards of Na, K, Ca, Mg and S, P, I, Br. For quality control 100 µl of an internal standard composed of 5 mg/L Ge-74, 1 mg/L Rh-103 and 1 mg/L Re-187 was added to each sample (10 ml).

Samples of precipitations from water surfaces were previously pulverised as it is described in chapter 4.4.6. For the purpose of ICP-MS analyses the pulverised samples were dissolved in distilled water, 1 M HNO_3 or n-Cyclohexane, respectively.

4.4.2. IC analysis

Major cations (Li^+, Na^+, NH_4^+, K^+, Mn^{2+}, Ca^{2+}, Mg^{2+}) were determined in the water chemistry lab of the Hydrogeology department of TUBAF with a Professional IC 850 from Metrohm using a guard column C4 guard and the separation column Metrosep C4 (150 mm). The system was run with a column temperature of 30°C and an eluent flow rate of 0.9 ml/min. The eluent consisted of 2 mM HNO_3 and 0.7 mM dipicolinic acid.

Determination of major anions (F^-, Cl^-, Br^-, PO_4, NO_3^-, SO_4^{2-}, SO_3^{2-}, $S_2O_3^{2-}$, SCN) [5] was carried out with a 881 Compact IC pro from Metrohm including the guard column Metrosep RP Guard and the separation column A Supp 5 (250 mm). The column temperature was set to 27 °C and the flow rate of the eluent was 0.7 ml/min. As eluent a solution of 3.2 mM Na_2CO_3, 1.0 mM $NaHCO_3$ and 10 % acetone was used.

The 858 Professional Sample Processor served as an autosampling device for ion analyses. Data interpretation was done with the software MagIC Net 2.2.

Considering ICP-MS results and EC values, samples for IC analyses were appropriately diluted in distilled water. Furthermore, samples for the determination of cations were acidified with 1 M HNO_3 to pH 3.5 to 2.5. Calibration of anions and

[5] The concentration of polythionates ($S_nO_6^{2-}$) is determined from the difference in thiosulfate ($S_2O_3^{2-}$) concentration between the cyanolysed and uncyanolysed samples

cations was carried out by measuring external standards of known concentrations. Standards of SO_3^{2-}, $S_2O_3^{2-}$ and SCN as well as samples stabilised in $Zn(CH_3COO)_2$ respectively $ZnCl_2$ were prepared under exclusion of oxygen in a glove box. Since SO_3^{2-} tends to oxidise quickly its standards were additionally stabilised in a solution of 37% formaldehyde and 1 M NaOH diluted in degassed distilled water.

Samples of precipitations from water surfaces were previously pulverised as it is described in chapter 4.4.6. For the purpose of IC analyses the pulverised samples were dissolved in distilled water, 1 M HNO_3 or n-Cyclohexane, respectively.

Laboratory quality assessment

On purpose of quality assessment, concentrations of F^-, Cl^-, NO_3^-, SO_4^{2-} and PO_3^- were additionally analysed for 15 samples in the laboratories of the *Kurdistan Institution for Strategic Studies & Scientific Research* (Sulaimani, Iraq). Measurements were carried out by ion chromatography. Eluent: Na_2CO_3 + $NaHCO_3$.

4.4.3. Total inorganic carbon (TIC) and dissolved organic carbon (DOC)

The contents of total inorganic carbon and dissolved organic carbon were determined in the water chemistry lab of the Hydrogeology department of TUBAF with the LiquiTOC element analyser (Elementar Analysesysteme GmbH). Calibration was performed by external standards. For TIC analyses, serial dilutions of different C concentrations were prepared for calibration by diluting a stock solution of 1 g C/L sodium carbonate with distilled and degassed water. For DOC analyses a stock solution of 1 g C/L potassium hydrogen phthalate was used for calibration.

Degassing of CO_2 due to low pH values at the sampling points DC-W-3, DC-W-4 and DC-W-6 resulted in low concentrations of total inorganic carbon. Therefore, these samples were measured in infrared range 1 (injected volume = 9.97 ml). All the other TIC samples were analysed in infrared range 2. DOC measurements were also performed in infrared range 1. The ranges of concentration are determined by the dilution series of the external standards. An overview of DOC and TIC analyses is given in Table 7.

.

Table 7: Infrared ranges (IR), Injected sampling volumes and ranges of concentration of TIC and DOC analyses

Analysis	IR	Injected sampling volume	Range of concentration
		ml	mgC/L
TIC	1	9.97	2.50 – 15.00
	2	2.38	10.00 – 80.00
DOC	1	9.97	0.25 – 20.00

4.4.4. Gas chromatographic analysis (GC)

Gas analyses were performed in the water chemistry lab of the Hydrogeology department of TUBAF by means of Thermoscientific Trace GC Ultra equipped with the column AT-Q (30 m x 0.32 mm) and a SSL injector. Gas samples of water and air were investigated with respect to methane, ethane, ethene and hexane using a FID detector. Nitrogen served as carrier gas. All samples were injected as gas (injection volume = 250 µl) by means of headspace technique: transfer of substances to be measured in the gas phase was achieved by injecting nitrogen into the sample vessels replacing a certain water volume and generating a gas phase (headspace). By shaking volatile substances equilibrate readily with the gaseous phase.

Calibration was performed with external standards. Data interpretation was realised using the software ChromQuest 5.0.

4.4.5. X-ray fluorescence spectrometry (XRF)

Co-author Anna Seither

Altogether 19 rock and mineral samples as well as 6 sediment samples were analysed for their elemental composition by X-ray fluorescence spectroscopy (XRF) with a SPECTRO XEPOS in the water chemistry lab of the Hydrogeology department of TUBAF.

Prior analysis, rock and mineral samples were crushed, dried and subsequently pulverised to about 20 µm by using the planetary mill Pulverisette 5. Sediment samples were dried, pestled and sieved. Only the grain fraction < 80 µm was analysed for its elemental composition. Approximately 4 g pulverised sample material was used for analysis.

4.4.6. X-ray diffraction (XRD)

XRD measurements were conducted at the mineralogical laboratory of the Institute of Mineralogy (Dr. R. Kleeberg) of TUBAF using the diffractometer URD-6 (Seifert-FPM) equipped with automatic divergence aperture and semiconductor detector Meteor DT.

For qualitative XRD measurements samples were prepared on a silicon plate. Parameters of measurements are: Scan: 2:1 sym.; constant area: 5.000°...80.000°; 0.030°; stepscan (0.50 sec), anode material: Co; voltage: 40 kV; current: 30 mA; cobalt radiation; fulltime: 0 h 20 min 50 s.

For quantitative measurements samples of precipitation from water surfaces were previously filtered (0.20 µm) and the solid residues were air-dried on the filter, subsequently. Afterwards, samples were pestled and sieved to a grain size < 35 µm. The stepscan was set to 2.00 sec and full time of analysis amounted to 2 h 5 min 2 s. Evaluation of results was done using the software "Analyze" (database: pdf4+, 2011). Quantification of peaks was accomplished by the Rietveld program BGMN and Autoquant.

All in all five sediment samples and two samples of precipitations from water surfaces in Darzila cave were analysed by XRD.

4.5. PhreeqC modelling

4.5.1. Check for plausibility

All water analyses were checked for their plausibility by different approaches. Firstly, the charge imbalance was calculated according to the following equation:

$$\text{Error}\,[\%] = \frac{(\sum \text{cations} - \sum \text{anions})\ [\frac{\text{mmol(eq)}}{\text{L}}]}{(\sum \text{cations} + \sum \text{anions})\ [\frac{\text{mmol(eq)}}{\text{L}}]} \times 100\% \qquad [11]$$

Calculation of errors [%] was carried out using the hydrogeochemical modelling program PhreeqC for Windows, Version 2.18.00 (Parkhust, Appelo 1999) and the database llnl.dat. Since regulations referred to DVWK 1992a are based on a modified equation, the calculated errors were multiplied by 2.

After DVWK (1992a) tolerable deviations are ±5% (total cations or anions up to 2 mmol(eq)/L) respectively ±2% (total cations or anions more than 2 mmol(eq)/L).

However, strict compliance with these limits is often not practicable (UBA 2000). Therefore, an extended acceptable deviation of ±10% will be taken into account in further data processing.

Errors that compensate each other, such as due to an overestimation of both an anion and a cation, remain undetected in the previous mentioned checks. Therefore, additionally, another plausibility check was applied comparing the difference between the measured and calculated conductivity as proposed in Rossum (1975). For this purpose, the conductivity was calculated with PhreeqC for Windows using the database phreeqc.dat. On the basis of the balance error and the measured vs. calculated conductivity following conclusions can be drawn:

Table 8: Statements from the plausibility checks of water analyses based on the calculation of the charge balance and a comparison of measured and calculated conductivity

	Negative charge balance	**Positive charge balance**
Measured EC > calculated EC	Deficiency of cations	Deficiency of anions
Measured EC < calculated EC	Surplus of anions	Surplus of cations

4.5.2. Saturation Indices

To evaluate if an aquatic solution is in equilibrium, undersaturated or supersaturated with regard to a solid phase, saturation indices are calculated using the program PhreeqC for Windows (database: llnl.dat).
The saturation index SI is defined as the logarithm of the quotient of the ion activity product (IAP) and the solubility product (K_{SP}):

$$SI = \log \frac{IAP}{K_{SP}} \quad [12]$$

An aqueous solution can be considered as saturated (dynamic equilibrium) in relation to a certain mineral phase if -0.05 < SI < 0.05. If the calculated saturation index is below -0.05 the solution is undersaturated with regard to the corresponding mineral phase, if SI exceeds +0.05 the solution is supersaturated with respect to this mineral phase. Undersaturation in relation to a certain mineral indicates net dissolution of the mineral, supersaturation in relation to a certain mineral may indicates net precipitation of the mineral in dependence on precipitation kinetics (Merkel et al. 2005; Ford, Williams 2007).

Saturation indices will be calculated for common karst rock minerals of carbonates, sulphates and silica. In addition, also selected sulphides, oxides and hydroxides, layered silica minerals as well as elemental sulphur will be taken into account for SI calculations. Saturation indices of halides like for instance halite, sylvite or carnallite will not be examined since salt solubility is so great and therewith salt indices are of little practical utility in karst studies (Ford, Williams 2007).

4.5.3. Ionic strength

The ionic strength is a sum parameter for ionic interactions and is calculated as one-half the sum of the molar concentrations of ions (m_i) in water multiplied by the square of their respective charges (z_i):

$$I = 0.5 \times \sum m_i \times {z_i}^2 \qquad [13]$$

Calculations of the ionic strength are carried out by means of PhreeqC (database: llnl.dat).

4.6. Multivariate statistical analyses

To identify homogeneous groups of waters of similar chemistry, hierarchical cluster analyses were performed using the program SPSS Statistics, version 20 (Bühl 2008). For applied statistical tests, a significance of 5% ($\alpha = 0.05$) was regarded as acceptable.

Initially, the Kolmogorov-Smirnov test was applied to all variables showing that a normal distribution cannot be assumed for all of them (Appendix C). Due to this, nonparametric methods will be used in the following section.

For the classification of water samples in-situ parameters, species of N, S, Fe and C, main cations and anions and selected elements were considered as input parameters. Species distributions of Fe and C were previously modelled with PhreeqC (Table A 24, Table A 25). Before cluster analysis, input parameters were checked in detail. To ensure an equal weighting of all variables and to avoid a distortion of the results, highly correlating variables have to be excluded previously. For that purpose, bivariate correlation analyses were carried out with the nonparametric Spearman correlation coefficient and a two-tailed test of significance. If two variables showed correlations > 0.9, one of them will usually not be considered in cluster analysis.

Moreover, variables that indicate the same values for almost all samples were also excluded previously, since they contribute to a levelling of differences and can therefore also cause distortions (Backhaus et al. 2011).

Cluster analyses were performed for the cases of 2 to 8 clusters. Because Ward's method yielded the most plausible results this algorithm was finally chosen. As interval measure squared Euclidian distance was set. Since values ranges over several orders of magnitude, transformation of data was required. Therefore, all variables were standardised to a range of [0 to 1] according to the following formula and rescaled.

$$x_{i,0\text{ to }1} = \frac{x_i - x_{min}}{x_{max} - x_{min}} \quad [14]$$

Where: X_i ... each data point i
X_{min} ... the minima among all data points
X_{max} ... the maxima among all data points
$X_{i,0\text{ to }1}$ ... the data point i normalised between 0 and 1

In order to figure out the optimal number of clusters, clustering was tested for significance by the nonparametric Kruskal-Wallis H test checking the equality of n independent samples by comparing their medians. For two independent samples the nonparametric Mann-Witney test was applied. Additionally, a sudden increase in heterogeneity during the agglomeration process can be used as a further indicator of the optimal number of clusters ("elbow criterion"). Therefore, the agglomeration coefficients $\hat{a}_i$ were plotted against the stages i of agglomeration. The number of clusters is determined by:

$$N_{cluster} = n - i \quad [15]$$

Where: $N_{cluster}$ ... optimal number of clusters
n ... number of cases to be clustered = 19
i ... stage at which a sudden increase in heterogeneity is visible

5. Results and interpretation

5.1. Description of cave patterns

5.1.1. Setting and dimensions of Darzila cave

Darzila cave is located close to Darzila village at 35°08’770’’N, 45°16’740’’E and 688 m asl (terrain surface). Hydrogen sulphide exhales (odour of rotten eggs) are characteristic for the whole region. The cave is entirely embedded in a limestone rock unit of Pila Spi Formation. Access to the cave enables a deep sinkhole that is probably formed by breakdown of instable parts of the cave (Figure 7). Those so-called collapse dolines are characterised by almost vertical rock walls and a debris floor sloping down into an open cave passage (Bell et al. 2005).

Figure 7: Great sinkhole providing access to Darzila cave

The diameter of the sinkhole is about 30 m (Figure 8). The cave entrance is on about 15 m below terrain surface, from where one gets into through a small and steep passage. The cave is located on approximately 38 m below terrain surface, about 650 m asl (Figure 8). However, it has to be taken in mind that these values are just approximations because precise measurement could not be performed. Total

explored length of the cave is about 200 m (Figure 9). Further exploration in easterly direction had to be interrupted due to bad air quality and the increased danger of rock fall. Thus, the end of the cave could not be reached yet.

In order to get a better idea about the dimension of the cave a map view as well as a cross sectional view were set up on the basis of surveying that has been conducted during field work (Figure 8, Figure 9). Karst symbols are used according to the official UIS list (Häuselmann, Neumann 1999). An overview of the location of sampling points inside of Darzila cave is provided in Figure 9.

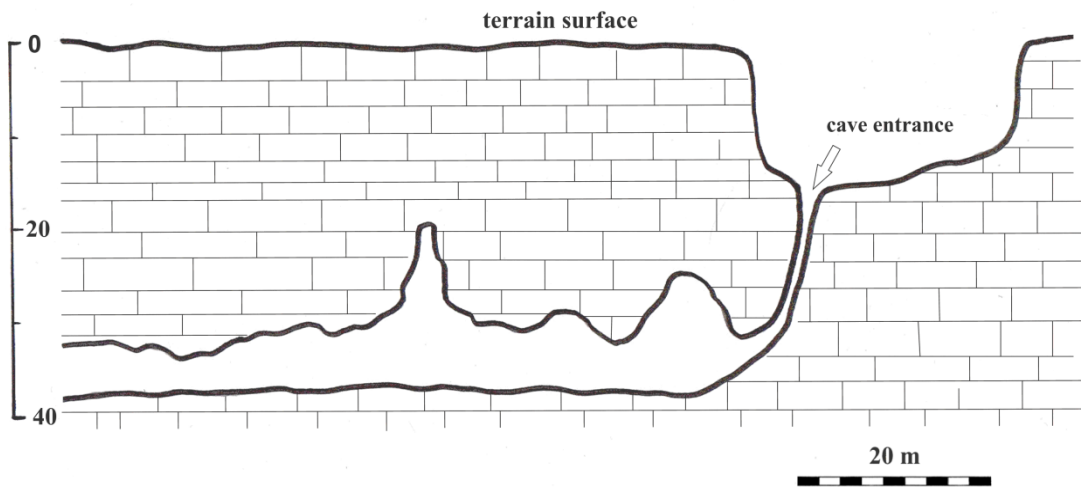

Figure 8: Cross sectional view of Darzila cave

As it is depicted in Figure 8, the cave shows an irregular profile with vaulted ceilings which are typical characteristics of gypsum replacement (Palmer, Palmer 2000). The floor is nearly flat over a large area. According to Palmer (1991) this is often an indication of subaqueous dissolution processes. Although they are not included in the cross sectional view, small skylights are present in the passage of ceilings nearby the entrance.

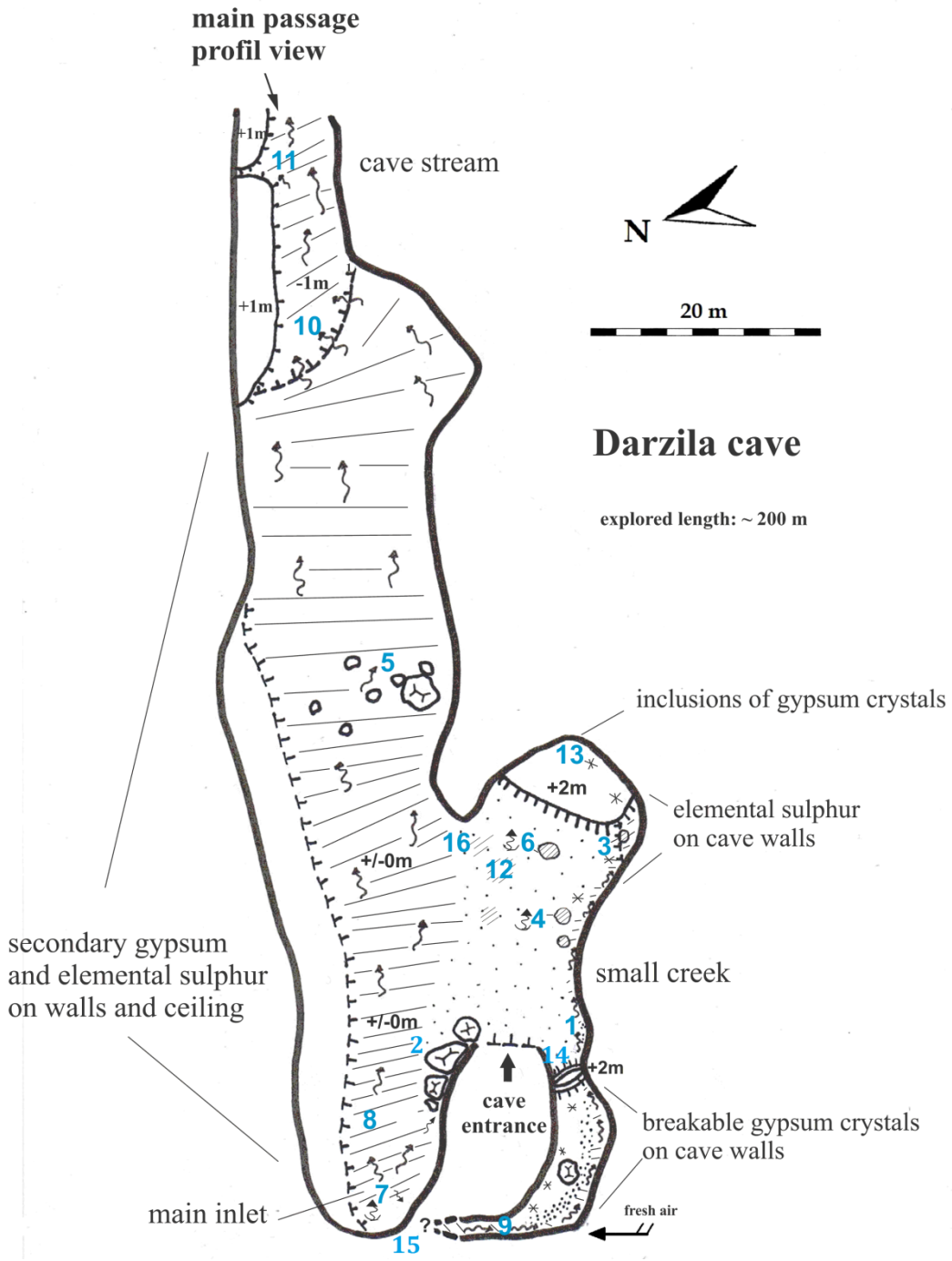

Figure 9: Map view of Darzila cave (blue numbers mark sampling points); karst symbols according to UIS guidlines (Häuselmann, Neumann 1999)

5.1.2. Brief hydrogeological description and location of sampling sites

Water in the cave is fed by different subterranean springs. Most parts of the cave floor are covered by water with a depth between a few cm to dm and of low stream velocity. The main inlet within Darzila cave is represented by sampling site DC-W-7 where water rises up a deep, steeply inclined fault. These types of springs (floor feeders) are typical characteristics of nonconventional karst caves (Palmer, Hill 2012).

Furthermore, a small creek was identified on the other site of the cave represented by the sampling points DC-W-1 and DC-W-9. Site DC-W-9 is located in an outstanding part of the cave only accessible by a narrow passage, characterised by fresh air supply and an overwhelming presence of readily breakable gypsum crystals covering the cave walls. However, the source of the creek could not be reached since the passage was too narrow and therefore not accessible.

Where the cave ground is not covered by water, small, acidic and isolated water pools are formed represented by sampling site DC-W-3, DC-W-4 and DC-W-6. The sampling points DC-W-4 and DC-W-6 are small springs with little discharge fed by water rising up from the underground (floor feeders). Because a subterranean source could not be identified, it is assumed that sampling site DC-W-3 exist due to overflow from the nearby water stream represented by DC-W-1 and DC-W-9.

In the rear part of the cave, a cave river of milky colour is formed consisting of a mixture of the different water inlets, best illustrated by the samples DC-W-10 and DC-W-11. This river represents the main discharge of the cave and outflows towards east. According to Khanaqa, Al-Manmi (2011) discharge rates vary in the range of 40 L/s (dry season, June) up to 60 L/s (wet season, April). However, since sampling was carried out at the end of the dry season in September and October lower values can be assumed. As the inlet at site DC-W-7 possesses the highest flow rate it probably mainly influence the hydrochemical composition of the main cave river.

Low water levels and decreased discharge in consequence of the ongoing dry season made the reconstruction of groundwater flow paths and the identification of springs difficult with regard to selected cases. For instance, the origin of the small river sampled at site DC-W-1 and DC-W-9 could not be clearly identified during field work. Moreover, it is uncertain whether the small water reservoir at site DC-W-8 is just formed due to overflowing water from DC-W-7 or if it is, beyond that, fed by

water ascending from the underground. In order to clarify these uncertainties, hydrochemical and isotopic investigation were carried out.

To investigate potential hydraulic connections between subterranean waters and surface waters in the surrounding of Darzila cave, five samples were also taken from the nearby river Awa Spi (Figure 10). During the investigation of Awa Spi river, two main subterranean feeders could be identified represented by DR-W-1 and DR-W-2. Moreover, a tributary of Awa Spi (DR-W-7), that was temporary waterless in the lower part and thus not connected to Awa Spi during the sampling period, as well as a small spring allocated some meters above the river level (DR-W-8) were sampled, too. In addition, sampling was also conducted at a well (DC-W-1) closely located to the cave entrance. Due to low water quality this well is not used by the locals neither for drinking nor irrigation. According to statements by village inhabitants the depth to water table is about 30 m (657 m asl). An overview of the sampling sites in the surrounding of Darzila cave is given in Figure 10.

Figure 10: Location of sampling points in the surrounding of Darzila cave

In summary, water sampling was carried out at 19 different sampling sites. The locations of sampling sites in Darzila cave as well as in the surrounding of the cave were defined considering groundwater inlets, tributaries and mixing zones.

5.2. Surface karst features

In addition to a thorough investigation of hydrogeochemical processes within Darzila cave and along Awa Spi river, also some selected surface karst features shall be presented in the following chapter. Surveying and mapping of surface karst features was carried out in the close vicinity of Darzila cave within a radius of about 1-1.5 km. GPS data and brief descriptions of documented karst features are provided in Table A 29.

The investigated karst region displays distinctive surface karst features. Where the limestone rock of the Pila Spi formation outcrops, common karren structures such as meandering karren, panholes or trittkarren are formed caused by solution on these massive bare limestone surfaces (Figure 11). Moreover, rillenkarren and several small pits allocated in a dry river bed could be found (Veress 2010; United States Environmental Protection Agency 2002; Pfeffer 2010).

Figure 11: (Left) Meandering karren (DS-K-3). (Middle) Etched surfaces (DS-K-5). (Right) Trittkarren with a straight riser (DS-K-23)

Figure 12: (Left) Rillenkarren (DS-K-1). (Middle) Small pits (DS-K-7). (Right) Panholes (DS-K-6)

Impressive karst features arise along the road from Sangaw to Darzila village. This area is marked by a cumulative occurrence of very deep crevasses and dolines which are frequently described as “diagnostic karst landforms” (Figure 13, Figure 14) (Bell et al. 2005; Ford, Williams 2007). In some cases, the murmuring of subterranean rivers can be heard, generally associated with the characteristic foul odour of

hydrogen sulphide. Dolines along the road are funnel-shaped and circular in plan with one dominant vertical joint and diameters of about 5-10 m. Nearby Darzila cave, another type of doline was located. As it can be seen in Figure 14 (left) this doline is characterised by an irregular shape and accumulated breccias. Apart from Darzila cave, also other cave systems could be found in the surrounding area. Some of them exhibit a strong odour of hydrogen sulphide. Some of the accessible caves have been partly explored by the locals.

Figure 13: (Left) Crevasse (DS-K-17). (Right) Roofed crevasse maybe providing access to a cave (DS-K15)

Figure 14: (Left) Collapse doline (DS-K-9). (Right) Funnel-shaped doline (DS-K-19).

5.3. Hydrogeochemistry

5.3.1. Data processing and evaluation of errors

5.3.1.1. Evaluation of methods and data processing

Raw data were initially checked with regard to missing values, concentrations below or above the detection limits and outliers.
For further modelling and data analyses, values below the detection limit were replaced by 0.3*detection limit. Due to appropriate dilutions, values exceeding the upper detection limit did not occur. Since missing values are problematic in terms of statistical data evaluation, they had to be replaced by other data. In a first step, missing values of parameters which were determined by different analytical approaches were substituted by values from other methods if available (for instance IC, ICP-MS data). Therewith, the water data sheet was successfully completed except for missing values of thiosulfates and polythionates with regard to sampling points outside of Darzila cave. Since their concentrations are low, these values were excluded from further statistical analyses. Furthermore, some of the elements determined with ICP-MS were discarded from further statistical analyses and modelling because most samples showed concentrations below the detection limits.

- **Redox potential and content of dissolved oxygen**

In general, increased concentrations of dissolved oxygen accompany with increased redox potentials (Matthess 1994). As it can be seen in Figure 15, a positive correlation between both measurements is generally given. However, increased deviations could be found with regard to DC-W-4, DC-W-6 and DC-W-9. Thus, measurements at these sites have to be taken with caution. Deviations may be caused due to the fact that electrochemical measurements of redox potentials in natural aquatic systems are often impeded by a lack of equilibrium on the one hand at the electrode and on the other hand among the various redox couples present in a given system. Measurements of individual redox species concentrations therefore would give more detailed and accurate information about the occurring redox processes and the actual redox state (Schüring et al. 2000).

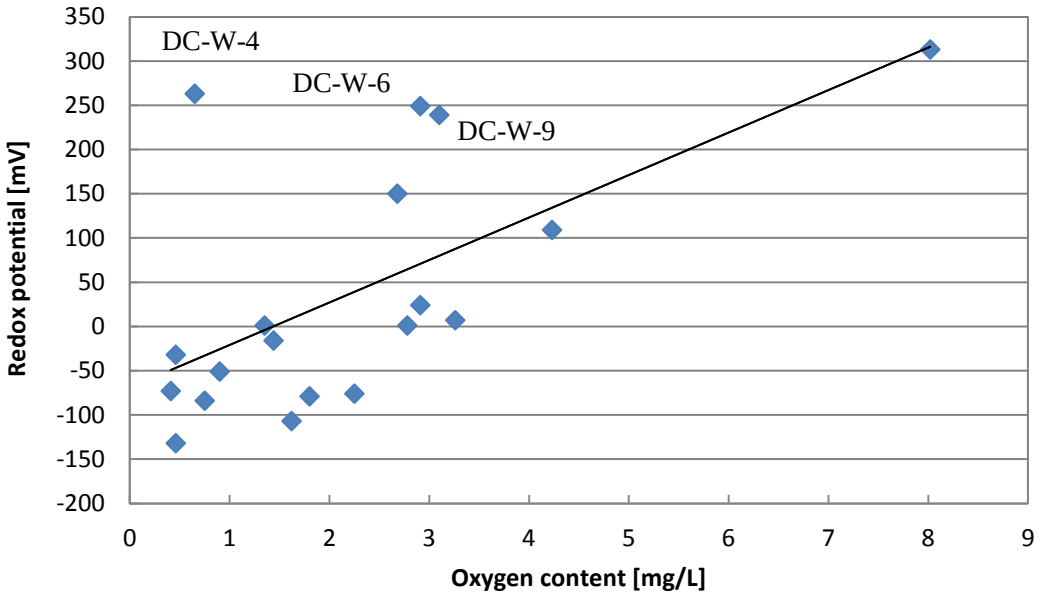

Figure 15: Redox potential vs. dissolved oxygen content

Measurements carried out at site DW-W-1 (well) should be regarded with caution since a flow through cell was not available and therewith redox conditions may have been already changed before measurement could be carried out. This assumption is strengthened by the fact that this site shows considerable concentration of sulphide ions (50 mg/L) (Table 12). But, sulphide is solely stable under reducing conditions (Figure 31) (Vitorge et al. 2007). Influences on the distribution of redox-sensitive elements have to be kept in mind, too.

- **Main anions and cations**

On purpose of verification, findings based on on-site photometry, IC and ICP-MS were compared to each other. Moreover, concentrations of S species were checked in detail.

Concentrations of calcium and magnesium were obtained by IC as well as by ICP-MS. The results can be accepted as being in good agreement since the relative deviation (RD) is 1.82% (Ca) respectively 2.83% (Mg) on average.

Significant diverging K-values were found for the samples DC-W-1, DC-W-2, DC-W-3 and DC-W-5 by comparing IC and ICP-MS results. If not considering these samples, the relative deviation is acceptable (5% on average). Since ICP-MS measurements can be disturbed by interferences with regard to K, results obtained by IC are more reliable (Kummer 2012).

Furthermore, results from ICP-MS and IC measurements were compared with regard to Br, Li and Mn indicating relative deviations of 12.77%, 9.10% and 11.18% on average. Considering that values are overall close to the detection limits, differences are considered as acceptable.

NH_4^+ concentrations measured by ion chromatography were generally lower compared to NH_4^+ concentrations measured by photometry. However, exceptions are the sampling sites DC-W-3 (RD = 28.3 %), DC-W-4 (RD = 99.3 %) and DC-W-6 (RD = 99.1 %). Characteristic differences of these sites compared to other sites are low pH ranges. Therefore, the photometrical determination was repeated after neutralising the water samples previously. In result, the relative deviation decreased to 6.4 % on average and values can be accepted as being in good agreement. For further data evaluation, photometrical determined NH_4^+ concentrations will be used except for the previously mentioned sampling sites for which IC results will be considered accordingly.

Problems also occurred in measuring concentrations of Fe^{2+} and Fe_{total} by photometrical methods. In some cases, photometrical determinations wrongly indicated Fe^{2+} concentrations which were higher than Fe_{total} concentrations obtained by ICP-MS. Furthermore, ICP-MS measurements revealed considerably higher concentrations of Fe_{total} at the sampling sites DC-W-4 and DC-W-6, which is not reflected by photometrical determinations. Since all sampling points are characterised by (partially) reducing redox conditions, Fe^{2+} should be predominant. However, this is not reflected by photometrical measurements because the reported Fe^{2+} concentrations are low. Thus, interferences by disturbing substances during photometrical analyses of Fe and Fe^{2+} ions are likely. In consequence, results from ICP-MS analysis will be used for further data evaluation and concentrations of Fe species will be modelled using the program PhreeqC for Windows.

Moreover, significant differences between IC analyses and photometrical measurements also occurred with regard to PO_4 representing relative deviations of 82.15% on average. Good agreements were only obtained for the samples DC-W-4 and DC-W-6 (RD = 6.12% on average). Because photometrical determinations are generally interference-prone (Table A 2), PO_4 contents measured by IC will be taken into account accordingly.

Recorded values of S species were checked in comparison with concentrations of total S determined by ICP-MS. The relative deviation between the sum of the four

species SO_4^{2-}, SO_3^{-}, S^{2-}, $S_2O_3^{2-}$ and S concentrations determined by ICP-MS was 13.01% on average with a maximum of 43.32% and a minimum of 0.95% whereas ICP-MS measurements generally showed higher values compared to total the sum of species except for sample DC-W-4 and DC-W-6. Based on experience, relative deviations of about 10 – 20% can be seen as sufficiently accurate considering that ICP-MS measurements of S are generally less exact, especially with respect to high S concentrations (Kummer 2012). However, in particular the samples DC-W-7 (22.55%), DC-W-8 (19.97%), DR-W-2 (43.32%), DR-W-3 (25.01%) and DW-W-1 (24.09%) indicated high diverging values. Possible source of error is the formation of volatile H_2S due to acidification of ICP-MS samples. In result, the efficiency of the nebuliser (1 to 2%) is raised and apparently increased S concentrations are detected (Kummer 2012).

- **Stabilisation of thiosulfates ($S_2O_3^{2-}$) and polythionates ($S_nO_6^{2-}$)**

In order to determine concentrations of the sulphur species $S_2O_3^{2-}$ and $S_nO_6^{2-}$ water samples were stabilised with the aid of $Zn(CH_3COO)_3$ respectively $ZnCl_2$ (Lauerwald 2007;Xu et al. 1998). It has to be mentioned that $ZnCl_2$, which was provided by Sulaimani hospital without an unambiguous labelling, already showed impurities before usage. Addition of $ZnCl_2$ to the water samples resulted in colourful precipitations. In result, concentrations of thiosulfates and polythionates in samples stabilised with $ZnCl_2$ were throughout lower compared to those stabilised with $Zn(CH_3COO)_3$. Hence, only the latter ones will be considered. Detailed laboratory tests are required in order to figure out the efficiency of both methods of stabilisations.

- **IC (Freiberg, Germany) vs. IC (Sulaimani, Iraq)**

On purpose of quality assessment, concentrations of F^-, Cl^-, NO_3^-, SO_4^{2-} and PO_4 measured in the laboratories of the *Kurdistan Institution for Strategic Studies & Scientific Research*, Sulaimani (Iraq) were compared to those measured in the laboratories of the Hydrogeology department, TU Freiberg (Germany). A comparative overview of results is given in Table A 27. Both laboratories detected generally low concentrations of F^-, NO_3^- and PO_4. Since values are close to the detection limits, significance of differences is limited. However, an outlier could be identified with regard to the PO_4 concentration of sample DR-W-1. Measurements of

the Kurdish institute reveal a remarkably high value of 491.8 mg/L. Since amounts of PO_4 were repeatedly determined by different approaches showing overall low concentrations of PO_4, the given value can be stated as an outlier. Good agreements were obtained with regard to Cl^- concentrations indicating only a minor relative deviation of 8.02% on average. With respect to SO_4^{2-}, overall lower values were measured with ion chromatography in Iraq. Highly diverging values of SO_4^{2-} could be found for sample DR-W-7 showing an aberration of 64.17%.

- **TIC vs. titration**

Concentrations of HCO_3^- and CO_2 of water samples were calculated on the basis of on-site K_A-/K_B-value titration. Furthermore, the content of total inorganic carbon of water samples was analysed with the LiquiTOC element analyser. Based on these findings, concentrations of HCO_3^- and CO_2 were modelled with PhreeqC for Windows. A comparison of results of both methods is given in Figure 16 displaying the sum of HCO_3^- and CO_2 ions. Further details are given Table A 4 and Table A 25.

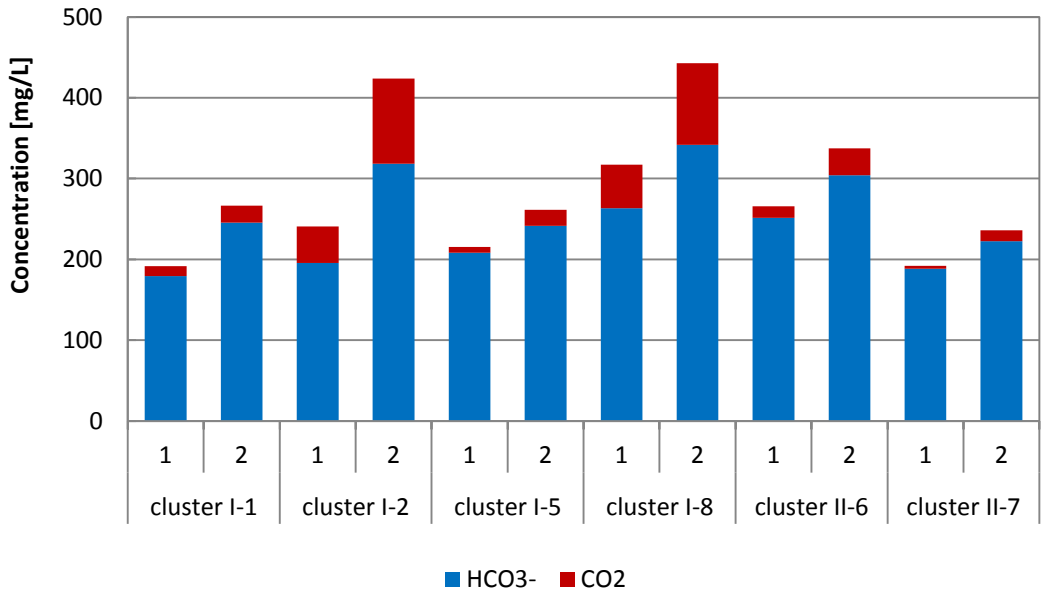

Figure 16: Comparison of concentrations of HCO_3^- and CO_2 of water samples determined by: 1 – TIC analyses and determination of C species with PhreeqC; 2 - K_A-/K_B-value titration (not considered: DC-W-3, DC-W-4, DC-W-6)

The samples DC-W-3, DC-W-4 and DC-W-6 are not considered since titration was not conducted for these samples. Generally, analyses based on LiquiTOC measurements and PhreeqC modelling (number 1) indicate values of 214.42 mg HCO_3^-/L and 22.69 mgCO_2/L on average whereas K_A-/K_B-value titrations (number 2) reveal overall higher values of 278.96 mg HCO_3^-/L and 48.95 mgCO_2/L on

average. With regard to K_A-/K_B-value titration, calculations of HCO_3^- and CO_2 are based on the assumption of a simple carbonate system. However, all samples are also characterised by high concentrations of sulphur. Thus, it is likely that the system S-O_2-H_2O also strongly contribute to the buffering capacity of the analysed waters. For this reason, values of HCO_3^- and CO_2 which were calculated based on results of the titrations are misleadingly too high. An overview of some sulphur species and acid-base-reactions that may contribute to the buffering behaviour of the water is provided in Table 9.

Table 9: Acid-Base-Reactions of some sulphur species (Langmuir 1997)

Species	Reaction	pH_{equ}*
HSO_4^-	$HSO_4^- \leftrightarrow H^+ + SO_4^{2-}$	1.99
HSO_3^-	$HSO_3^- \leftrightarrow H^+ + SO_3^{2-}$	7.36
$HS_2O_3^-$	$HS_2O_3^- \leftrightarrow H^+ + S_2O_3^{2-}$	1.75
H_2S	$H_2S \leftrightarrow H^+ + HS^-$	6.99
HS^-	$HS^- \leftrightarrow H^+ + S^{2-}$	(18.5)

*pH at which the acid and conjugate base have equal concentrations (calculations are based on thermodynamic data at 25°C and 1 bar pressure)

5.3.1.2. PhreeqC modelling and evaluation of analytical errors

- **Ionic strength**

Ionic strengths were calculated with the program PhreeqC. The results are represented in Figure 17. The acidic water pools are characterised by the overall highest ionic strengths ranging from 0.05 mol/kg to 0.2 mol/kg. The flowing water bodies of the cave indicate values of 0.03 mol/kg on average whereas Awa Spi river and its tributary show lower values of about 0.02 mol/kg. Similar characteristics can be also depicted by comparing specific electrical conductivities respectively TDS values.

PhreeqC modelling can be performed based on the theory of ion association and Debye-Hückel expressions (Parkhust, Appelo 1999). Since this approach uses ionic strength-dependent activity coefficients, it is only valid up to 1 mol/kg. Some authors even recommend an upper limit of 0.7 mol/kg. For higher ionic strengths SIT (species interaction theory) or Pitzer equation are usually applied (Merkel et al. 2005). However, calculations of the ionic strengths reveal values up to about 0.2 mol/kg. Therefore, ion interactions at high ionic strengths do not have to be considered. An additional overview of ionic strengths is given in Table A 21.

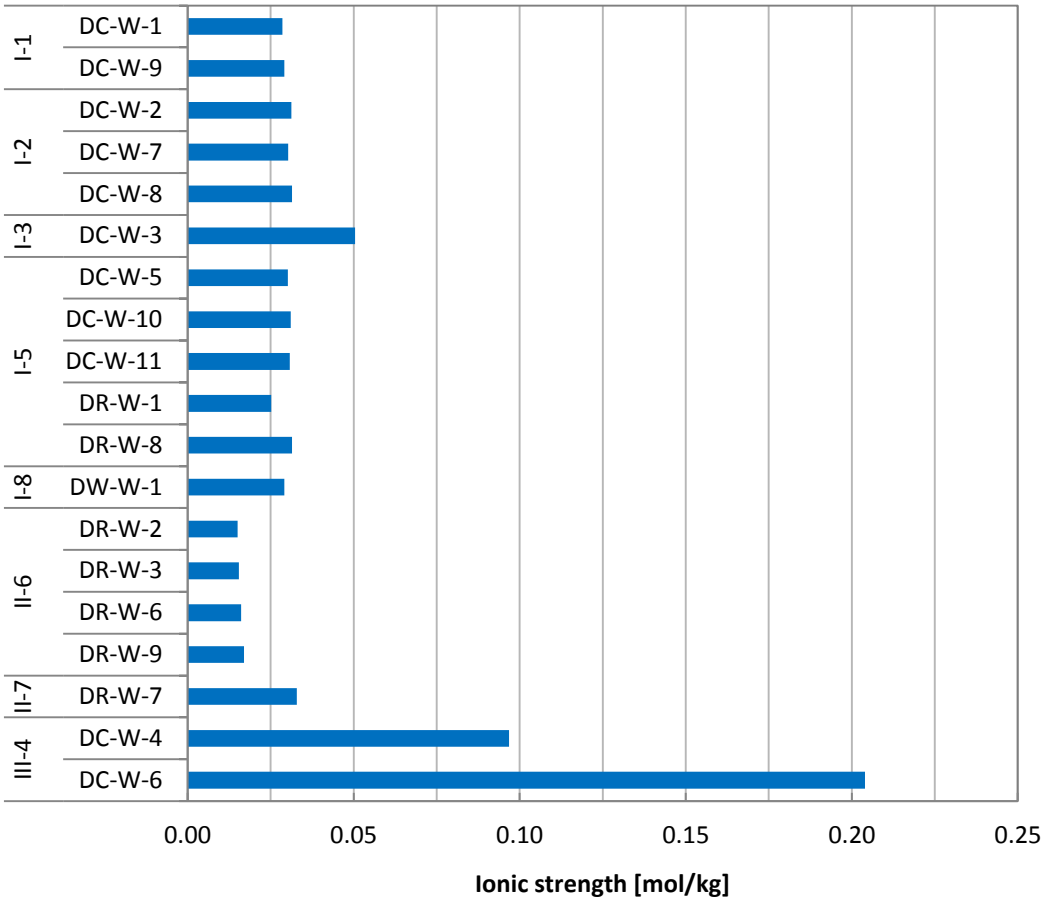

Figure 17: Ionic strengths of water samples calculated with PhreeqC using the database llnl.dat based on ion association theory and Debye-Hückel expressions

➢ Plausibility check

For water data check charge imbalance as well as the range of recorded to modelled conductivity were calculated with PhreeqC for Windows using the database llnl.dat and phreeqc.dat, respectively (Table A 21). Since the dataset of phreeqc.dat is less completed than that of llnl.dat less parameters were considered in modelling. A list of input parameters is given in Table A 17. From multiple determinations in different dilutions or on different equipment, values with the better findings of analytical errors and smaller deviations of measured to modelled conductivity were selected.

Sampling point DC-W-4 and DC-W-6, both acidic waters, initially indicated very high charge balance errors of -69.30% and -30.18%. Because problems occurred with regard to pH measurements at these sites during fieldwork, the pH value could be identified as the major source of error. Upon collecting water samples at site DC-W-4 and DC-W-6, in-situ measurement of the pH values could not be accomplished because the pH electrode did not work probably within the low pH ranges. Therefore,

measuring the pH value was firstly conducted on the next field day (4 days later) using another pH electrode. Because charge balance errors and comparisons of modelled to recorded conductivities indicated deficiencies of cations at both sites (Table A 21), the pH values were appropriately reduced (DC-W-4: pH = 2.05 → 1.55, DC-W-6: pH = 1.13 → 1.03). Thereby, an improvement of charge imbalances (Figure 18) could be achieved.

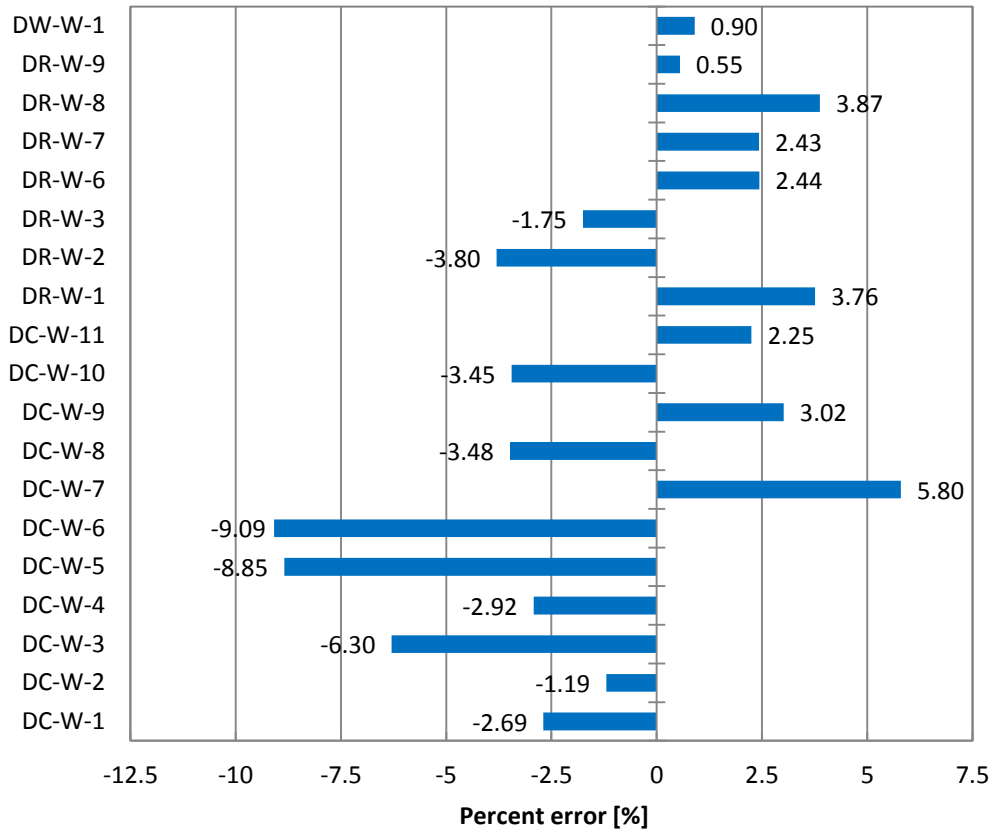

Figure 18: Final charge balance errors [%] of the water samples computed with PhreeqC for Windows (llnl.dat database) referred to DVWK (1992a)

After revising, all charge balance errors are in the range of +6% to -9%. For 15 out of 19 samples errors are even lower than ±4% (Figure 18). Therewith, analytical errors are within an acceptable range and data can be used for further evaluation and modelling.

5.3.2. Clustering of water samples

For an easier and more clearly laid out interpretation of chemical water analyses, the examined sampling points were divided in groups of similar chemistry by cluster analysis. Moreover, uncovering of potential hydraulic connections between the different sampling points is targeted.

- **Bivariate correlation analysis (Spearman)**

In order to discover dependencies between variables, bivariate correlation analyses were conducted for all water samples (Appendix C). As an initially conducted Kolmogorov test showed that not all data are normal distributed, the Spearman correlation coefficient was used (also see chapter 4.6; Appendix C). High correlations (correlation coefficient > 0.9) could be found with regard to the following variables:

- pH ↔ $CaCO_3^0$ ↔ CO_3^{2-} ↔ $MgCO_3^0$
- EC ↔ Li
- Na ↔ Be ↔ Cl
- Fe^{2+} ↔ $FeSO_4^0$
- $FeHCO_3^+$ ↔ $FeCO_3^0$
- Ca ↔ SO_4^{2-}
- K ↔ SiO_2
- Mg ↔ F
- Pb ↔ Cd

To ensure an equal weighting of variables only one of the significantly correlating variables should be considered for purposes of cluster analysis (Backhaus et al. 2011). However, in order to increase the weighting of certain key features such as pH value, EC, Ca^{2+} and SO_4^{2-} concentration etc., only the variables $MgCO_3^0$, CO_3^{2-}, Be, $FeCO_3^0$ and Cd will be excluded from cluster analysis. Beyond that, the variables Pb, As, Cr, Cu, Co and $Fe(OH)_3^0$ showed the same values for almost all samples and will consequently also be excluded. Since the relevance of the in-situ parameters oxygen content and temperature is supposed to be low, these parameters also will not be considered in the classification of water samples. Hence, 36 instead of 49 parameters

will be taken into account in cluster analysis. A summary of input parameters is given in

Table A 18.

➢ Cluster analysis

The results of the hierarchical cluster analysis are shown in form of a dendrogram in Figure 19. The optimal number of clusters was determined under consideration of the Kruskal Wallis test respectively the Mann-Witney test. With regard to a significance of $\alpha = 0.05$ (5%) good results yielded a classification in eight groups (28 out of 36 significant parameter) (Appendix C). The "elbow criterion" does not provide clear results and shall therefore not be further considered herein (Figure B 1).

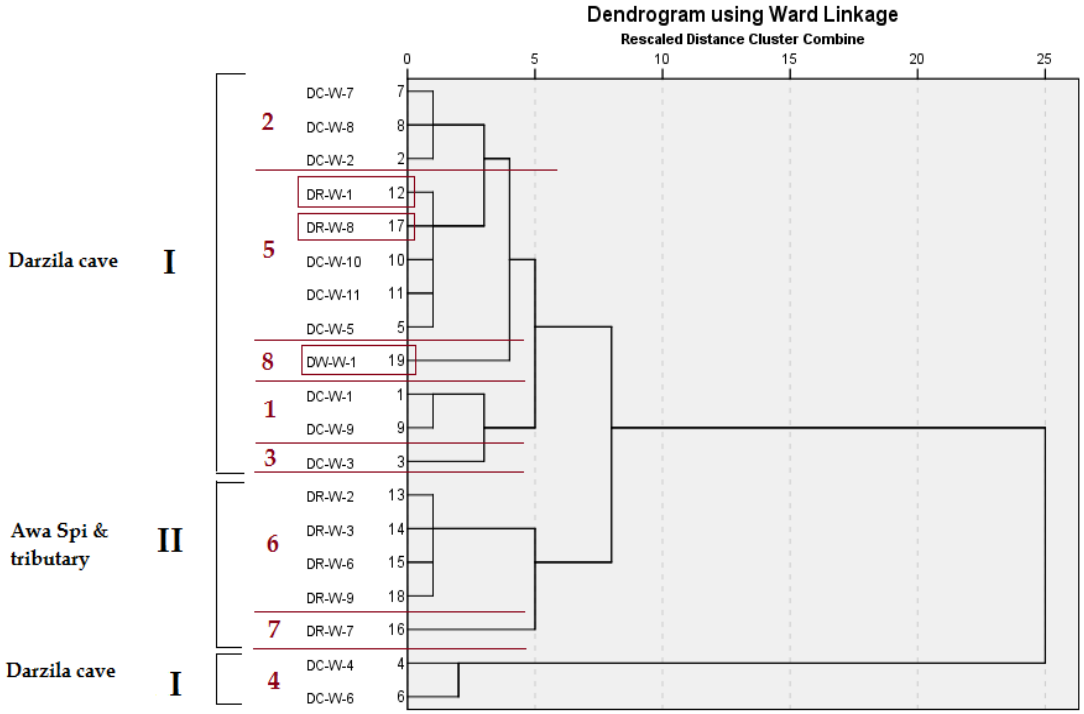

Figure 19: Dendrogram of hierarchical cluster analysis of 19 water samples including 31 parameters (Ward's method, Euclidian distances, program: SPSS for Windows, version 20)

It can be seen that, disregarding the samples DC-W-4 and DC-W-6, the dendrogram reflects the geographical proximity of the sampling sites, since on the one hand sampling points located in Darzila cave (cluster 1, 2, 3, 5, 8) and on the other hand sampling points located along Awa Spi river (cluster 6) and its tributary (cluster 7) are each more closely related. Accordingly, clusters are summarised to two major groups (I - Darzila cave and II - Awa Spi river) in order to allow an easier interpretation of data (Figure 19). Since DC-W-4 and DC-W-6, which are characterised by low pH ranges in combination with high EC values and especially

high concentrations of SO_4^{2-} ions, differ highly from all the other sampling points, they need to be considered separately. However, because they are located within Darzila cave these sampling points also will be assigned to the major group I.

Interesting relations indicate the sampling points DW-W-1, DR-W-8 and DR-W-1 (red bordered). Even though the sampling site DW-W-1 (well water) cannot be clearly assigned to any group, the cluster analysis reveals that the groundwater of the well nearby the cave and cluster 2 and 5, which are located within the cave, are distantly related. Thus, it can be assumed that both, cave and well water are fed by the same aquifer. According to information provided by village inhabitants the water table is on about 657 m asl at the well. Measurements of the cave depth reveal water levels of about 650 m asl inside the cave. However, both approximations are subject to uncertainty. Thus, no clear statement about an assumed connection between cave and well water can be made on the basis of the performed cluster analysis. However, isotopic analyses may provide more precise evidences (data not given in this paper).

Furthermore, a close relationship between the sampling points DC-W-5, DC-W-10, DC-W-11 (Darzila cave), which represent the main discharge of Darzila cave, and the sampling point DR-W-1, which is a subterranean feeder of Awa Spi river, is visible (group 5). Thus, a hydraulic connection by underground passages can be concluded. As the cave river discharges towards east in the direction of DR-W-1, DR-W-1 is potentially the main outlet of Darzila cave. Another close relationship to the main cave discharge was found for DR-W-8.

Moreover, it can be seen that sample DR-W-7 differs highly from the other sampling points and cannot be assigned to any group. Since DR-W-7 represents a sampling point at a small tributary of Awa Spi river that was temporary waterless in its lower part during the sampling period (dry season), a low similarity to the other sampling points with regard to water chemistry and in-situ parameters was expected. Another sampling point that indicates no close relationships to any other sampling sites is DC-W-3. However, a distant relationship to the sampling sites DC-W-1 and DC-W-9 can be found and was also expected since these sites are located nearby.

➢ Piper diagram

In addition, a piper diagram was created to display the different groups of water in a graphical form (Figure 20). Since a piper diagram just takes into account the concentrations of the main anions and cations, it yields slightly different results of grouping in comparison to those of the cluster analysis.

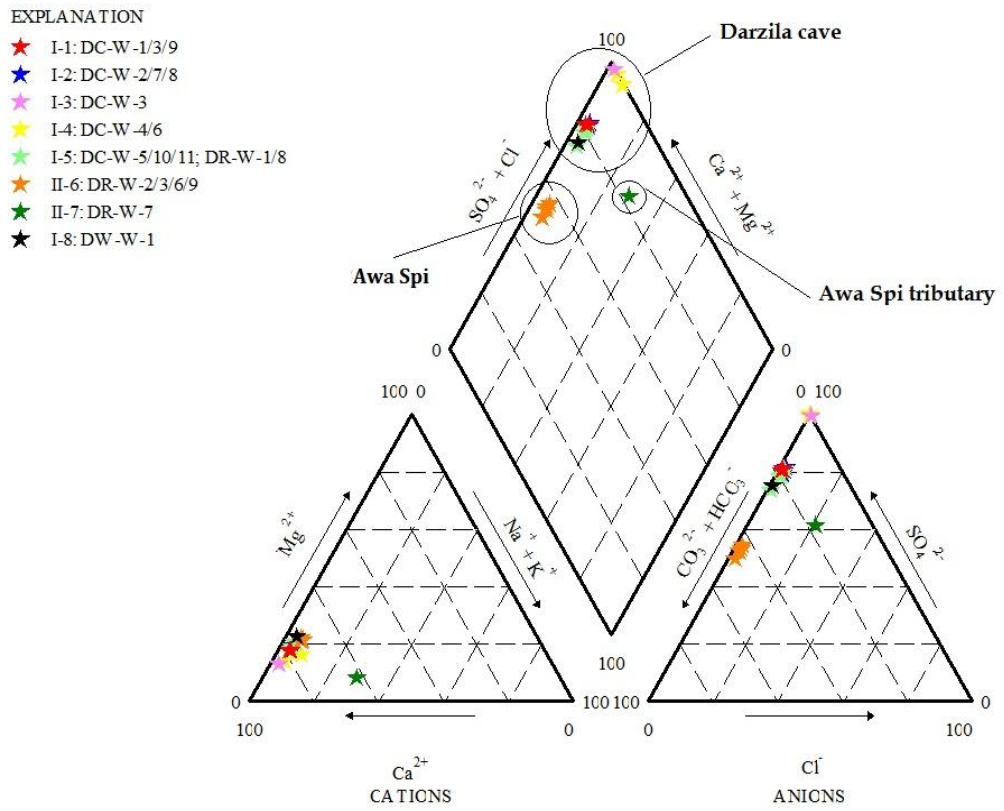

Figure 20: Piper diagram, concentrations in meq/L (software: GW_Chart, version 1.23.5.0, USGS), colours are related to groups of water determined by cluster analysis

It can be seen that especially the concentrations of anions strongly influence the formation of diverging groups whereas differences in cation concentrations are of minor importance. Based on the diagram, two main groups can be identified. The first group consists of sampling points located along the river Awa Spi, which are characterised by higher concentrations of HCO_3^- and lower SO_4^{2-} contents. The second group mainly comprises sampling points located in Darzila cave, which are predominated by higher SO_4^{2-} concentrations and lower contents of HCO_3^-. Therewith, the local distribution of sampling points is also well reflected by the piper diagram (compare to Figure 9 and Figure 10).

Furthermore, the sampling points DC-W-3, DC-W-4 and DC-W-6 form an extraordinary subgroup within Darzila cave strongly dominated by the overall highest concentrations of SO_4^{2-} ions.

According to the cluster analysis, a close similarity of the sampling points DR-W-1, DR-W-8 and DW-W-1 to the cave waters with regard to water chemistry can generally be confirmed with the aid of the Piper diagram.

Moreover, sample DR-W-7 cannot be assigned to any group by means of a piper diagram. This conclusion is also consistent with the results of the cluster analysis. Furthermore, it can be seen that there are only slightly differences in the composition of ions that are displayed in a Piper diagram between the cluster I-1, I-2, I-5 and I-8.

- **Summary of clustering of water samples**

In summary, the two major groups Darzila cave (group I) and Awa Spi (group II) and their subgroups will be regarded separately in further evaluations. Due to different sources and several mixing processes, waters of diverse characteristics are located in Darzila cave. However, four homogeneous subgroups could be found represented by cluster I-1 (DC-W-1/9), cluster I-2 (DC-W-2/7/8), cluster I-4 (DC-W-4/6) and cluster I-5 (DC-W-5/10/11, DR-W-1/8). To ensure a high homogeneity within the groups sampling sites DW-W-1 (cluster I-8) and DC-W-3 (cluster I-3) will be regarded separately. Awa Spi river will be considered as one small group composed of cluster II-6 (DR-W-2/3/6/9) and sampling site DR-W-7 (cluster II-7) which will be discussed as an outlier since it represents a tributary of Awa Spi river.

5.3.3. In-situ parameters

A complete list of in-situ parameter can be found in Table A 7. In the following, only in-situ parameters determined in Darzila cave will be regarded. Afterwards, a short description of changes of in-situ parameters in the course of the river Awa Spi will be presented.

5.3.3.1. Darzila cave

An overview of in-situ parameter measured in Darzila cave is provided in Table 10.

Table 10: Overview of mean in-situ parameters and ranges of water samples of group I summarised according to cluster analysis

Cluster ID		n	pH	EC	TDS	E_H	T	DO
				µS/cm	mg/L	mV	°C	mg/L
I-1	mean	2	7.32	1586	1150	174	22.9	3.67
	range		*0.02*	*6*	*4*	*130*	*0.2*	*1.13*
I-2	mean	3	6.80	1732	1255	-96	26.1	1.50
	range		*0.36*	*15*	*11*	*56*	*0.2*	*1.79*
I-3		1	3.30	2840	2059	-84	21.4	0.75
I-5	mean	5	7.71	1634	1185	37	24.9	2.60
	range		*0.78*	*315*	*228*	*149*	*1.3*	*1.91*
I-8		1	6.83	1605	1164	313	26.6	1.62

n - number of sampling points

- **pH conditions**

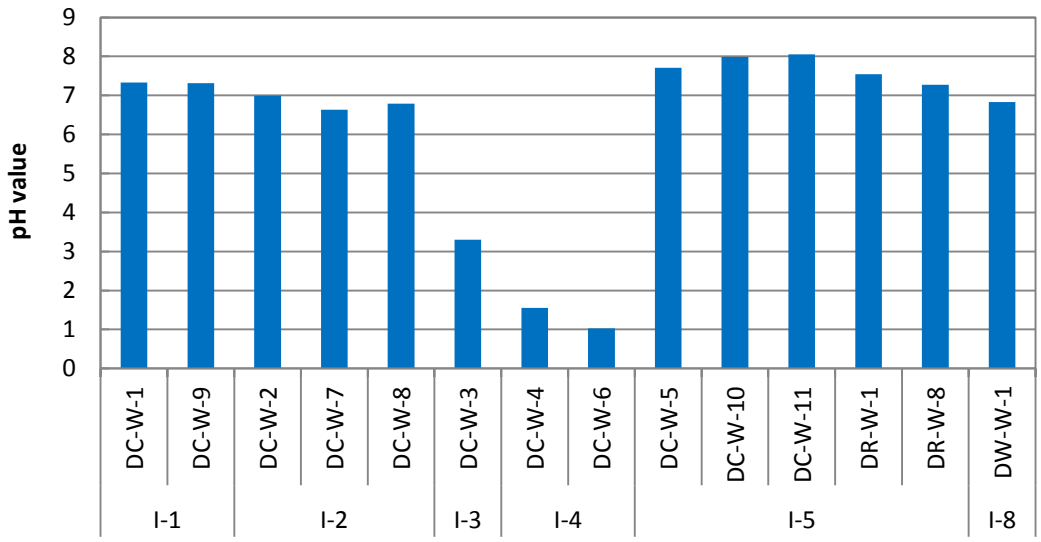

Figure 21: pH values of water samples of group I

The water within Darzila cave predominantly indicate pH values in the range of 6.63 (DC-W-7) and 8.05 (DC-W-11) with a slight tendency towards alkaline conditions. Because of elevated CO_2 contents at site DC-W-7 (Table A 25), where the water first emerges to the cave from deep sites, the pH value is lowered at this site. With increasing distance to this main inlet, a slight increase in pH can be observed potentially reasoned by CO_2 degassing.

According to Hölting, Coldewey (2005) bedrock aquifers mainly composed of limestone and gypsum as it is also present in the investigation area generally indicate pH values of 7 to 7.4. Hence, the recorded pH values of 7.31 on average fit well to the present bedrock. In contrast, separated water bodies like the sampling points DC-W-3, DC-W-4 and DC-W-6 show significantly decreased pH values of 3.30, 1.55 and 1.03. A shift toward acidic can be caused by, among others, due to the presence of sulphuric acid. A more detailed discussion will be given in chapter 5.3.10.

- **Redox conditions (E_H) and content of dissolved oxygen (DO)**

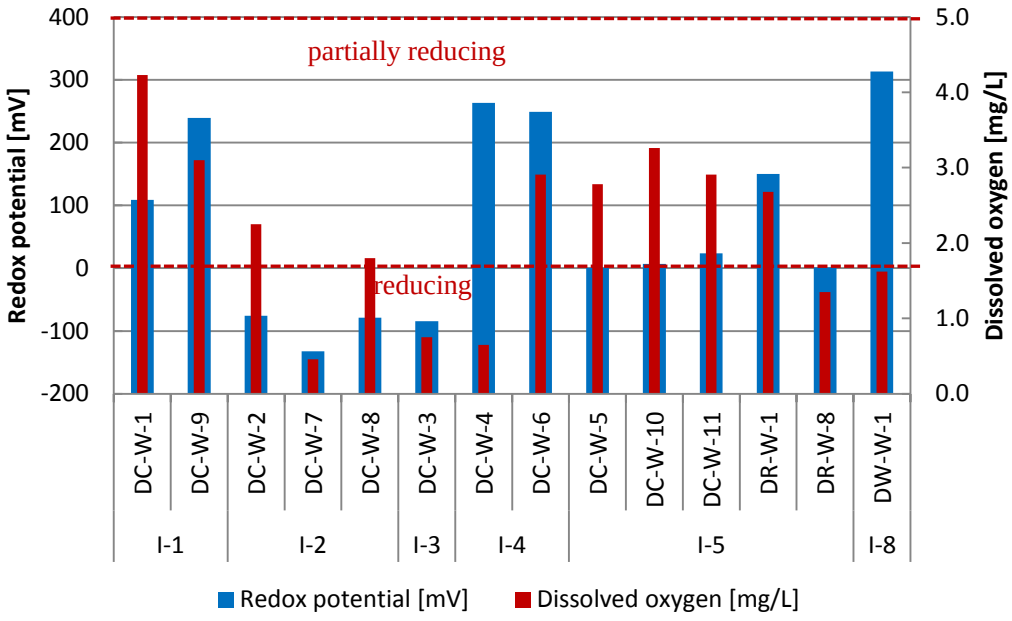

Figure 22: Redox potential and oxygen content of water samples of group I

Measured redox potentials are generally low. Cluster I-1, I-5, I-8 and I-4 indicate partially reducing conditions with a minimum of 1 mV and a maximum of 313 mV. In contrast, cluster I-2 and I-3 show overall reducing redox conditions in the range of -132 mV and -76 mV. Concentrations of dissolved oxygen range from 4.23 mg/L (DC-W-1) to 0.46 mg/L (DC-W-7). Thus, the amount of dissolved oxygen is generally low compared to common values of 6–12 mg/L in groundwater (Matthess

1994). Due to the fact that atmospheric oxygen is relatively insoluble in water (at saturation: 8.25 mg/L of O_2 [at 1bar, 25°C]) small amounts of reductants such as DOC can deplete the water oxygen content at a rate greatly exceeding the rate of O_2 replenishment (Langmuir 1997). Organic matter as well as hydrogen sulphide can be considered as the major reductants with regard to Darzila cave. Other potential reductants are Fe^{2+}, Mn^{2+} and ammonia (Langmuir 1997).

Stumm and Morgan (1996) provide a rough classification of groundwaters in representative ranges of redox intensity in soil and water (Figure 23).

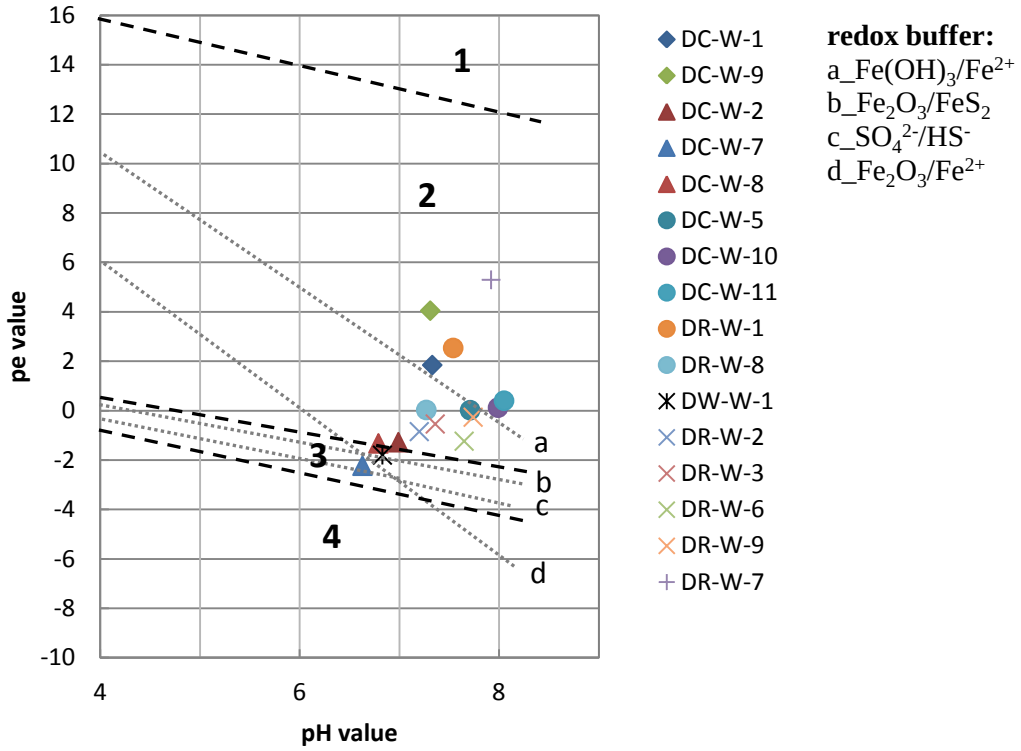

Figure 23: pe-pH diagram including sampling sites, selected redox buffer and representative redox ranges (bold lines): 1 – oxygen-bearing waters, no degradation processes; 2 – O_2 has been consumed (by degradation of organic matter), but SO_4^{2-} is not yet reduced; 3 – characteristics are SO_4^{2-}/HS^- or SO_4^{2-}/FeS, SO_4^{2-}/FeS_2 redox equilibria, high contents of organic matter; 4 – anoxic sediments and sludges (Stumm, Morgan 1996; Merkel et al. 2005) (disregarded are the acidic sampling sites DC-W-3, DC-W-4, DC-W-6, samples are listed and marked according to cluster analysis)

According to Figure 23, analysed waters are predominantly in the second range that is representative for many ground and soil waters where O_2 has been consumed (by degradation of organic matter), but sulphate is not yet reduced (Figure 23). Sampling sites summarised to cluster I-2 as well as DW-W-1 are characterised by slightly decreased pH and pe conditions. Thus, these sampling sites can be partly assigned to the third redox range, which is generally characterised by increased contents of

organic matter and SO_4^{2-}/HS^- or SO_4^{2-}/FeS, SO_4^{2-}/FeS_2 redox equilibria. In addition, common redox buffers in the prevailing pe-pH ranges according to Merkel et al. (2005) are given in Figure 23.

- **Specific electrical conductivity (EC) and total dissolved solids (TDS)**

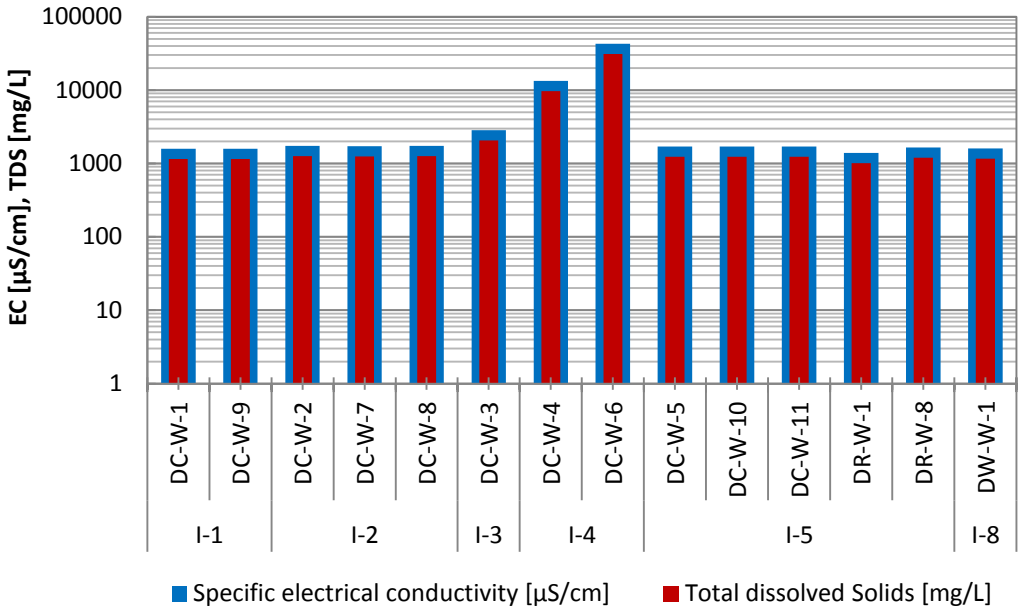

Figure 24: Specific electrical conductivity and concentration of total dissolved solids of water samples of group I (note: logarithmic scale)

The amount of total dissolved solids was calculated on the basis of the specific conductivity multiplied by a factor of 0.725 (Hölting, Coldewey 2005). Bodies of flowing water reveal specific conductivities of 1649 µS/cm on average and concentrations of total dissolved solids of 1196 mg/L on average. Hence, flowing waters investigated within Darzila cave can be described as brackish waters (Davis, DeWiest 1967). In contrast, small and isolated water reservoirs represented by DC-W-4 and DC-W-6 indicate remarkably high EC values of 13.34 mS/cm (TDS = 9.67 g/L) and 42.70 mS/cm (TDS = 30.96 g/L). Thereby, they can be described as (moderately) saline waters, respectively (Davis, DeWiest 1967). Only slightly elevated EC values of 2840 µS/cm were measured at the sampling point DC-W-3 that strengthens the assumption of just a temporary separation of this water body from the flowing water during the dry season.

Elevated TDS values in groundwater can be caused by a variety of processes. In particular, it has to be considered that the cave water is of deep-seated origin. In most cases, flow velocities are decreased at deep sites resulting in long retention periods that favour dissolution processes (Matthess 1994). Moreover, an increase in pressure

with increasing depth enhances the dissolution of the adjacent carbonate rock, insofar as the dissolution of gases such as CO_2 increases. Beyond that, the high solubility of gypsum rocks of the Lower Fars Formation (K_{SP} = 2.31*10^{-5} at 25°C) also strongly contribute to elevated TDS values in water. Significantly decreased pH values can be regarded as a main reason for remarkable increased TDS values at the sampling sites DC-W-4, DC-W-6 and DC-W-3. In addition, also evaporation processes may attribute to elevated contents of TDS with regard to these almost stagnant water bodies. However, also a potential influence of hydrocarbon-bearing layers has to be taken into account.

5.3.3.2. Awa Spi river and its tributary

Table 11 provides an overview of in-situ parameter measured at Awa Spi river and its tributary. A complete list of parameters is given in Table A 7.

Table 11: Overview of mean in-situ parameters and ranges of group II summarised according to the results of cluster analysis

Cluster ID		n	pH	EC	TDS	E_H	T	DO
				µS/cm	mg/L	mV	°C	mg/L
II-6	mean	4	7.49	914	662	-43	21.9	0.80
	range		*0.54*	*131*	*95*	*57*	*1.8*	*1.03*
II-7		1	7.92	2092	1517	-107	17.3	8.02

n - number of sampling points

Changes of in-situ parameter in the course of the river Awa Spi from the uppermost source DC-W-1 downstream to the last sampling point DC-W-9 are depicted in Figure 25.

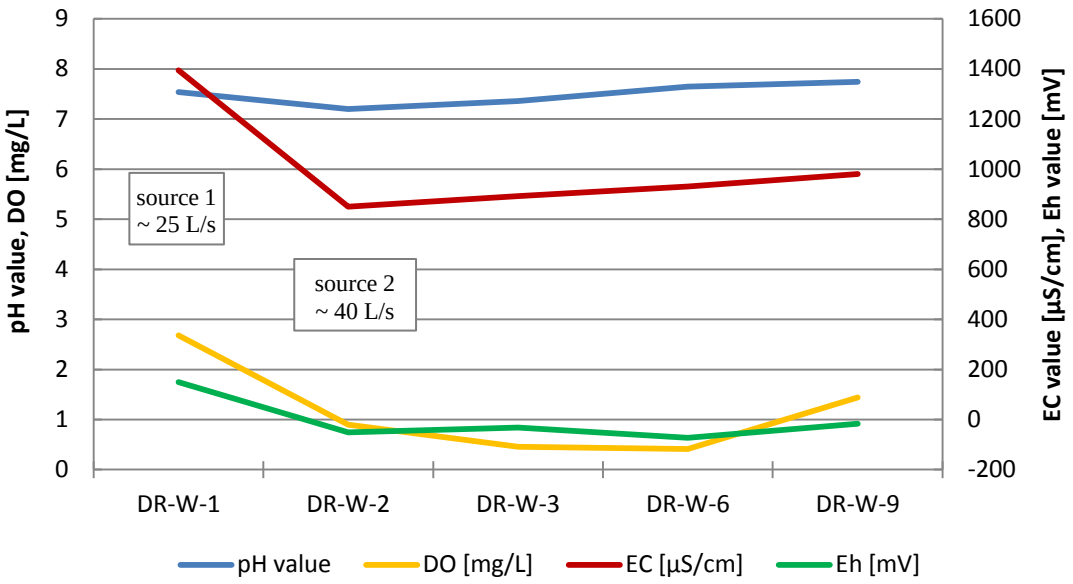

Figure 25: Changes of in-situ parameters in the course of Awa Spi river (the order of sampling points on the x-axis is downstream from the left to the right)

As it is obvious in Figure 25, the water composition of Awa Spi is mainly governed by the second source (DR-W-2) at which a higher discharge of approximately 40 L/s was determined. Compared to the uppermost source (DR-W-1) that represents an outlet of Darzila cave, the second source (DR-W-2) possesses significantly lower EC values. Therewith, mean TDS values of flowing water in Darzila cave are almost twice as high as mean TDS values of Awa Spi. Based on these facts, it can be concluded that source 1 and source 2 originate from different rock formations. It is likely that the second source (DR-W-2) is also influenced by the Sagirma Qaradagh anticline that is located to the east of the investigation area (also see chapter 2.2).

Generally, Awa Spi is characterised by alkaline pH conditions. After an initial decrease in pH from site DR-W-1 to DR-W-2, a slight increase from 7.2 to 7.74 in the direction of flow can be observed potentially reasoned by CO_2 degassing (Table A 25).

Just like the pH value, also the EC value increases from the second source (850µS/cm) downstream to DR-W-9 (981 µS/cm). The amount of total dissolved solids increases from 616 mg/L (DR-W-2) to 711 mg/L (DR-W-9). With regard to the arid to semi-arid climate in that region, increases in TDS along the flow path are most probably reasoned by evaporation processes.

Considering the redox potential, the river is dominated by reducing conditions. As in particular the second source, DR-W-2, possesses elevated concentrations of sulphide (7.8 mg/L), it can be regarded as the main reducing agent.

The tributary of Awa Spi is characterised by a pH of 7.92. Indicative is a significantly higher electrical conductivity of 2093 µS/cm (TDS = 1517 mg/L). The influence of agriculture could be one of the reasons. Measurements of the redox potential indicate partially reducing conditions.

5.3.4. Dissolved organic carbon (DOC)

According to Sigg and Stumm (2011), common DOC values are in the range of 0.5 to 1.5 mg/L with regard to normal groundwater. However, as it is depicted in Figure 26 particularly high concentrations were measured at site DC-W-4 (14 mg/L) and DC-W-6 (20 mg/L).

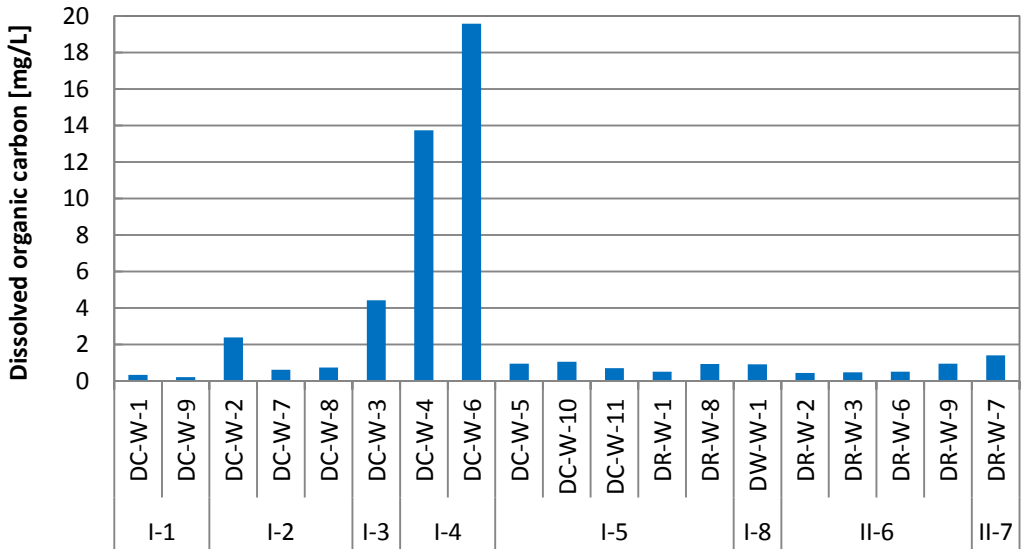

Figure 26: Contents of dissolved organic carbon (DOC)

Due to the arid to semiarid climate, vegetation and fertile soils are generally absent in the investigation area (also see chapter 2.4) and cannot be the source of organic matter. Beyond that, elevated DOC contents in water can be attributed to the release of organic substances originating from sedimentary organic carbon (Artinger et al. 2000). Indeed, Palmer (2007) mentions that petroleum is the most common deep subsurface source of carbon. Chilingar et al. (2005) also denominate the presence of organic components as the most typical feature of oilfield waters. Thus, a potential influence of hydrocarbon associated solutions from deep oil-bearing reservoirs on the water chemistry in particular at site DC-W-4 and DC-W-6 can be assumed.

Furthermore, organic matter acts as a substrate for microbial catabolism and as electron donor for anaerobic respiration (Reineke, Schlömann 2007). Hence, it also

exerts an important control on microbial enhanced redox processes in groundwater systems. Due to high DOC values and the presence of biofilms it can be concluded that there is an enhanced microbiological activity at site DC-W-2, DC-W-3, DC-W-4 and DC-W-6. A detailed analysis of microbiological activities within Darzila cave will be given elsewhere.

The contribution of active biomass to elevated DOC values can be ruled out, since 0.2 µm filters were used and most microorganisms are larger than 0.2 µm (Reineke, Schlömann 2007).

5.3.5. Main anions and cations

Anions and cations in water were mainly analysed by IC. Supplementary, results of on-site photometry will be also considered. Concentrations HCO_3^- and Fe^{2+} were determined by PhreeqC modelling on the basis of TIC and ICP-MS results.

5.3.5.1. Darzila cave

Average concentrations and ranges of the major anions and cations are displayed in Figure 27. Because the sample DC-W-4 and DC-W-6 indicate exceptionally high concentration levels compared to the other sampling sites, concentrations at these sites are represented separately in Figure 28.

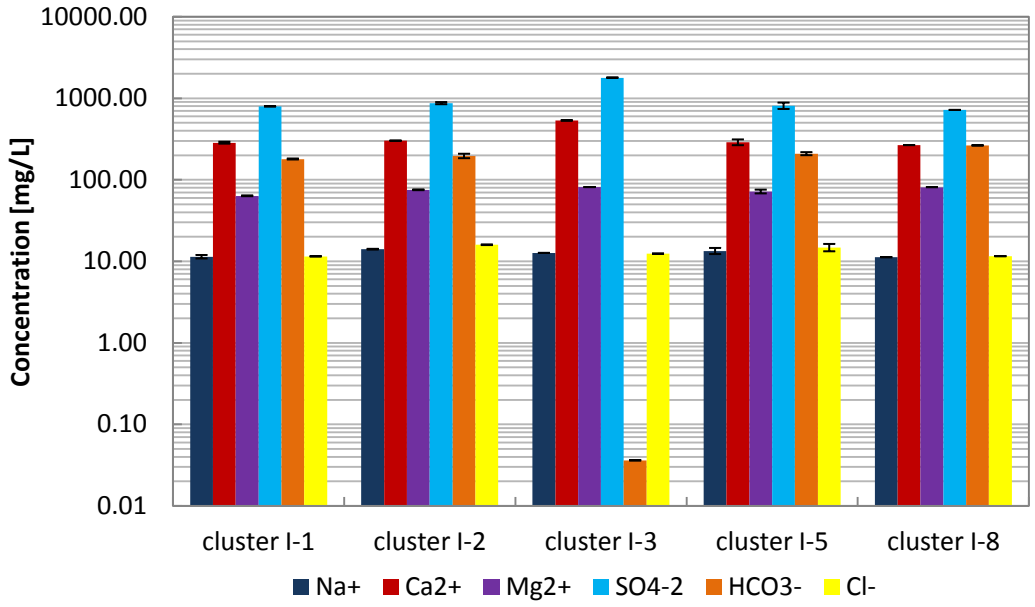

Figure 27: Main cations and anions of group I according to clusters

By far the highest concentrations were measured for sulphate. With regard to flowing water bodies within Darzila cave, concentrations range between 627 mg/L (DR-W-1) and 889 mg/L of SO_4^{2-} (DC-W-2). Other predominant ions are Ca^{2+}, HCO_3^- and Mg^{2+} ions.

Considerably high sulphate concentrations exhibit the acidic sampling sites DC-W-4 and DC-W-6. Sulphate contents range from 4840 to 13210 mg/L (Figure 28). Beyond that, these sites are predominated by Ca^{2+} ions. Moreover, high concentrations of Mg^{2+}, but also appreciable concentrations of Na^+, K^+, Fe^{2+}, Cl^- and $NH4^+$ were detected. In addition, also noteworthy contents of Al were determined at these sites (DC-W-4: 40.01 mg/L; DC-W-6: 32.61 mg/L).

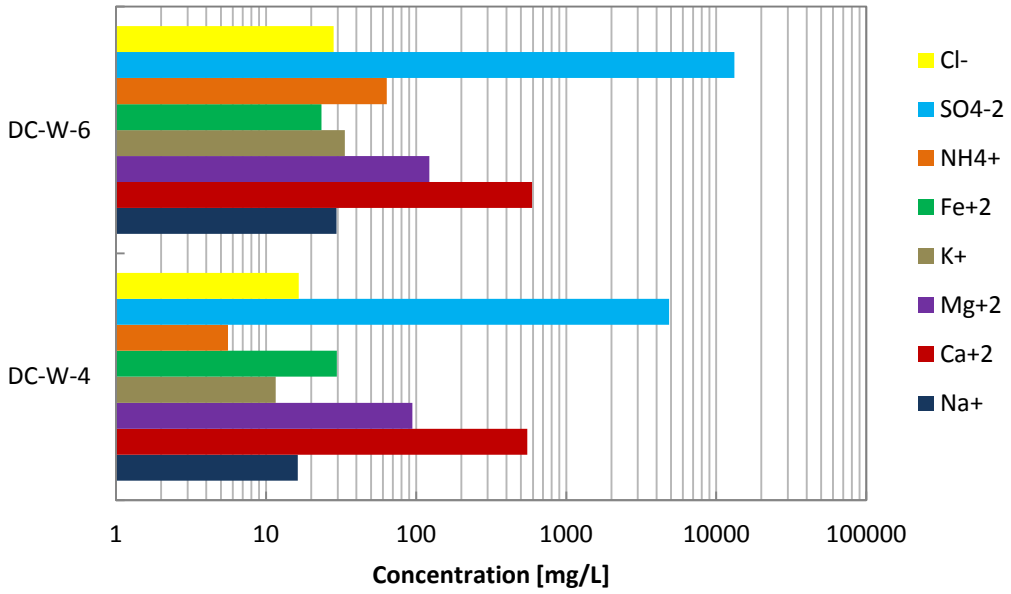

Figure 28: Main cations and anions of the samples DC-W-4, DC-W-6 (note: only 5% of the SO_4^{2-} concentrations and 50% of Ca^{2+} concentrations are represented)

Considering a water type criterion of 20% the cave water can be generally described as Ca-Mg-SO_4-type. With regard to the acidic and isolated water pools, a tendency to the Ca-(Mg)-SO_4-type can be observed (Table A 28). Although the cave waters show high concentrations of HCO_3^-, their percentage is low compared to the overall predominant SO_4^{2-}. Only the sampling site DR-W-1 (cluster I-5) indicates an increased percentage of HCO_3^- and can be named as Ca-Mg-(HCO_3)-SO_4-type. DR-W-1, which is a subterranean feeder of Awa Spi river, represents an intermediate state between the cave water (Ca-Mg-SO_4-type) and the river water (Ca-Mg-HCO_3-SO_4-type) influenced by both the cave atmosphere and the fresh air.

5.3.5.2. Awa Spi river and tributary

The water composition of Awa Spi is mainly determined by the second source (DC-W-2) that do not show any hydraulic connection to the cave water by underground passages. As the content of SO_4^{2-} ions is significantly lowered at site DC-W-2 while the concentration of HCO_3^- differs only slightly compared to the cave water, the percentage of HCO_3^- is increased in Awa Spi water. Therefore, the water of Awa Spi can be described as Ca-Mg-HCO_3-SO_4-type (Table A 28). It seems that the groundwater that emerges to Awa Spi at the sampling site DC-W-2 is less influenced by gypsum-bearing layers resulting in decreased contents of SO_4^{2-} and Ca^{2+}.
In the course of the river, slight increases in Na^+, Ca^{2+}, Mg^{2+}, Cl^- and SO_4^{2-} ions from the sampling site DR-W-2 to DR-W-9 can be observed as it was already apparent by an increase in EC values. Evaporation processes can be regarded as the major reason of concentration increases.

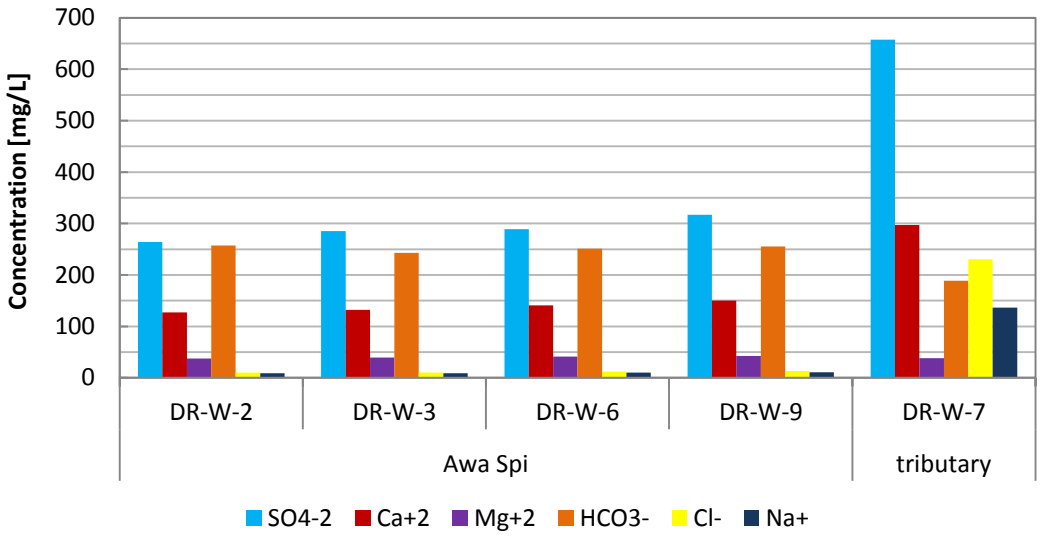

Figure 29: Main cations and anions of water samples of Awa Spi river and tributary

The tributary indicates significantly higher concentrations of Na^+ and Cl^- and can therefore be described as Ca-Na-Cl-SO_4-type (water type criterion: > 20%). Elevated concentrations of Na^+ and Cl^- are probably reasoned by an additional influence of halite-bearing layers. Moreover, the tributary indicates significantly higher concentrations of SO_4^{2-} compared to Awa Spi. Thus, intensive interactions with gypsum-bearing layers such as the Lower Fars Formation or also the Sagirma Formation in its catchment area can be considered as the main agent of increased SO_4^{2-} contents.

5.3.6. Elemental ratios

In order to identify water-rock-interactions such as ion exchanges and other processes that influence the hydrogeochemistry at different sampling points, the individual water constituents must be evaluated by reference to a solute that is practically nonreactive. Major characteristic of a solute that behaves conservatively is that its concentration in a solution increases directly with increasing TDS value. Langmuir (1997) mentions that the best common species is probably Cl^-. But, according to Spearman correlation analysis, Li seems to be most suitable since it exhibits the highest correlation with EC values (correlation coefficient = 0.905) (Appendix C). However, Cl^- with a correlation coefficient of 0.825 might be suitable as well. According to XRF analysis of rocks the concentration of Cl^- is consistently low (Table A 13). As incorporations of Cl^- ions in e.g. clay minerals can be regarded as negligible, Cl^- will be used in the following as a relative constant.

Results are represented in Figure 30. Only sampling sites summarised to group I will be considered in the following section.

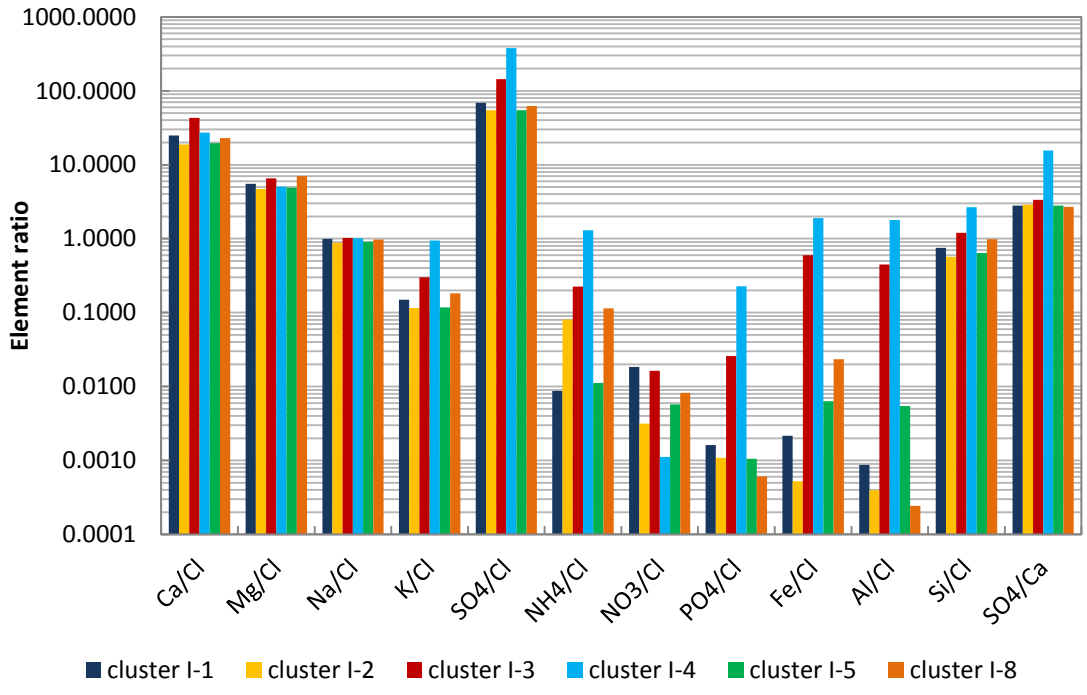

Figure 30: Selected elemental ratios of water samples of group I

Si, Al, Fe and K^+ are common elements that are incorporated in clay minerals. As the ratios Si/Cl^-, Al/Cl^-, Fe/Cl^- and K^+/Cl^- are throughout increased with regard to the acidic samples (cluster I-3, I-4), ion exchange with clay minerals as well as the

destruction of clay minerals at pH values below 3 to 4 (Langmuir 1997) are the most likely factors that contribute to enhanced concentrations of the previously mentioned ions at these sites.

Furthermore, the acidic samples show remarkably high relative concentrations of SO_4^{2-} ions. In contrast, relative concentrations of Ca^{2+}, Mg^{2+} and Na^{+} are almost constant over the wide range of salinity in Darzila cave. In addition, an increase in SO_4^{2-} concentrations relative to Ca^{2+} concentrations at site DC-W-4 and DC-W-6 is also highlighted by the calculated ratio r(SO_4^{2-}/Ca^{2+}). Since dissolution of gypsum result in an increase of both Ca^{2+} and SO_4^{2-} in water, it is most likely that there is an additional input of sulphate at site DC-W-4 and DC-W-6 (cluster I-4). With regard to Darzila cave, two sources of SO_4^{2-} are assumed: firstly, dissolution of gypsum from Lower Fars Formations and secondly, ascent of H_2S from hydrocarbon-bearing layers. Therewith, it can be assumed that there is an additional input of S deriving from hydrocarbon-bearing layers. A slightly increased relative concentration of SO_4^{2-} was also found at the sampling point DC-W-3 (cluster I-3). However, the relative Ca^{2+} content increases as well indicating an elevated dissolution of gypsum caused by a lowered pH value at this site.

Relative declines in NO_3^{-} contents, which are unlikely to react inorganically, probably reflect the biological uptake of it as nutrient (Langmuir 1997). Based on this, an increased biological activity can be assumed with regard to the strongly acidic sites (cluster I-4). Highest measured DOC values strengthen this assumption. Slightly decreased ratios were also determined at the main inlet of the cave (cluster I-2). The biological activity of the small creek southwards the entrance can be stated as low because of a high NO_3^{-}/Cl^{-} ratio accompanied with low contents of dissolved organic carbon (DOC) (also see chapter 5.3.4). Moreover, enhanced relative values of PO_4 and NH_4^{+} also come along with increased DOC values measured at the acidic pools.

Absolute increases in species, which are generally unlikely to derive from rock weathering such as Cl^{-}, NO_3^{-} and Na^{+}, probably result from their concentration by evaporation (Langmuir 1997). Significant enhanced values of Cl^{-} and Na^{+} could be detected at site DC-W-6 (Table A 8). Hence, concentration of water constituents by evaporation also has to be taken in mind with regard to isolated pools of water. Therewith, different concentration levels between DC-W-6 and DC-W-4 may be

explained. In contrast, measureable amounts of NO_3^- could not be found at this site, which may result from biological uptake of NO_3^-.

In summary, distinct differences could be found with regard to acidic pools compared to neutral to slightly alkaline waters in Darzila cave. Indeed, elevated absolute and relative concentrations of ions attribute to a sum of different factors. It needs to be considered that the solubility and mobility of many species is greatly increased under acidic conditions. Beyond that, also evaporation processes may contribute to elevated salinities in the acidic pools. However, conspicuous characteristics of the acidic pools are increased SO_4^{2-} concentrations relative to Ca^{2+} as well as elevated contents of elements commonly incorporated in clay minerals. Differences between water samples from Darzila cave are generally low with respect to concentrations relative to Cl^-. However, noticeable deviations were found between the small creek in the southern part of the cave (cluster I-1) and the main inlet on the other side of the entrance in the northern part of the cave (cluster I-2). Moreover, it is evident that the main cave discharge represented by cluster I-5 is mainly dominated by the water chemistry of cluster I-2.

5.3.7. Distribution of species

As the S-O-H system appears to be predominant in initiation and enlargement of nonconventional karst systems, a detailed representation of the distribution of sulphur species will be given in the following chapter. Moreover, also the distribution of carbon species will be represented.
Species distribution was modelled by means of the program PhreeqC for Windows under consideration of prevailing pH and E_H conditions. Results will be summarised according to the results of cluster analysis.

5.3.7.1. Sulphur species

Sulphate and sulphide as well as metastable sulphur species, such as thiosulfates, polythionates and sulphites, were determined by ion chromatography and photometry. An overview of the concentrations of analysed sulphur species is given in Table 12.

Table 12: Concentrations of analysed dissolved sulphur species

Cluster ID	Sample ID	SO_4^{2-}	$HS^-/H_2S/S^{2-}$	SO_3^{2-}	$S_2O_3^{2-}$	$S_nO_6^{2-}$
		mg/L	mg/L	mg/L	mg/L	mg/L
I-1	DC-W-1	797	0.06	0.01	0.02	0.06
	DC-W-9	790	<0.01	0.01	0.01	0.00
I-2	DC-W-2	889	0.12	0.01	0.14	0.10
	DC-W-7	828	0.07	0.01	0.05	0.07
	DC-W-8	888	0.11	0.00	0.07	0.09
I-3	DC-W-3	1783	3.36	0.00	0.16	0.15
I-4	DC-W-4	4840	3.92	0.01	0.07	n.d.
	DC-W-6	13210	0.05	0.06	0.06	0.02
I-5	DC-W-5	863	6.32	0.01	1.17	0.85
	DC-W-10	855	4.32	0.00	1.72	0.71
	DC-W-11	830	1.30	0.01	3.04	0.70
	DR-W-1	627	0.09	0.01	n.d.	n.d.
	DR-W-8	868	0.02	0.01	n.d.	n.d.
I-8	DW-W-1	717	49.92	0.40	n.d.	n.d.
II-6	DR-W-2	264	7.84	0.03	n.d.	n.d.
	DR-W-3	285	6.40	0.00	n.d.	n.d.
	DR-W-6	289	4.24	0.00	n.d.	n.d.
	DR-W-9	317	5.12	0.31	n.d.	n.d.
II-7	DR-W-7	657	<0.01	0.00	n.d.	n.d.

n.d. - not determined (not looked for)

The results reveal an overwhelming predominance of sulphate ions in water. Their percentage in relation to total dissolved sulphur species ranges between 93% and 100%. Lowest contents of sulphate in cave water possess the small creek to the south of the entrance (cluster I-1) with concentrations of 794 mg/L on average. Highest concentrations exhibit the acidic pools whereupon most remarkable amounts were measured at site DC-W-6 (13.21 g/L).

Moreover, considerable concentrations of sulphide could be measured. The highest content of sulphide were found in the sample DW-W-1 (well) with a concentration of about 50 mg/L. Within Darzila cave, highest concentrations were measured at site DC-W-5 (7.84 mg/L). Towards the rear part of the cave, contents of sulphide in water decrease down to 1.30 mg/L (DC-W-11). Losses due to degassing as H_2S and oxidation to sulphate can be regarded as the main processes that cause a decrease of sulphide contents in water.

Despite of the fact that the main inlet of the cave, DC-W-7, shows the lowest redox potential (-132 mV) and the lowest pH (6.6) of sampled flowing waters in Darzila cave only very low amounts of sulphides could be measured by photometry. In contrast, addition of ammonium Zn-acetate in order to precipitate sulphide for isotopic analysis yielded appreciable amounts of ZnS at this site (work of Seither,

A.). Therefore, it can be speculated that the photometrical determination of HS^- /H_2S/S^{2-} must be disturbed at this site and also at site DC-W-8 and DC-W-2. Potential interfering substances are generally strongly reducing ions that prevent the formation of the blue colour during photometry (Table A 2).

Sampling and stabilisation in order to determine polythionates and thiosulfates were performed at eleven sampling sites within Darzila cave. Concentrations of thiosulfates range between 0.01 mg/L and 3.04 mg/L. An increase in thiosulfates along the pathway from site DC-W-7 to DC-W-11 is obviously. Only low values were measured with regard to polythionates. Site DC-W-6 exhibited the highest contents with 0.85 mg/L.
In addition, concentrations of sulphites were determined by ion chromatography. However, the results have to be taken with caution since sulphite is a metastable species relative to sulphate and samples were not stabilised with regard to sulphites (also see chapter 4.1.1). Appreciable concentrations were only measured at site DW-W-1 (0.40 mg/L) and site DC-W-9 (0.31 mg/L).
Thiosulphates and sulphites are most abundant near groundwater redox interfaces, where they can complex with borderline or soft metal cations (Daskalakis, Helz 1992). Less common among the metastable sulphur species are the polythionates, which are themselves metastable relative to sulphite, thiosulfate, S^0 and the sulphide species (Langmuir 1997).

Along Awa Spi river, significant amounts of sulphides were measured at the main subterranean inlet of Awa Spi river, DR-W-2. At this site, exhalations of H_2S were quite strong and concentrations of 7.84 mg/L could be determined. Contents of sulphides tend to decrease in the course of the river. Moreover, Awa Spi river is characterised by overall lower sulphate concentrations compared to the cave water. However, an increase in SO_4^{2-} ions along the flow path is obvious. In this process, oxidation of H_2S to SO_4^{2-} is solely or even principally responsible.

However, analytical results have to be taken with caution. As it is obviously in Figure 31, distribution of sulphur species changes at low pH and low pe values.

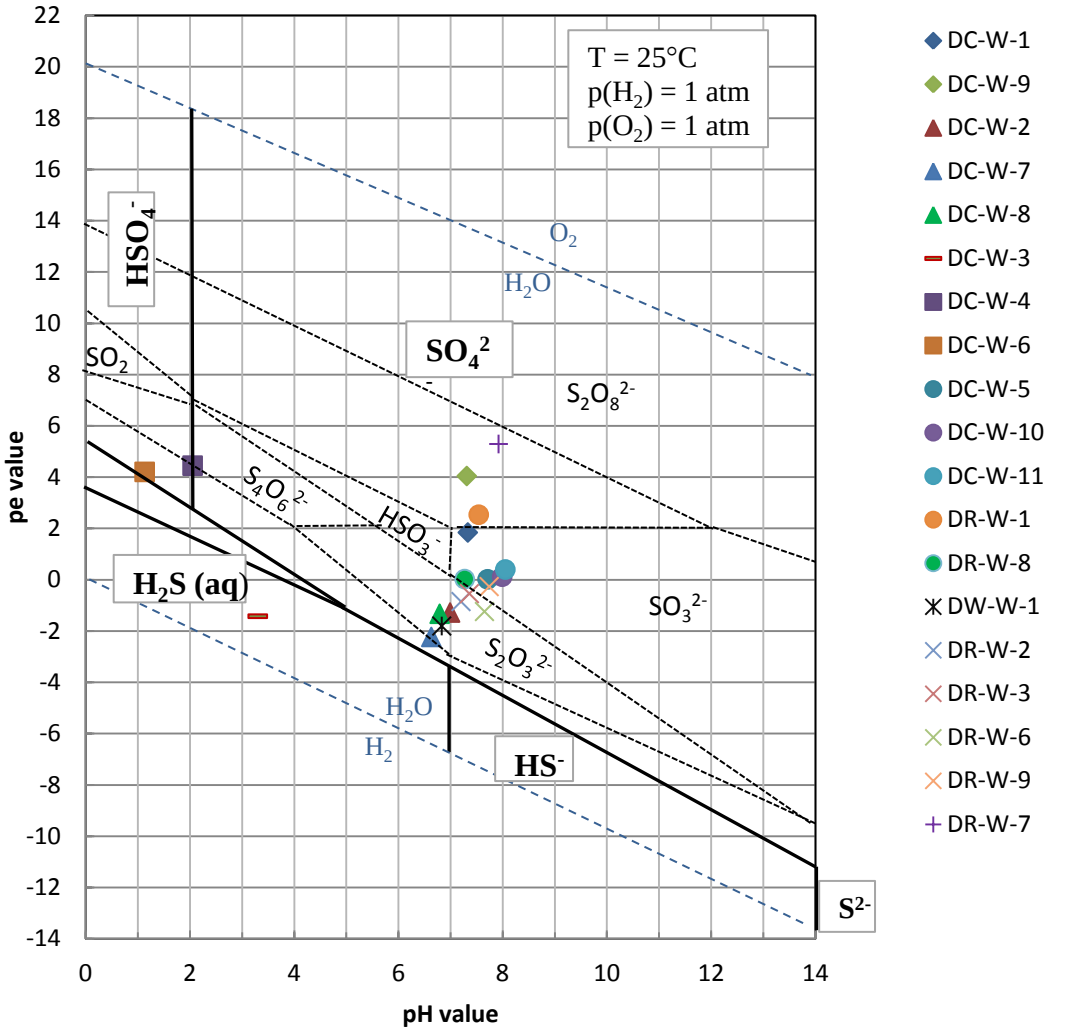

Figure 31: pe-pH diagram of thermodynamically most stable sulphur species (in bold, thick lines) and minor sulphur species (dashed lines) in the system S-O_2-H_2O at standard conditions (T = 25°C, p(O_2) = 1 atm, p(H_2) = 1atm, activity of all dissolved species = 10^{-3} mol/L = 96 mg SO_4^{2-}/L) (modified after Vitorge et al. 2007).

In order to determine the distribution of S species under consideration of prevailing pH and pe values PhreeqC modelling was applied. Additionally, complexation is regarded. In Figure 32, only the most prevalent sulphur species will be presented. A complementary list of S species of concentrations >1 mg/L is given in Table A 24.

Considering flowing waters, sulphur is prevalently present in its highest oxidation state +6. The overall predominant species is the free anion sulphate with a percentage of 67% on average. Additionally, sulphate forms stable complexes with the predominant cations Ca^{2+} and Mg^{2+}. As concentrations of free Ca^{2+} ions are higher compared to those of Mg^{2+} ions $CaSO_4^0$ complexes are predominant (23% on average). The percentage of $MgSO_4^0$ complexes amounts to 12% on average in flowing waters (Figure 32).

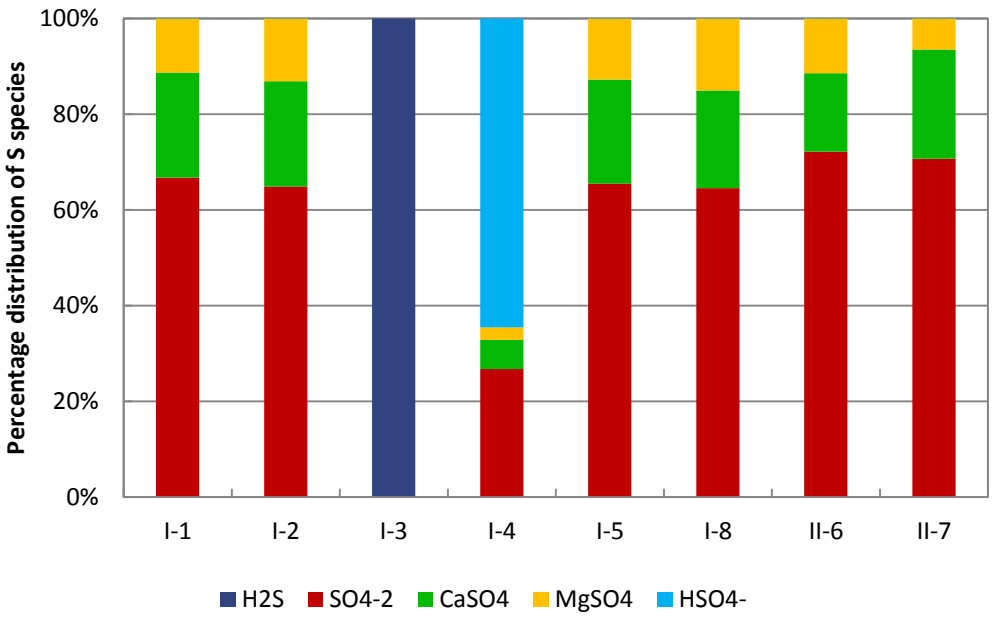

Figure 32: Distribution of sulphur species according to clusters

Since sulphur is a redox- and pH-sensitive element the distribution of S species is changed with regard to strongly acidic pools represented by cluster I-3 and I-4. The water at the sampling sites DC-W-4 and DC-W-6 (cluster I-4) are predominated by HSO_4^- (65%) whereas the percentage of sulphate decreases to 27%. Low pH values in combination with a decreased redox potential cause an overall predominance of H_2S at site DC-W-3 (cluster I-3) (Figure 32, also see Figure 31).

In contrary to analytical results, PhreeqC modelling does not provide any appreciable concentrations of sulphide species in flowing waters. It needs to be considered that modelling the distribution of species with PhreeqC is commonly based on equilibrium thermodynamics (Merkel et al. 2005). Equilibrium models describe boundary conditions defined by assuming attainment of equilibrium (Langmuir 1997). However, the establishment of equilibrium is generally slow in natural waters (Matthess 1994). In particular, the sulphate/sulphide couple is often far from equilibrium (Schüring et al. 2000). Therewith, diverging results between modelling and analytical findings of S species can be explained. However, it needs to be taken in mind that sulphide concentrations determined by photometry are often interference-prone.

5.3.7.2. Species of inorganic carbon

The distribution of inorganic carbon species was calculated on the basis of TIC values determined with the LiquiTOC element analyser. A summary of results is given in Table A 25. In the following, only the most prevalent C species will be considered.

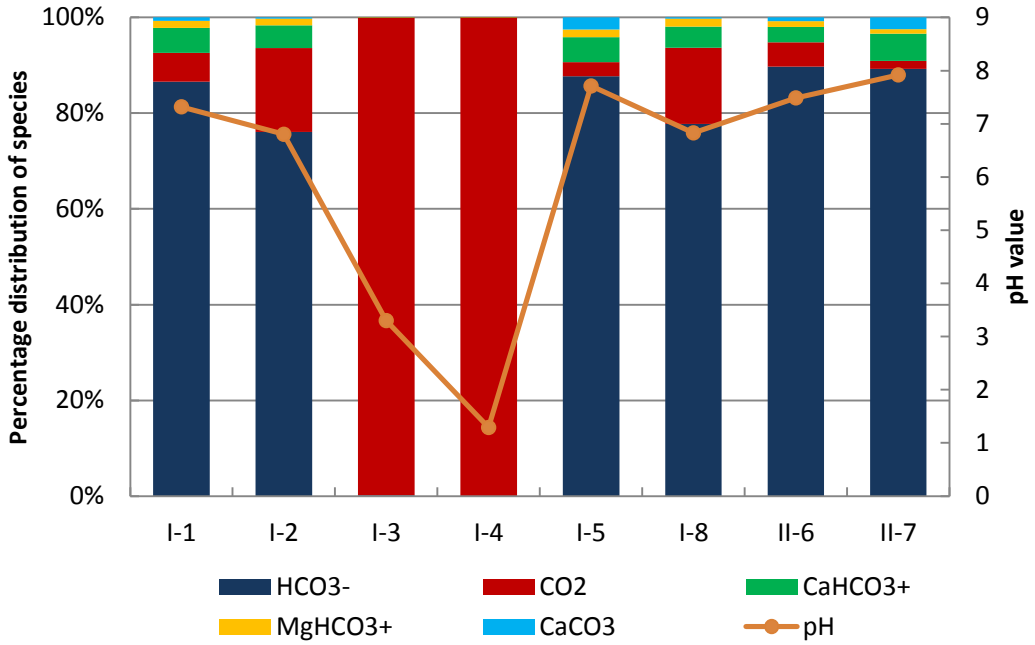

Figure 33: Distribution of C species according to clusters modelled with PhreeqC for Windows based on results from measurements of total inorganic carbon (TIC) with the LiquiTOC element analyser

The distribution of carbon species is strongly influenced by pH conditions (Figure 33). As the sampling sites represented by cluster I-3 and I-4 are characterised by low pH values, the total inorganic carbon is mainly present in form of CO_2. Since CO_2 easily degasses to the atmosphere, total amounts of inorganic carbon are by far the lowest at these sites (Table A 3). Under almost neutral conditions, HCO_3^- is the overall predominant specie. Complexes are formed with Ca^{2+} and Mg^{2+} ions.

5.3.8. Major, minor and trace elements

Altogether 55 elements were measured by ICP-MS. A complete overview of measured concentrations, modes of measurement and detection limits is given in Table A 10 to Table A 12. To provide a better overview of results, all elements were classified into major, minor and trace elements as it is shown in Table 13. Considered are the mean concentrations of elements of all 19 samples.

Concentrations below the detection limit were previously replaced by 0.3*detection limit (see section 5.3.1.1).

Table 13: Classification of elements measured by ICP-MS considering mean element concentrations

Classification	Criterion	Elements measured by ICP-MS
Major elements	> 5 mg/L	K, Mg, Si
	> 100 mg/L	Ca, S
Minor elements	0.1 – 5 mg/L	Al, Fe, P, Sr,
Trace elements	< 0.1 mg/L	B, Ba, Br, Ce, Co, Cr, I, In, La, Li, Mn, Mo, Nd, Ni, Rb, U, V, Y, Zn
	< 0.001 mg/L	Ag, As, Be, Bi, Cd, Cs, Cu, Dy, Er, Eu, Ga, Gd, Ho, Lu, Pb, Pr, Sb, Sc, Se, Sm, Sn, Tb, Te, Th, Tl, Tm, Yb,

Overall predominant elements are Ca and S, but also K, Mg, Si. Moreover, Al, Fe, P and Sr also indicate significant amounts.

Rather extraordinary are Sr contents of 4.22 mg/L on average. According to Matthess (1994) contents of Sr are generally low and amount to about 0.01-1.0 mg/L with regard to most groundwaters. In limestone bedrocks, the ratio of Sr/Ca*1000 is commonly about 1.5. However, flowing waters within the cave indicate ratios of 16.19 on average which is very close to ratios determined in granites containing 0.1-1.0% Ca (Matthess 1994). But granite does not occur in the surrounding geological formations (see chapter 2.2). Apparently, there must be another source of elevated Sr concentrations. According to Satyanarayana (2011) and Chilingar et al. (2005), Sr constitutes a supplementary indicator of oilfield waters. However, since flowing waters in Darzila cave obviously do not indicate any other common characteristics of oilfield waters, clear statements cannot be done.

However, in the previous sections, common characteristics of hydrocarbon-associated solutions could already be pointed out at the sampling points DC-W-4 and DC-W-6, e.g.:

- High concentrations of total dissolved solids (TDS)
- High concentrations of dissolved organic carbon (DOC)
- Particularly high relative concentrations of SO_4^{2-}

In order to substantiate a potential influence of oil-bearing layers on the water composition of the samples DC-W-4 and DC-W-6, a more detailed investigation of the hydrochemistry with regard to water constituents commonly associated with

hydrocarbons will be given in the following section (also see Table 3 in chapter 3.3). Chilingar (2005) and Satyanarayana (2011) mention a variety of elements that are commonly present in oilfield waters (Table 3). However, only trace elements will be considered herein. To illustrate enrichments of indicative elements at the sampling sites DC-W-4 and DC-W-6 also the concentrations at the sampling point DC-W-7 will be displayed as a reference value. Concentration levels are represented in Figure 33.

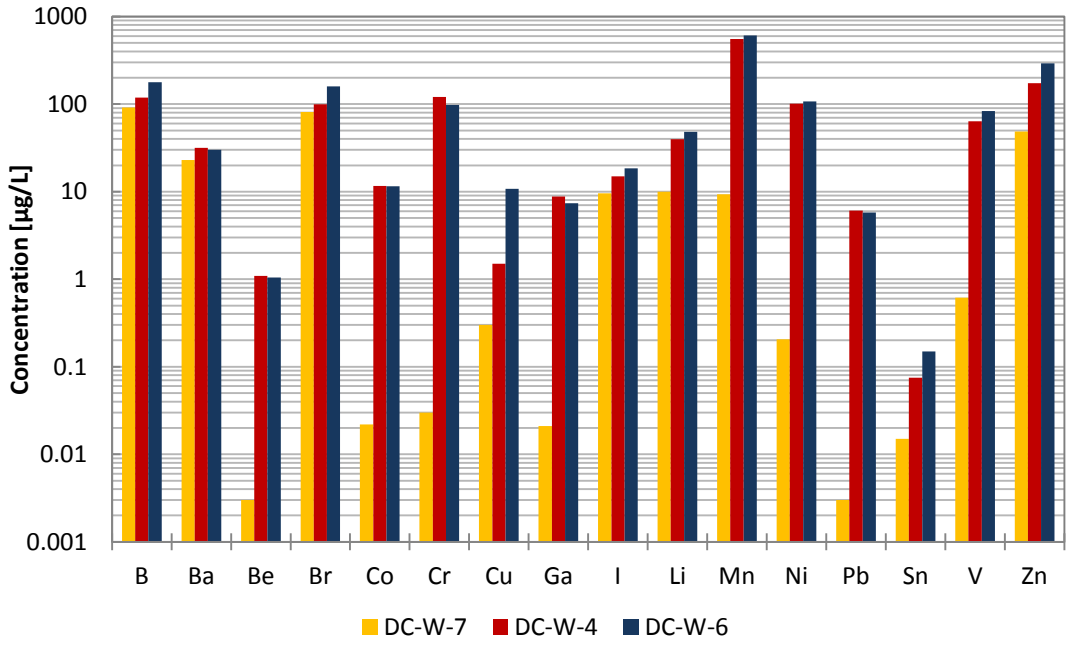

Figure 34: Concentration levels of trace elements commonly enriched in groundwaters of oil-bearing layers

In comparison to the sample DC-W-7, DC-W-4 and DC-W-6 possess partially strong enrichments with respect to certain elements, such as Be, Co, Cr, Ga, Mn, Ni, Pb and V. However, according to Chilingar et al. (2005) and Satyanarayana (2011) in particular I and Br are strong indicators for the presence of oil. But, only slight enrichments could be found with regard to these elements. Though, it has to be considered that the measurement of I by ICP-MS is problematic due to the high volatility of this element (Oliveira et al. 2010). Since no special approach for I measurement was performed the obtained concentrations are probably not reliable.

Although elevated concentrations of selected elements commonly present in oilfield waters could be shown, further investigations are required due to the complexity of oilfield waters. For instance, the presence of naphthenic acids would be a strong argument (Chilingar et al. 2005). Additionally, isotopic analysis carried out but not

shown in here may provide more clear results about the potential influence of hydrocarbon-bearing layers allocated in the vicinity of the cave.

5.3.9. Precipitation and dissolution processes

5.3.9.1. Saturation indices

Figure 35 shows the mean saturation indices of selected mineral phases averaged according to the results of the cluster analysis. Since the acidic samples DC-W-3, DC-W-4 and DC-W-6 differ strongly compared to the rest of sampling points, these sites will be discussed separately in chapter 5.3.10. A complete list of calculated saturation indices is given in Table A 22 and Table A 23.

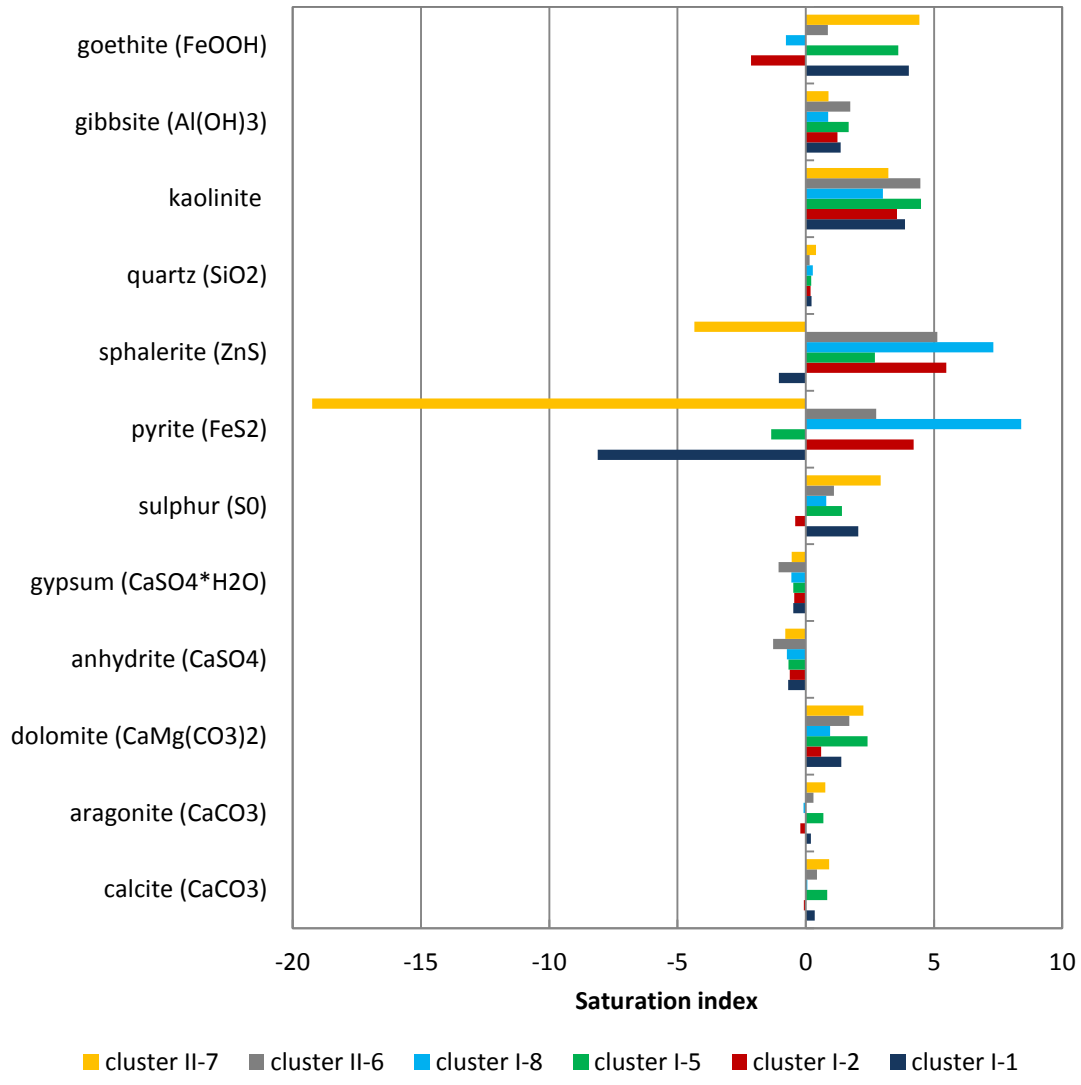

Figure 35: Mean saturation indices of selected mineral phases calculated with PhreeqC and summarised according to clusters

Generally, there are only minor differences between the sampling sites in the number of under- and supersaturated solutions with regard to the given minerals. However, the sites DC-W-7 and DC-W-8 (cluster I-2) are characterised by a slight undersaturation in relation to calcite and aragonite. Common characteristics of dissolution of the limestone bedrock close to these sampling sites could be found in-situ (Figure 36, right). Palmer (2007) mentions that the dissolution rate is greatest at or near the water table because oxygen is most abundant in the open air, e.g. in the cave atmosphere. Due to this fact, most cave rooms are widest at the present or former levels of the cave water (Palmer 2007). This was also observed in most parts of Darzila cave. Close to the sampling sites of cluster I-2 to the north of the entrance, the cave walls showed the highest dissolution (implied in Figure 9). But also walls at former water levels of the small creek in the northern part of the cave were in parts deeply dissolved (DC-W-1, DC-W-9).

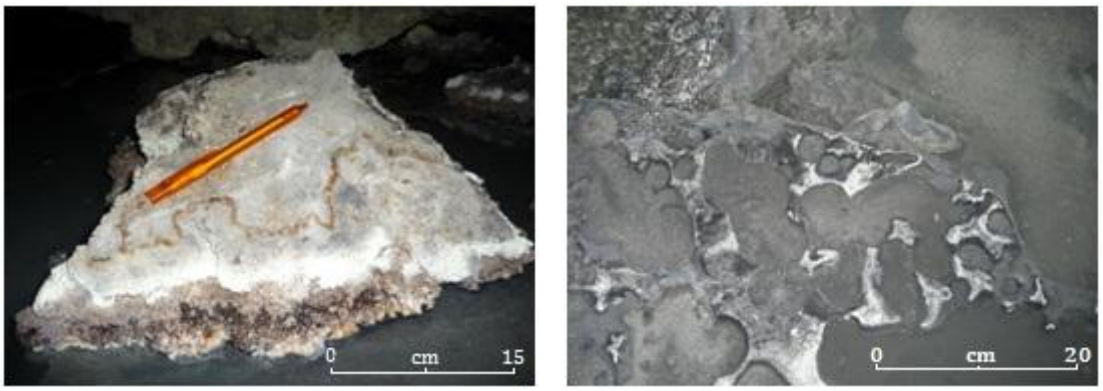

Figure 36: (Left) Precipitations of carbonates and iron bearing minerals close to DC-W-5, DC-W-10 (cluster I-5). (Right) Dissolution of calcite close to DC-W-7 and DC-W-8 (cluster I-2)

In contrast, water samples that were taken in the rear part of the cave are characterised by a supersaturation with respect to carbonates. Precipitations of carbonates were found in-situ, for instance close to site DC-W-5 (Figure 36, left). According to Matthess (1994) precipitation and dissolution of carbonates are, amongst others, influenced by kinetic effects in relation to the release of CO_2. If CO_2 degasses into the atmosphere the capacity for dissolution of limestone is decreased even in presence of sulphuric acid (Figure B 2) (Palmer 1991).

Comparing the distribution of C species and the amount of total inorganic carbon between the main cave spring (DC-W-7) and the main discharge in the cave (towards DC-W-11) it can be seen that water that rises at site DR-W-7 is subject to CO_2 degassing in contact with the cave atmosphere resulting in a decrease of total

inorganic carbon in water (Figure 37). Hence, changes in the saturation indices of carbonates are most likely a result of CO_2 degassing along the flow path. Moreover, the aggressiveness of the water also decreases as H_2S becomes more dilute and degasses in the direction of flow. Thus, generation of sulphuric acids diminishes (Palmer 2007).

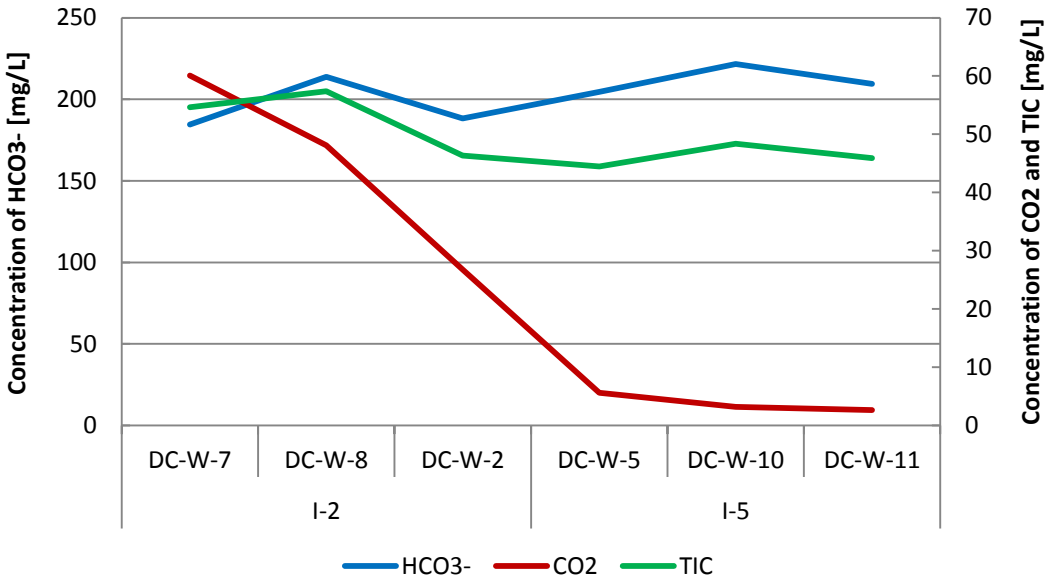

Figure 37: Changes in the distribution of C species and in the total amount of inorganic carbon from the main cave spring (DC-W-7) downstream towards the main discharge in the cave (DC-W-11)

Furthermore, all investigated flowing waters are undersaturated with regard to the sulphate minerals gypsum and anhydrite. Since the solubility product of gypsum is high it dissolves easily and precipitations of gypsum are generally rare in contact to water (Matthess 1994). However, considering changes in SO_4^{2-} contents along the flow path from the sampling site DC-W-8 to DC-W-11 there is an obvious decrease from 888 mg/L to 830 mg/L while Ca^{2+} contents are almost constant (about 300 mg/L) (Table A 8). Thus, it seems that the solubility of gypsum decreases with increasing pH resulting in precipitation of gypsum even though it is not reflected by the calculated saturation indices. In result of gypsum precipitation SO_4^{2-} concentrations decreases. Because of dissolution of the adjacent limestone bedrock the concentration of Ca^{2+} remains almost constant.

While water samples are throughout undersaturated with respect to sulphate minerals, most of the samples are supersaturated with regard to sulphide minerals, e.g. pyrite and sphalerite, and sulphur. The milky colour of most of the investigated

waters in Darzila cave and Awa Spi river potentially results from suspended elemental sulphur. Similar phenomena are also mentioned by Hose et al. (2000). According to Langmuir (1997) incomplete oxidation of H_2S at total sulphur concentrations exceeding the solubility of sulphur (~$5*10^{-5}$ mol/L) may lead to the precipitation of colloidal elemental sulphur. Analysed water samples exhibit total sulphur concentrations in the range of $2.86*10^{-3}$ to $1.41*10^{-1}$ mol/L. Exceptionally the main cave inlet (DC-W-7) is composed of clear water indicating a saturation index of -1.95 with regard to elemental sulphur.

Beyond that, the investigated waters are prevalently supersaturated with regard to iron-bearing minerals such as goethite, hematite and magnetite. Exceptions are the sampling sites which are summarised to cluster I-2. These ones are characterised by a strong undersaturation with respect to iron-bearing minerals. However, precipitations of iron-bearing minerals in other parts of the cave can be confirmed by observations (brownish line in Figure 36, left).

Moreover, all investigated waters are supersaturated with regard to clay minerals, e.g. kaolinite, illite, montmorillonite-Ca. Clay minerals occurred at various sites in Darzila cave. However, a detailed investigation of their mineralogical composition was not carried out.

5.3.9.2. Precipitations on cave ceilings and walls due to degassing

Much of the cave enlargement of sulphuric acid caves takes place above the water table (Palmer, Hill 2012). Thereby, gypsum is the most abundant by-product of H_2S/H_2SO_4 speleogenesis (Provencio et al. 1998). Buck et al. (1994) described the origin and petrology of five types of gypsum in Guadalupe caves: subaerial gypsum crust that has replaced bedrock by sulphuric acid reaction, subaqueous gypsum crust of the same origin, subaqueous gypsum sediment, breccias of fallen gypsum blocks, evaporitic gypsum. In Darzila cave, subaerial gypsum formed by replacement reactions is predominant. The ceilings are smooth and arched which is a typical characteristic of gypsum replacement (Palmer, Palmer 2000) (also see Figure 8). According to Palmer and Palmer (2004) replacement gypsum is only poorly bonded to the host rock since gypsum occupies in a larger molar volume compared to carbonate. Hence, fragments of gypsum easily fall to the cave floor. In Darzila cave, large and smaller gypsum blocks are widely distributed on the cave floor. Thereby,

the frequency of occurrence increases towards the rear part of the cave. As flowing waters in Darzila cave are throughout undersaturated with regard to gypsum, blocks of gypsum can be dissolved easily. Subsequently, it can be carried away in solution by the main cave stream. This process seems to be the main contributor to the cave enlargement in Darzila cave.

An overwhelming presence of gypsum crystals was found in a small part of the cave located to the southwest of the entrance containing the sampling site DC-W-9 (Figure 38, right). Fresh-air supply is distinctive for this part of the cave. Because of the additional fresh-air supply H_2S oxidises completely to SO_4^{2-}. Therefore, the formation of elemental sulphur as an intermediate product of incomplete oxidation of hydrogen sulphide on the gypsum crust is prevented. Thus, gypsum can crystallise. Beyond that, crystal growth is probably slowed down due to low H_2S contents in water (Table 12). These facts may attribute to the formation of larger gypsum crystals compared to other parts in Darzila cave.

Figure 38: (Left) Elemental sulphur at the cave ceiling above the acidic sampling sites. (Right) Crystalline gypsum at the cave ceiling at site DC-W-9

The formation of speleogenetic gypsum at the cave ceilings is attributable to degassing of H_2S from the water, which is thereupon absorbed, along with oxygen from the cave air, by water films and droplets on the cave walls. Subsequently, H_2S reacts to sulphuric acid dissolving the limestone bedrock. Speleogenetic gypsum is formed according to equation 4 (Figure 38, right). Moreover, incomplete dissolution of hydrogen sulphide can produce sulphur according to the following equation (Palmer 2007):

$$2H_2S + O_2 \rightarrow 2S^0 + 2H_2O \qquad [16]$$

Since sulphur is most stable in acidic environments (Palmer 2007), remarkably thick crusts of elemental sulphur were in particular found at the cave ceilings in the vicinity of site DC-W-3, DC-W-4 and DC-W-6 (Figure 38, left).

Palmer and Hill (2012) also mentions that sulphur tends to concentrate on non-carbonate materials, such as gypsum, because condensed water of low pH value would be easily neutralised by limestone (also compare chapter 3.2). Hence, crusts of elemental sulphur are built up on gypsum incrustations in Darzila cave and were also found in other parts of the cave.

5.3.9.3. Precipitations on water surfaces

At different sites in Darzila cave white precipitations on water surfaces could be observed where temporary stagnant water bodies are formed (Figure 39). Samples were taken at two sites namely DC-P-2 and DC-P-16 according to their location (see Figure 9).

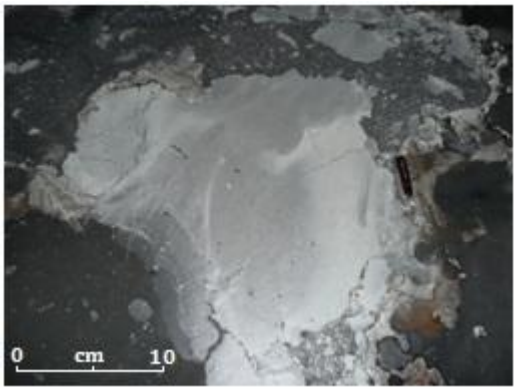

Figure 39: Precipitation on water surfaces

In order to investigate the mineralogical and chemical composition of these white precipitations ICP-MS and XRD measurements were carried out. Anions were determined by means of IC. With regard to the instability of compounds, e.g. gypsum, and the small sample size only qualitative XRD analysis could be conducted. Results are given in Table 14.

Table 14: Mineralogical composition of precipitations in water surfaces according to results of qualitative XRD measurements

Sample ID	Organoleptic parameter	Mineralogical composition
DC-P-2	Light brown, odour of organics	$S^0 + CaSO_4{}^0 * 2H_2O + SiO_2$
DC-P-16	Yellow-green, odour of organics	$S^0 + CaSO_4{}^0 * 2H_2O + CaCO_3{}^0$

As it can be seen in Table 14, precipitations are mainly composed of elemental sulphur (S^0), gypsum ($CaSO_4{}^0*H_2O$) and quartz (SiO_2) respectively calcite ($CaCO_3{}^0$). These findings can be compared to calculated saturation indices. Waters in Darzila cave are generally oversaturated with regard to the minerals sulphur, quartz and calcite (see chapter 5.3.9). Thus, precipitation of these minerals is likely. However, the analysed precipitations also consist of gypsum whereas saturation indices indicate an overall undersaturation with respect to this mineral. Since precipitations typically only occur on stagnant water bodies concentration of water constituents at these sites is favoured. According to Matthess (1994) the solubility product of $CaCO_3{}^0$ is $3.31*10^{-9}$ and that of $CaSO_4{}^0*H_2O$ is $2.31*10^{-5}$ (at 25°C). Therewith, calcite precipitates first since its solubility product is very low. On contrary, the solubility of gypsum in water is high and the precipitation of gypsum in contact with water is generally rare. However, the production of sulphuric acid in contact with the atmosphere enhances the dissolution of the calcite bedrock and more Ca^{2+} is provided. These additional constituents may drive gypsum to supersaturation if the influx of fresh water is low (Palmer, Palmer 2000). Evaporation, as it is likely with regard to the stagnant, small water bodies in Darzila cave, would boost this process (Palmer 2007). Thus, also the solubility product of gypsum might be exceeded and small amounts of gypsum can precipitate.

Because of small sample sizes analytical correctness of ICP-MS and IC measurements cannot be ensured at all and have to be taken with caution. However, IC results and selected elements of concentrations >1 mg/g will be presented to get an idea about the chemical composition of the precipitations (Table 15).

Table 15: Selected elements in precipitations on water surfaces

mg/g	F^-	Cl^-	PO_4	$SO_4{}^{2-}$	Al	Ca	Fe	K	Mg	Na	Si
DC-P-2	2.73	0.97	0.51	92.75	0.34	154.06	0.14	0.93	1.38	1.77	1.63
DC-P-16	0.15	0.71	2.74	255.49	4.36	31.10	4.00	5.40	2.93	1.56	1.36

As it already was concluded from the mineralogical composition of the precipitations as well as from hydrochemical analysis of water samples, the ions $SO_4{}^{2-}$ and Ca^{2+} are predominant. Sample DC-P-16 indicates significant higher values of $SO_4{}^{2-}$ whereas the concentration of Ca^{2+} is lower. Beyond that, DC-P-16 is characterised by generally higher contents of Al, Fe, K and Mg. These differences are potentially a result of the nearness of sample DC-P-16 to the acidic sampling sites which differ from the other sampling sites by overall increased concentrations.

Since the powdered samples did not dissolve completely neither in water nor in 1 M HNO_3, it can be assumed that the precipitations also consist of organic substances. This was approved by adding cyclohexane (organic solvent) whereby a complete dissolution of the part which could not be dissolved in HNO_3 could be attained.

5.3.10. The formation of acidic pools in a limestone bedrock

The pH of water in limestone terrains is usually in the range of 6.5 and 8.9 (Ford, Williams 2007). However, isolated pools such as DC-W-3, DC-W-4 and DC-W-6 indicate low pH values of 3.3 down to 1.03. According to Palmer (2007) the pH can decrease greatly in waters where sulphuric acid is produced and the water body is shielded from the carbonate rock by non-carbonate coatings, e.g. gypsum, clay or chert. In order to figure out which processes are most likely to cause the formation of acidic pools in Darzila cave saturation indices will be regarded initially.

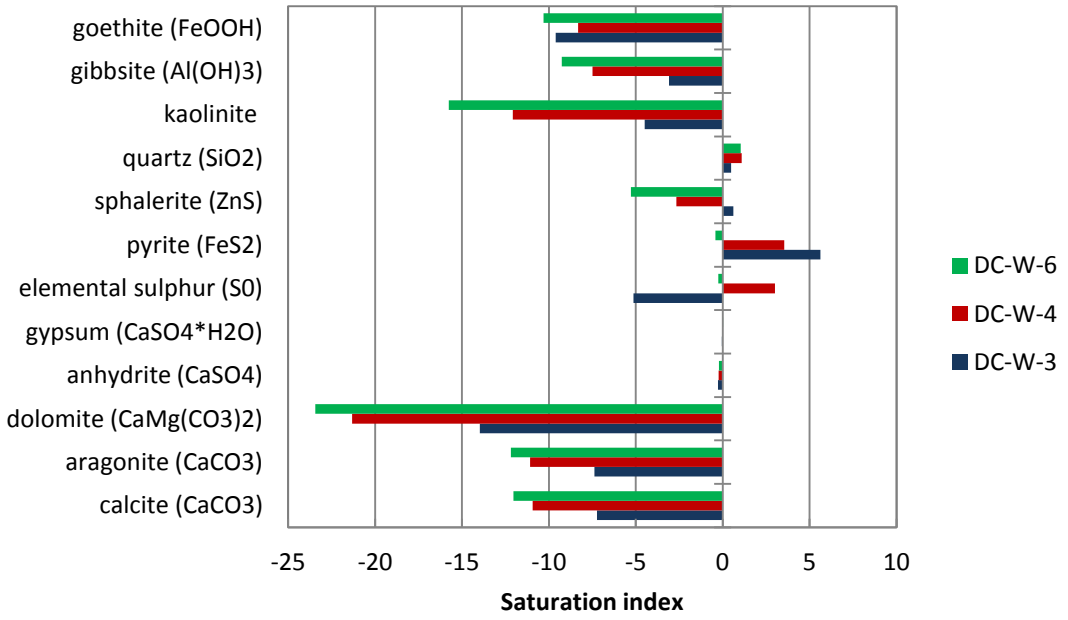

Figure 40: Saturation indices of selected mineral phases of acidic, isolated pools in Darzila cave

As it can be seen in Figure 40, the investigated pools are strongly undersaturated with regard to carbonates whereas they are in equilibrium with gypsum even though Darzila cave is solely embedded in limestone bedrock. Moreover, these sampling sites are strongly undersaturated with regard to clay minerals and iron-bearing hydroxides, such as goethite and gibbsite. Significant differences in saturation indices between the three sampling sites were only found with regard to elemental S^0 and sulphide minerals, such as ZnS^0, $FeS_2{}^0$. Differences in saturation indices can be

explained by the availability of pH-dependent species. Undersaturation with regard to a certain mineral phase is generally caused by a lack of appropriate ions in solution, e.g. sulphide ions. Moreover, influences of microbiological activity have to be considered (also see chapter 5.3.4).

Even though the formation of a gypsum layer in the acidic pools was not investigated yet, it can be concluded from the calculated saturation indices that the formation of incrustations of gypsum is most likely since all three sampling sites are in equilibrium with regard to gypsum. Although it was mentioned in chapter 5.3.9 that speleogenetic gypsum is only rarely formed under water, gypsum incrustations can be formed if the concentration of dissolved sulphate is great enough (Palmer 1991). Sequence of reactions explaining the origin of Guadalupe caves largely discussed by Palmer and Palmer (2000) can also be partially invoked in here. A rough outline of chemical reactions potentially occurring in Darzila cave shall be presented in the following. A conceptual model is provided in Figure 41.

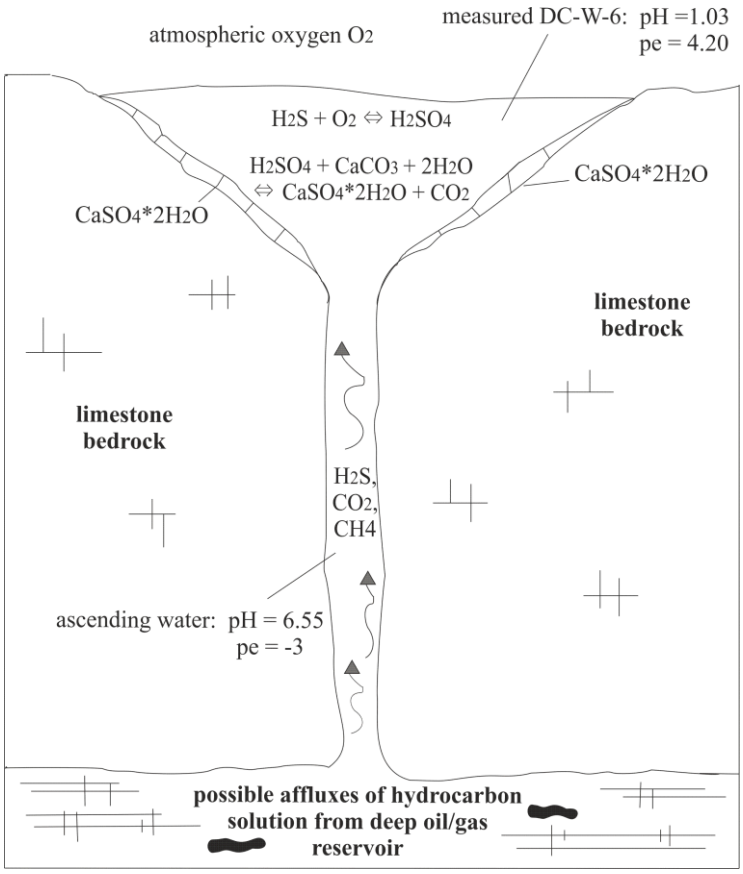

Figure 41: Conceptual model of the formation of incrustations of gypsum in contact to the cave atmosphere causing a drop in pH value

H_2S ascend, either in solution or as a distinct gas phase, into the carbonate rocks of the Pila Spi formation and oxidises at the water table due to the presence of atmospheric oxygen according to equation 2 (chapter 3.2). In consequence, carbonate rocks will be dissolute by sulphuric acids as it is described in equation 3 (chapter 3.2).

By far the most common by-product of sulphuric acid cave formations is gypsum that is formed where the acid is fairly concentrated. Gypsum can precipitate even in fairly acidic water, but at pH below about 2 (depending on temperature and dissolved species) sulphate is consumed in the following way (Palmer, Hill 2012):

$$SO_4^{2-} + H^+ \leftrightarrow HSO_4^- \quad [17]$$

In order to approve the approach of incrustations of gypsum in the acid pools, PhreeqC modelling was conducted. As representative site DC-W-6 was selected. Based on the hydrochemical composition of DC-W-6, following parameters were assumed to describe the ascending water that is rich in H_2S: pH = 6.5, pe = -3 (reducing conditions), H_2S = 4686.48 mg/L (calculated from measured concentrations of SO_4^{2-}).

In a first step, the reaction of the ascending water in contact to oxygen was modelled under consideration of calcite bedrock (equilibrium phase: calcite). As a result, the concentration of H_2S/HS^- decreases strongly and the amount of SO_4^{2-} and Ca^{2+} ions increases simultaneously with increasing input of oxygen (see reaction 18) (Figure 42). Due to an increase in H^+ and SO_4^{2-} ions more calcite dissolve resulting in an increase in Ca^{2+} ions according to equation 19. In consequence, the water becomes supersaturated with regard to gypsum (Table 16). If reaction kinetics are sufficiently fast, gypsum will precipitate according to reaction 4.

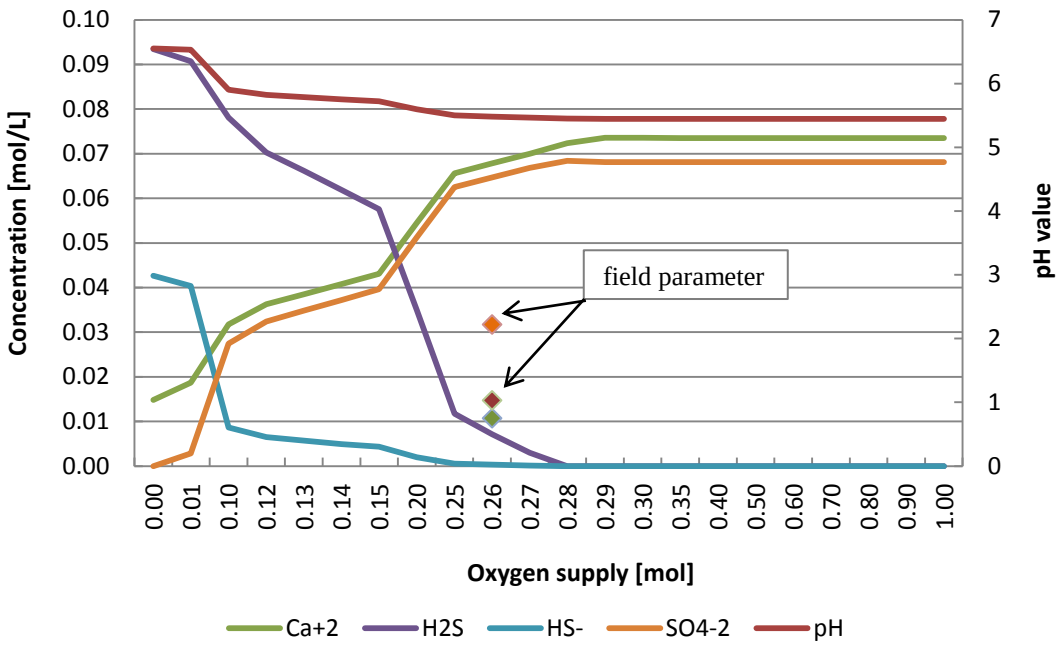

Figure 42: Modelled concentrations of Ca^{2+}, H_2S, HS^- and SO_4^{2-} ions in dependence on oxygen input under consideration of calcite as equilibrium phase (model 1)

However, it can be shown that the pH value only decreases slightly in contact with oxygen but the measured values of 3.3 to 1.03 cannot be achieved since the buffer capacity of the carbonate system limits the pH drop (Langmuir 1997).

Assuming precipitation of gypsum as it derives from model 1, the reaction of ascending water in contact with oxygen was modelled again but under consideration of incrustations of gypsum inhibiting the dissolution of the limestone bedrock according to equation 19. For that propose, gypsum was set as equilibrium phase.

The second model shows a significant decrease in H_2S/HS^- ions quite similar to that obtained by the first model. On the contrary, the concentration of SO_4^{2-} only increases slightly and the amount Ca^{2+} ions even decreases, because precipitation of gypsum prevents further dissolution of the limestone bedrock (Figure 43). In consequence, the water is strongly undersaturated with respect to calcite and the pH of the water decreases significantly (Figure 43, Table 16). Furthermore, it can be seen that the concentration of SO_4^{2-} ions as well as the pH value increase slightly again with increased input of oxygen. This might be due to the fact that sulphate is consumed again at pH values less than about 1.5 (reaction 20). In consequence, more gypsum may dissolve to replace it, which would also explain the fact that the amount of Ca^{2+} ions slightly increases again in the course of oxidation. Moreover, a further decrease in pH is limited since the acid is moderated by reaction 20 (Figure 43).

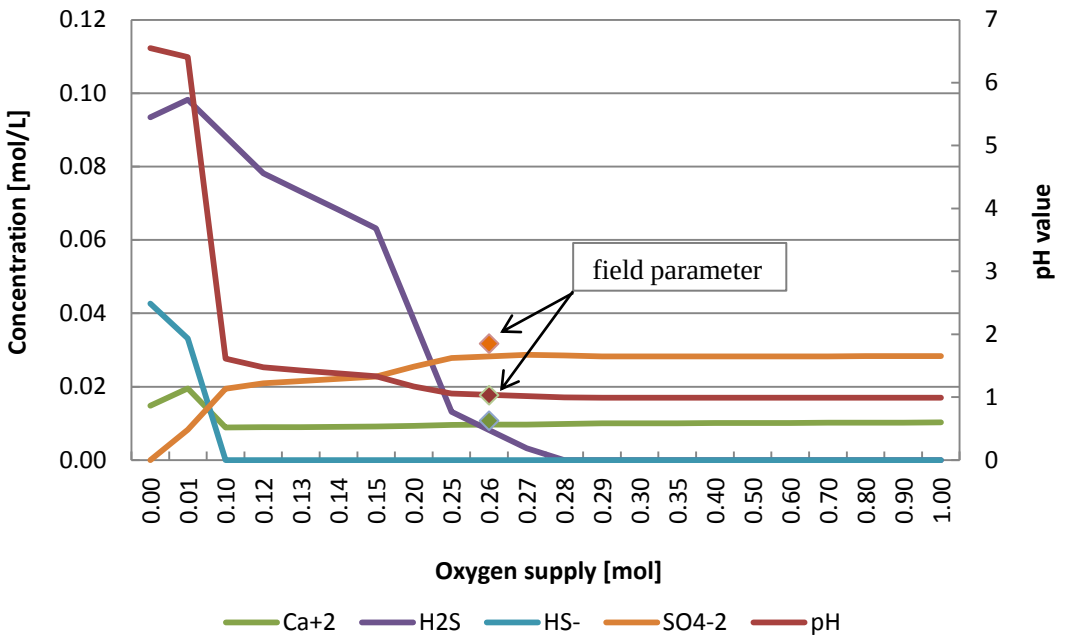

Figure 43: Modelled concentrations of Ca^{2+}, H_2S, HS^- and SO_4^{2-} ions in dependence on oxygen input under consideration of gypsum as equilibrium phase (model 2)

Considering incrustations of gypsum in modelling, a pH value of 1.03 like it was obtained in the field can be achieved by adding 0.260 moles O_2 to the assumed solution. In order to compare modelled values to those measured in the field, selected parameters related to an input of 0.260 moles O_2 are given in Table 16.

Table 16: Selected variables based on field measurements at site DC-W-6 compared to results of PhreeqC reaction modelling; model 1: equilibrium phase = gypsum, model 2: equilibrium phase = calcite (only parameters related to an input of 0.260 moles O_2 are represented)

O_2 = 0.260 mol	DC-W-6	Model 1	Model 2
pH	1.030	5.483	1.037
pe	4.200	-1.656	3.858
ionic strength [mol/kg]	0.204	0.285	0.194
S_{tot} [mmol/L]	139.54	138.05	141.43
Ca_{tot} [mmol/L]	15.02	132.51	18.04
Ca^{2+} [mmol/L]	10.71	67.83	9.63
SO_4^{2-} [mmol/L]	31.72	64.70	28.24
H_2S [mmol/L]	0	7.15	8.20
$SI_{calcite}$	- 12.038	0	- 12.091
$SI_{dolomite}$	- 23.429	- 1.336	- 24.551
SI_{gypsum}	+ 0.006	+ 1.100	0
SI_{quartz}	+ 1.031	+ 0.993	+ 0.984
$SI_{kaolinite}$	- 15.751	+ 8.928	- 17.017
$SI_{gibbsite}$	- 9.248	+ 3.065	- 9.898
$SI_{geothite}$	- 10.301	- 2.423	- 9.245

With regard to pH, pe as well as ionic strength results of model 2 agree quite well to the measured values whereas results of model 1 differ significantly. Due to an assumed equilibrium with respect to calcite in model 1 the concentration of calcium is strongly overestimated. In contrast to model 1, good agreements between DC-W-6 and model 2 were obtained with regard to the saturation indices of carbonates (e.g. calcite, dolomite), sulphates (e.g. gypsum), oxides and hydroxides (e.g. gibbsite) and layered silica minerals (e.g. kaolinite).

In conclusion, the second model generally agrees very well to the parameters that were obtained in the field. Thus, the chemical characteristics of the investigated acidic pools in Darzila cave can be well explained by the given approach.

6. Summary of the main results

Darzila cave offers remarkable opportunities to investigate an active cave system of deep-seated sulphuric acid origin. But detailed field studies are rare. Therefore, the main objective of the present work was to gain a first survey about fundamental processes of sulphuric acid speleogenesis in Darzila cave. Hydrogeochemical and hydrogeological investigations of the cave as well as explorations in the vicinity were carried out at the end of the dry season in September and October 2011. In the following section, a summary of the main results will be given.

- **Hydrogeochemical description**

The cave is fed by several groundwater inlets, commonly present as floor feeders. The main inlet is represented by DC-W-7 (cluster I-2), which is located to the north of the cave entrance and mainly influences the hydrogeochemical composition of the main cave discharge represented by cluster I-5. A small creek to the south of the cave entrance (cluster I-1) can be regarded as a further inlet even though the source could not be identified yet. Differences in the hydrogeochemical composition between both inlets are visible. Compared to cluster I-2, cluster I-1 is influenced by fresh air supply resulting in elevated E_H values and increased DO contents. Sulphide concentrations are diminished due to long time exposition to aerated conditions. Moreover, contents of TDS and DOC are slightly decreased.

Waters flowing in the cave represented by cluster I-1/2/5 can be generally described as brackish waters with TDS contents of about 1200 mg/L on average. Predominant ions in cave waters are SO_4^{2-}, Ca^{2+}, Mg^{2+}, but also significant concentrations of HCO_3^- ions were measured. The pH values range from 6.63 to 8.05 whereupon an increase along the flow path from DC-W-7 to DC-W-11 in result of CO_2 degassing can be observed. Throughout (partially) reducing conditions are characteristic for the cave waters. H_2S and organic compounds can be considered as the major reductants. Although, oxidation processes become more and more predominant in contact to the cave atmosphere.

In addition to the previous mentioned main inlets, further small springs were identified. In small and isolated pools, where the formation of gypsum coatings shields ascending water from the limestone rock, highly acidic, (moderately) saline waters are found. Distinctive features are low pH values, elevated contents of DOC

(up to 20 mg/L), remarkable high TDS values (up to 31 g/L) and the omnipresence of biofilms on the water surfaces. Moreover, increases in SO_4^{2-} contents relative to Ca^{2+} contents as well as elevated contents of elements commonly incorporated in clay minerals (e.g. Si, Fe, Al) are indicative for these sites.

In addition to a thorough investigation of Darzila cave also the nearby river Awa Spi was investigated. Cluster analysis based on hydrogeochemical parameters reveal a hydraulic connection between Awa Spi and Darzila cave. DR-W-1, which represents a subterranean feeder of Awa Spi, could be identified as the main outlet of Darzila cave. Moreover, DR-W-8 also shows a high similarity to the cave water. However, the hydrogeochemical composition of the river water is mainly governed by the second subterranean inlet (DR-W-2) which possesses the highest discharge rate. Compared to the cave water, Awa Spi shows significantly lower contents of TDS (662 mg/L on average) and can be described as Ca-Mg-HCO_3-SO_4- type. The influence of gypsum-bearing layers seems to be decreased. The river is characterised by alkaline pH conditions whereupon a slight increase in flow direction can be observed - potentially caused by CO_2 degassing. The river water is characterised by throughout reducing conditions probably mainly reasoned by a high input of sulphide (8 mg/L) at site DR-W-2. The milky colour of the river is probably caused by colloidal sulphur.
The tributary of Awa Spi indicates increased TDS values of 1517 mg/L and partially reducing conditions and a pH of 7.92. As the predominant ions are Ca^{2+}, Na^{+}, Cl^{-} and SO_4^{2-}, there seems to be an additional influence of halite-bearing layers.

- **Distribution of sulphur species**

As the establishment of an equilibrium between sulphate and sulphide is generally slow in natural waters, considerable amounts of sulphide could be still measured even though sulphate is the predominant species under the prevailing pH-pe-conditions in flowing water bodies (stability field of sulphur species, PhreeqC modelling). In cave water, maximum sulphide contents of 6.32 mg/L could be determined whereupon concentrations decrease along the flow path due to degassing and oxidation to sulphate. The highest sulphide concentrations were measured at the well (DW-W-1) with amounts of about 50 mg/L of sulphide indicating strong reducing conditions at deep sites. A shift towards acidic conditions, as it is given in the small and isolated pools, favours the predominance of H_2S and HSO_4^{-} ions. Due

to high concentrations of Ca^{2+} and Mg^{2+} ions in solution, $CaSO_4^0$ and $MgSO_4^0$ complexes are preferably formed (PhreeqC modelling). Concentrations of metastable sulphur species are generally low. However, an increase of thiosulphates up to a maximum of 3.04 mg/L along the flow path from DC-W-7 to DC-W-11 is obvious.

- **Cave origin and cave enlargement processes**

Morphological features and cave deposits commonly associated with sulphuric acid cave origin are omnipresent in Darzila cave. Main cave enlargement processes that could be identified are:

- Subaerial dissolution of the limestone bedrock and gypsum replacement
- Subaqueous dissolution of cave walls at or near the water table
- Limestone dissolution by acidic drips on the cave floor

Because of the high frequency of gypsum blocks and secondary gypsum coatings, in particular in the rear part of the cave, subaerial dissolution seems to be the main contributor to cave enlargement in Darzila cave. Subaqueous dissolution processes are greatest where water first emerges to the cave. Indicative are cave walls that are highly dissolved at or near former water tables close to DC-W-7. Though, separation of the effect of sulphuric acid from that of carbonic acid is difficult in this regard (Palmer, Palmer 2000). Contribution of acidic drops to cave enlargement seems to be low since this effect was only observed in the rear part of the cave where an accumulation of potholes was found.

- **Origin of cave sulphur**

Gypsum of Lower Fars formation might be the main source of cave sulphur. However, based on hydrogeochemical parameters a potential influence of hydrocarbon-related waters was pointed out with respect to the small and isolated pools DC-W-4 and DC-W-6. Strong indices are:

- Elevated concentrations of total dissolved solids (TDS)
- Elevated concentrations of dissolved organic carbon (DOC)
- Particularly high enrichment of SO_4^{2-} ions relative to Ca^{2+} ions
- Relative enrichments of trace elements, such as Cr, Be, Ga, Ni, Co, Mn, Pb and V

7. Recommendations

During data acquisition and analyses, various problems and errors occurred. Beyond that, also several questions raised by this thesis and new ideas evolved for following studies. Therefore, some recommendations will be given:

- Further exploration of Darzila cave and complementing of cave plans (only about 200 m are explored up to now). For that purpose an appropriate equipment including e.g. helmet, gas mask, head lamp, gloves is necessary.
- More detailed investigation of cave pattern and study of the geomorphic history and evolutional sequences of Darzila cave (e.g. dating, investigation of former water tables) (compare Palmer 2012)
- Study of seasonal changes and of the contribution of oxygenated meteoric water to carbonate corrosion during the wet season (compare Galdenzi et al. 2008)
- More detailed investigation of the karst system (e.g. tracer tests, exploration of other caves in the surrounding)
- Repeat sampling for determining sulphites in water but stabilising in 37% formaldehyde and 1 M NaOH (Metrohm manual – recommendations) or shock-freeze
- Repeat measurements of sulphides in water, in particular at site DC-W-2/7/8 (cluster I-2), and in air
- Conducting of laboratory tests checking the efficiency of stabilisation methods for thiosulfates and polythionates
- Repeat measurement of iodine by ICP-MS but sample preparation (e.g. adding of alkaline NH_3- or TMAH- or acidic HCl-solution) in order to circumvent difficulties caused by formation of volatile iodine species. A review of iodine determination by ICP-MS is provided by Oliveira et al. (2010)
- Detailed analysis of organics in water

8. References

Angert, E.R; Northup, D. E.; Reysenbach, A.-L; Peek, A.S; Goebel, B.M; Pace, N.R (1998): Molecular phylogenetic analysis of a bacterial community in Sulphur River, Parker Cave, Kentucky. In *American Mineralogist* (83), pp. 1583–1592.

Artinger, R.; Buckau, G.; Geyer, S.; Fritz, P.; Wolf, M.; Kim, J. I. (2000): Characterisation of groundwater humic substances: influence of sedimentary organic carbon. In *Applied Geochemistry* (15), pp. 97–116.

Aziz, M. (2001): Climate of North Iraq, Brief - Note (unpublished working document of FAO AM SS). FAO documentation Fund. Erbil.Backhaus, K.; Erichson, B.; Plinke, W.; Weiber, R. (2011): Multivariate Analysemethoden: Eine Anwendungsorientierte Einfuhrung. 13th ed. Berlin: Springer.

Barton, H.A; Luiszer, F. (2005): Microbial metabolic structure in a sulfidic cave hot spring: Potential mechanisms of biospeleogenesis. In *Journal of Cave and Karst Studies* 67 (1), pp. 28–38.

Bell, F. G.; Waltham, T.; Culshaw, M. (2005): Sinkholes and subsidence. Karst and Cavernous Rocks in Engineering and Construction. 1st ed. Berlin: Springer-Verlag.

Buck, M. J.; Ford, D. C.; Schwarcz, H. P. (1994): Classification of cave gypsum deposits derived from oxidation of H2S. In: Breakthrough in karst geomicrobiology. In *Karst Water Institute. Special Publication 1:*, pp. 5–9.

Bühl, A. (2008): SPSS Version 16. Einführung in die moderne Datenanalyse. 11th ed. München: Pearson Studium.

Canfield, D. E. (2001): Biogeochemistry of Sulfur Isotopes. In *Reviews in Mineralogy and Geochemistry* 43 (1), pp. 607–636.

Chilingar, G. V.; Buryakovsky, L. A.; Eremenko, N. A.; Gorfunkel, M. V. (2005): Geology and geochemistry of oil and gas. Amsterdam: Elsevier.

Cunningham, K. M.; Wright, W. G.; Nordstrom, D. K.; Ball, J. W.; Schoonen, M. A. A.; Xu, Y. (1996): Water-quality data for Doughty Springs, Delta County, Colorado, 1903-1994, with emphasis on sulfur species. In *USGS Open-File Report*, pp. 96–619.

Daskalakis, D. K.; Helz, G. R. (1992): Solubility of CdS (greenockite) in sulfidic waters at 25°C. In *Environmental Science and Technology* (26), pp. 2462–2468.

Davis, S. N.; DeWiest, R. J. M. (1967): Hydrogeology. 2nd ed. New York, London Sydney: Wiley.

DVWK (1992a): Entnahme und Untersuchungsumfang von Grundwasserproben (DVWK - Regel 128).

Egemeier, S.J (1973): Cavern Development by Thermal Waters with a Possible Bearing on Ore Deposition. PhD. Stanford University.

Egemeier, S.J (1981): Cavern Development by thermal waters. In *Bulletin of the National Speleological Society* 43, pp. 31–51.

Ehrlich, H.L (2002): Geomicrobiology. 4th ed. New York: M. Dekker.

Engel, A. S.; Stern, L. A.; Bennett, P. C. (2004): Microbial contributions to cave formation: New insights into sulfur acid speleogenesis. In *Geology* 32 (5), pp. 369–372.

Ford, D. (2006): Karst geomorphology, caves and cave deposits: a review of North American contributions during the past half century. In: R. S. Harmon, Carol M. Wicks, Derek Ford and William B. White (Hg.): Perspectives on Karst geomorphology, hydrology, and geochemistry. A tribute volume to Derek C. Ford and William B. White. Boulder, Colorado: Geological Society of America.

Ford, Derek; Williams, Paul W. (2007): Karst hydrogeology and geomorphology. [Rev. ed.]. Chichester, England ;, A Hoboken, NJ: John Wiley & Sons.

Galdenzi, S.; Cocchini, M.; Morichetti, L.; Amici, V.; Scuri, S. (2008): Sulfide ground-water chemistry in the Frasassi Caves, Italy. In *Journal of Cave and Karst Studies* (70(2)), pp. 94–107.

Galdenzi, S.; Maruoka, T. (2000): Gypsum deposits in the Frasassi Caves, Central Italy. In *Journal of Cave and Karst Studies* 65 (2), pp. 111–125.

Galdenzi, S.; Menichetti, M. (1995): Occurrence of hypogenic caves in a karst region: Examples from Italy. In *Environmental Geology* 26(1), pp. 39-47.

Gunn, J. (2004): Encyclopedia of Caves and Karst Science. London: Fritzroy Dearborn.

Hach Company: DR/890 Colorimeter - Procedures Manual.

Haddad, R. H. Smoor P. B. (1973): Groundwater Survey of Erbil Project Area. In *IARNR Techn. Bull.* 50.

Hassan, I. O.; Surdashy, A. M.; Sherawani, G. H.; Aqrawi, A. M.; Naqishbandi, S. F.: Lithostratigraphic Map of Northern Iraq (1:50000): Groundwater Unit of WRI Sub-Sector and Mapping Unit, FAO Coordination Office Northern Iraq.

Häuselmann, P.; Neumann, A. (1999): Cave Symbols: The Official UIS List. voted by the national delegates. Available online at www.uis-speleo.org, checked on 16/04/2012.

HAZRA Eng.Co. (1963): Hydrogeological Survey of Iraq. Chicago, Baghdad.Hill, C. A. (1990): Sulfuric acid speleogenesis of Carlsbad Cavern and its relationship to hydrocarbons, Delaware basin, New Mexico and Texas. In *AAPG* 74 (11), pp. 1685–1694.

Hölting, Bernward; Coldewey, Wilhelm Georg (2005): Hydrogeologie. Einführung in die allgemeine und angewandte Hydrogeologie ; 69 Tabellen. 6th ed. München: Elsevier, Spektrum Akad. Verl.

Hose, L. D.; Palmer, A. N.; Palmer, M.; Northup, D. E.; Boston, P. J.; DuChene, H. R. (2000): Microbiology and geochemistry in a hydrogen-sulphide rich karst environment. In *Chemical Geology* 169 (3-4), pp. 399–423.

Hose, L.D; Pisarowicz, J.A (1999): Cueva de Villa Luz, Tabasco, Mexico-Reconnaissance Study of an Active Sulfur Spring Cave and Ecosystem. In *Journal of Cave and Karst Studies* 61 (1), pp. 13–21.

Iurkiewicz, A. A.; Stevanovic, Z. P. (2010): Reconnaissance study of active sulfide springs and cave systems in the southern part of the Sulaimani Governorate (NE Iraq). In *Carbonate Evaporites* (25), pp. 203–216.

Jassim, Saad Z.; Goff, J. C. (2006): Geology of Iraq. 1st ed. Prague, Brno: Dolin; Moravian Museum.

Kaasalainen, H.; Stefánsson, A. (2011): Sulfur speciation in natural hydrothermal waters, Iceland. In *Geochimica et Cosmochimica Acta* 75 (10), pp. 2777–2791.

Khanaqa, P. A.; Al-Manmi, D. A. (2011): Hydrogeochemistry and geomicrobiology of Darzila spring in Sangaw, Sulaimani, NE Iraq. In *Iraqi Bulletin of Geology and Mining* 7(3), pp. 63–79.

Klimchouk, A. B. (2007): Hypogene Speleogenesis. Hydrogeological and Morphogenic Perspective. Special Paper no. 1. 1st ed. Carlsbad: National Cave and Karst Research Institute, checked on 12/01/2012.

Klimchouk, A. B.; Ford, D. C.; Palmer, A. N. (2000): Speleogenesis. Evolution of karst aquifers. 1st ed. Huntsville (Ala.): National Speleological Society.

Kummer, N. A. (2012): Accurancy of ICP-MS measurements, pH calibration. personal communication. Freiberg, 2012.

Langmuir, Donald (1997): Aqueous environmental geochemistry. Upper Saddle River, N.J, London: Prentice Hall; Prentice-Hall International.

Lauerwald, F. (2007): Sulfur geochemistry of hot springs at Yellowstone National Park - investigating the importance of sulfur oxidation versus microbial sulfate reduction by species selective sampling and isotopic investigations (Diploma thesis). Universität Bayreuth, TU BAF.

Lawa, A. F. (2004): Sequence stratigraphic analysis of the Middle Paleocene-Middle Eocene in the Sulaimani district (Kurdistan region). PhD thesis, University of Sulaimani Iraq.

Le Faou, A. (1990): Thiosulfate, polythionates and elemental sulfur assimilation and reduction in the bacterial world. In *FEMS Microbiology Letters* 75 (4), pp. 351–382.

Kanemoto, M.; Shiragami, T.; Pac, C.; Yanaginda, S. (1992): Semiconductor photocatalysis. Effective photoreduction of carbon dioxide catalyzed by ZnS quantum crystallites with low density of surface defects. In *J. Phys. Chem.* 96, pp. 3512–3526.

Maala, K. A. (2006): Geological Map of Sulaymaniayah Quadrangles, scale 1:250000. Iraq-Baghdad: State Company of Geological Survey and Mining.

Machel, H.G (2001): Bacterial and thermochemical sulfate reduction in diagenetic settings - old and new insights. In *Sedimentary Geology* 140 (1-2), pp. 143–175.

Matthess, Georg (1994-): Lehrbuch der Hydrogeologie. 3rd ed. Berlin: Borntraeger.

Merkel, Broder; Planer-Friedrich, B.; Nordstrom, Darrell Kirk (2005): Groundwater geochemistry. A practical guide to modeling of natural and contaminated aquatic systems. Berlin ;, New York: Springer.

Oliveira, A. A.; Trevizan, L. C.; Nóbrega, J. A. (2010): REVIEW: Iodine Determination Review: Iodine Determination by Inductively Coupled Plasma Spectrometry. In *Applied Spectroscopy Reviews* 45 (6), pp. 447–473.

Onac, B. P.; Wynn, J. G.; Sumrall, J. B. (2011): Tracing the sources of cave sulfates: a unique case from Cerna Valley, Romania. In *Chemical Geology* 288 (3-4), pp. 105–114.

Osseo-Asare, K. (1989), Solution chemistry and separation process in precious and rare metals systems. In *Precious and Rare Metals Technologies.* (Eds.) Torma, A.E. and Gundiler, I.H. (Elsevier: Amsterdam).pp 113-135

Palmer, A. N. (1991): Origin and morphology of limestone caves. In *Geological Society of America Bulletin, v. 103* (1), pp. 1–21.

Palmer, A. N. (2007): Cave geology. Dayton, Ohio: Cave Books.

Palmer, A. N. (2011): Distinction between epigenic and hypogenic maze caves. In *Geomorphology* 134 (1-2), pp. 9–22.

Palmer, A. N. (2012): Hypogenic sulfuric acid caves: morphology and evolution. personal communication (unpublished), checked on 0.4/05/2012.

Palmer, A. N.; Hill, C. A. (2012): Sulfuric Acid Caves. In *Encyclopedia of Caves*, pp. 810–819.

Palmer, A. N.; Palmer, M. V. (2004): Sulfate-carbonate interactions in the development of karst. In *Northeastern geology and environmental science* 26 (1), pp. 93–106.

Palmer, A.N; Palmer, M.V (2000): Hydrochemical interpretation of cave patterns in the Guadalupe Mountains, New Mexico. In *Journal of Cave and Karst Studies* 62 (2), pp. 91–108.

Parkhust, D. L.; Appelo, C. A. J. (1999): User's Guide to PreeqC (Version 2) - a computer program for speciation, batch-reaction, one-dimensional transport, and inverse geochemical calculations, checked on 26/01/2012.

Pfeffer, Karl-Heinz (2010): Karst. Entstehung - Phänomene - Nutzung. Stuttgart: Borntraeger.

Provencio, P.; Polyak, V. J.; Mosch, C. J. (1998): By-products of H2S/H2SO4 speleogenesis. Proceedings of the Society: Selected Abstracts 1998 NSS Convention in Sewanee, Tennessee. In *Journal of Cave and Karst Studies* (60/3).

Reber, J.; Meier, K. (1984): Photochemical production of hydrogen with zinc sulfide suspensions. In *J. Phys. Chem.* 88, pp. 5903–5913.

Reineke, Walter; Schlömann, Michael (2007): Umweltmikrobiologie. 1st ed. München: Spektrum.

Rossum, J. R. (1975): Conductance Method for Checking Accuracy of Water Analyses. In *AWWA* (Vol. 67 Iss. 4), pp. 204–205.

Satyanarayana, D. (2011): Petroleum Geochemistry. Delhi: Daya Publishing House.

Schüring, J.; Schulz, H. D.; Fischer, W. R.; Böttcher, J.; Duijnisveld, W. H. M. (Eds.) (2000): Redox : fundamentals, processes and applications ; with 21 tables. Berlin Heidelberg New York: Springer - Verlag.

Sigg, L.; Stumm, W. (2011): Aquatische Chemie. Einführung in die Chemie natürlicher Gewässer. 5th ed. Stuttgart: UTB.

Stevanovic, Z. P.; Iurkiewicz, A. A. Maran A. (2009): New insights into karst and caves of northwestern Zagros (Northern Iraq). In *ACTA CARSOLOGICA* (38/1), pp. 83–96.

Stevanovic, Z. P.; Markovic, M. (Eds.) (2003a): Hydrogeology of Northern Iraq, Vol.1. Climate,, Hydrology, Geomorphology & Geology. FAO Northern Iraq Coordination Office. 2nd ed. Erbil, checked on 11/04/2012.

Stevanovic, Z. P.; Markovic, M. (Eds.) (2003b): Hydrogeology of Northern Iraq, Vol.2. General Hydrogeology and Aquifer Systems. FAO Northern Iraq Coordination Office. Erbil.

Stumm, W.; Morgan, J. J. (1996): Aquatic chemistry. 3rd ed. New York, N.Y: John Wiley & Sons.

Tang, K.; Baskaran, V.; Nemati, M. (2009): Bacteria of the sulphur cycle: An overview of microbiology, biokinetics and their role in petroleum and mining industries. In *Biochemical Engineering Journal* 44 (1), pp. 73–94.

Trüper, H.G (1984): Microorganisms and the Sulfur cycle. In: A. Müller und B. Krebs (Ed..): Sulfur. Its significance for chemistry, for the geo-, bio- and cosmosphere and technology. Bielefeld sulfur meeting. Amsterdam: Elsevier.

UBA (Ed.) (2000): Entwicklung von Erfassungs- und Auswertungsverfahren für Grundwasserzustandsdaten zur Erfüllung internationaler Berichtspflichten des Bundes gegenüber der Europäischen Union. Umweltbundesamt. Berlin (Forschungsbericht, 298 23 241).

United States Environmental Protection Agency (Ed.) (2002): A lexicon of cave and karst terminology with special reference to environmental karst hydrology. Available online at www.epa.gov/ncea, updated on 16/04/2012.

Veress, Márton (2010): Karst environments. Karren formation in high mountains. New York: Springer.

Vitorge, P.; Phrommavanh, V.; Siboulet, B.; You, D.; Vercouter, T.; Descostes, M. et al. (2007): Estimating the stabilities of actinide aqueous species. Influence of sulfoxy-anions on uranium (IV) geogechemistry and discussion of Pa(V) first hydrolysis. In *C. R. Chimie* (10), pp. 978–993.

Worden, R.H; Smalley, P.C (1996): H2S-producing reactions in deep carbonate gas reservoirs: Khuff Formation, Abu Dhabi. In *Chemical Geology* 133, pp. 157–171.

World Weather Online (2011): Sangaw Weather, Iraq Weather Averages. Available online at http://www.worldweatheronline.com/Sangaw-weather-averages/As-Sulaymaniyah/IQ.aspx.

Xu, Y.; Schoonen, M. A. A.; Nordstrom, D. K.; Cunningham, K. M.; Ball, J. W. (1998): Sulfur geochemistry of hydrothermal waters in Yellostone National Park: I. The origin of thiosulfate in hot spring waters. In *Geochimica et Cosmochimica Acta* 62 (23/24), pp. 3729-2743.

9. Appendix

List of Tables

List of Figures

9.1. Appendix A – Tables

Table A 1: Photometrical determinations: Applied methods and their ranges, precisions and estimated detection limits (EDL)

Compound	Method (HACH)	Range	Precision	EDL
Unit		mg/L	mg/L	mg/L
NH_4^+	8155	0 - 0.5 (NH_3-N)	±0.02	0.02
NO_2^-	8507	0 - 0.35 (NO_2-N)	±0.001	0.005
Fe_{total}	8008	0 - 3.0	±0.017	0.03
Fe^{2+}	8146	0 - 3.0	±0.017	0.03
PO_4	8048	0 - 2.5	±0.05	0.05
$HS^-/H_2S/S^{2-}$	8130	0 - 0.7	±0.02	0.01

Table A 2: Common interferences in the test procedures of photometrical determinations

Compound	Interferences
NH_4^+	Ca > 1 g/L as $CaCO_3^0$; all levels of iron; Mg > 6 g/L as $CaCO_3^0$; NO_3^- > 100 mg/L as NO_3^--N; NO_2^- > 12 mg/L as NO_2^--N; PO_4 > 100 mg/L as PO_4-P; SO_4^{2-} > 300 mg/L; sulphide intensifies the colour; turbidity and sample colour give erroneous high values
NO_2^-	Fe^{2+} and Cu^{2+} cause low results; Fe^{3+} and lead ions interfere by causing precipitation; NO_3^- > 100 mg/L as NO_3^--N; all levels of strong oxidising and reducing substances
Fe_{total}	Ca^{2+} > 10 g/L as $CaCO_3^0$; Cl^- > 185 g/L; Mg > 100 g/L as $CaCO_3^0$; high sulphide levels, S^{2-}, turbidity
Fe^{2+}	-
PO_4	Al > 200 mg/L; all levels of arsenate; Cr > 100 mg/L; Cu > 10 mg/L; all levels of hydrogen sulphide; Fe > 100 mg/L; Ni > 300 mg/L; silica > 50 mg/L; silicates > 10 mg/L; turbidity or sample colour, Zn > 80 mg/L, highly buffered samples or extreme sample pH (pH 2 to 10 is recommended)
$HS^-/H_2S/S^{2-}$	Strong reducing substances (sulphite, thiosulfate, hydrosulfite) reduce the blue colour or prevent its development; turbidity

Table A 3: Contents of total inorganic carbon (TIC) and dissolved organic carbon (DOC) in water determined with the LiquiTOC element analyser (laboratories of the chair for hydrogeology, TU Freiberg)

Sample ID	TIC	DOC
	mg/L	mg/L
DC-W-1	39.92	0.34
DC-W-2	46.35	2.39
DC-W-3	7.01	4.42
DC-W-4	5.08	13.73
DC-W-5	44.49	0.95
DC-W-6	4.70	19.58
DC-W-7	54.63	0.61
DC-W-8	57.40	0.74
DC-W-9	41.30	0.22
DC-W-10	48.37	1.05
DC-W-11	45.87	0.70
DR-W-1	47.49	0.50
DR-W-2	59.04	0.43
DR-W-3	53.85	0.47
DR-W-6	53.89	0.52
DR-W-7	40.85	1.41
DR-W-8	43.49	0.92
DR-W-9	54.59	0.96
DW-W-1	69.25	0.91

Table A 4: Titration of water samples with HCl respectively NaOH; concentrations of HCO_3^- and CO_2 are calculated based on equation [10] (M_{HCO3-} = 61.02 g/mol; M_{CO2} = 44.01 g/mol; $c_{NaOH;HCl}$ = 0.1 mol/L)

Sample ID	Date	pH_0	HCl	HCO_3^-	pH_0	NaOH	CO_2	C_{total}
			ml	mg/L		ml	mg/L	mg/L
DC-W-1	20.09.2011	7.2	3.6	219.6	7.2	0.7	30.8	51.6
DC-W-2	20.09.2011	7.2	5.2	317.2	7.2	1.6	70.4	81.6
DC-W-3*								
DC-W-4*								
DC-W-5	20.09.2011	7.8	4.8	289.8	7.8	0.2	8.8	59.4
DC-W-6*								
DC-W-7	25.09.2011	6.9	5.4	326.4	6.7	3.3	145.2	103.8
DC-W-8	25.09.2011	7.1	5.1	311.1	7.1	2.3	101.2	88.8
DC-W-9	01.10.2011	7.3	3.7	222.7	7.4	0.6	26.4	51.0
DC-W-10	01.10.2011	8	4.8	292.8	8.0	0.2	6.6	59.4
DC-W-11	01.10.2011	7.7	2.5	149.5	8.0	0.3	13.2	33.0
DR-W-1	01.10.2011	7.5	4.4	268.4	7.5	0.7	30.8	61.2
DR-W-2	01.10.2011	7.4	5.8	353.8	7.6	1.3	55.0	84.6
DR-W-3	01.10.2011	7.7	5.4	326.4	7.7	0.7	28.6	72.0
DR-W-6	08.10.2011	7.9	5.2	314.2	7.8	0.5	22.0	67.8
DR-W-7	08.10.2011	7.8	3.7	222.7	7.8	0.3	13.2	47.4
DR-W-8	08.10.2011	7.3	3.4	207.4	7.2	0.9	39.6	51.6
DR-W-9	08.10.2011	8	4.5	271.5	7.9	0.3	11.0	56.4
DW-W-1	08.10.2011	7.2	5.6	341.6	7.1	2.3	101.2	94.8

*Titration was not conducted

Table A 5: Gases in water (nomenclature: GW) and air (nomenclature: GA) measured by gas chromatography (laboratories of the chair for hydrogeology, TU Freiberg)

Sample ID	CH_4	C_2H_6	C_2H_4	C_6H_{14}
	µg/l	µg/l	µg/l	µg/l
DC-GW-1	1.57	0.14	0.23	0
DC-GW-2	186.56	4.79	0	32.34
DC-GW-3	1.19	0	0.19	0
DC-GW-4	1.35	0	0	0
DC-GW-5	38.7	1.16	0	0
DC-GW-6*				
DC-GW-7	141.67	3.61	0	0
DC-GW-8	100.95	2.59	0.35	0
DC-GW-9	1.54	0.4	0.31	0
DC-GW-10	24.36	0.76	0	0
DC-GW-11*				
DR-GW-1	5.5	0	0	20.78
DR-GW-2	128.4	5.87	0	15.64
DR-GW-3	57.91	2.78	0	0
DR-GW-6	59.71	2.56	0	0
DR-GW-7	467.36	7.4	0	0
DR-GW-8	43.47	0	0.23	0
DR-GW-9	19.26	0.9	0	0
DW-GW-1*				
DC-GA-3	1.28	0	0	0
DC-GA-9	1.33	0	0	0

*DC-GW-6, DC-GW-11, DW-GW-1 got broken during travelling

Table A 6: Correction of the redox potential and calculation of pe [EMF = readings, E_R = measured redox potential of the reference solution (E_{ref} = 220 mV), $EMF_{(ref)}$ = EMF-(E_R-E_{ref}), $E_{H(25°C)}$ = $EMF_{(ref)}$-0.198*(T-25)+207, E_H = $E_{H(25°C,pH=7)}$ = $E_{H(25°C)}$-(-59.1*(pH-7)), pe = 16.9*E_H/1000]

Sample ID	EMF	E_R	$EMF_{(ref)}$	T	$E_{H(25°C)}$	pH	$E_{H(25°C,pH=7)}$	pe
	mV	mV	mV	°C	mV		mV	
DC-W-1	-111	227	-118	23	89	7.3	109	1.8
DC-W-2	-275	227	-282	26	-75	7.0	-76	-1.3
DC-W-3	-66	227	-73	21	134	3.3	-84	-1.4
DC-W-4	358	230	348	22	556	2.1	263	4.5
DC-W-5	-241	227	-248	25	-41	7.7	1	0.0
DC-W-6	400	232	388	21	596	1.1	249	4.2
DC-W-7	-307	230	-317	26	-110	6.6	-132	-2.2
DC-W-8	-263	230	-273	26	-66	6.8	-79	-1.3
DC-W-9	27	234	14	23	221	7.3	239	4.0
DC-W-10	-245	234	-259	25	-52	8.0	7	0.1
DC-W-11	-232	234	-246	25	-38	8.1	24	0.4
DR-W-1	-85	224	-89	24	118	7.5	150	2.5
DR-W-2	-266	224	-270	22	-62	7.2	-51	-0.9
DR-W-3	-257	224	-261	23	-53	7.4	-32	-0.5
DR-W-6	-296	244	-320	22	-112	7.7	-73	-1.2
DR-W-7	72	242	50	17	259	7.9	313	5.3
DR-W-8	-198	244	-222	25	-15	7.3	1	0.0
DR-W-9	-244	244	-268	21	-60	7.7	-16	-0.3
DW-W-1	-280	244	-304	27	-97	6.8	-107	-1.8

Table A 7: In-situ parameter (corrected E_H values; redox conditions: if $E_H \leq 0$ mV then reducing, if $0 < E_H < 400$ mV then partially reducing, if $E_H \geq 400$ mV then oxidising) and on-site photometry

Sample ID	Date	pH	EC	DO	T	Turbidity	E_H	Redox conditions	NH_4^+	*NH_4^+	**Fe_{total}	**Fe^{2+}	NO_2^-	PO_4	$HS^-/H_2S/ S^{2-}$
			µS/cm	mg/L	°C	NTU	mV		mg/L	mg/L	mg/L	mg/L	mg/L	mg/L	mg/L
									± 0.02	± 0.02	± 0.017	± 0.017	± 0.001	± 0.05	± 0.02
DC-W-1	15.09.2011	7.3	1583	4.2	22.8	1	109	partially reducing	0.09		0.09	0.25	0.02	0.11	0.06
DC-W-2	15.09.2011	7.0	1730	2.3	26.0	106	-76	reducing	2.40		< 0.03	0.06	0.03	1.86	0.12
DC-W-3	15.09.2011	3.3	2840	0.8	21.4	38	-84	reducing	1.56	3.10	7.12	6.76	0.01	1.78	3.36
DC-W-4	19.09.2011	1.6	13340	0.7	21.6	18	263	partially reducing	0.02	4.80	15.04	9.88	0.03	4.60	3.92
DC-W-5	15.09.2011	7.7	1710	2.8	25.3	26	1	partially reducing	0.12		< 0.03	0.17	0.02	0.52	6.32
DC-W-6	22.09.2011	1.0	42700	2.9	21.4	57	249	partially reducing	0.29	56.00	n.d.	0.04	0.03	6.68	0.05
DC-W-7	19.09.2011	6.6	1725	0.5	26.2	56	-132	reducing	0.70		n.d.	0.09	0.03	2.30	0.07
DC-W-8	19.09.2011	6.8	1740	1.8	26.1	36	-79	reducing	0.74		n.d.	0.06	0.02	2.07	0.11
DC-W-9	27.09.2011	7.3	1589	3.1	23.0	5	239	partially reducing	0.11		n.d.	< 0.03	0.01	0.18	< 0.01
DC-W-10	27.09.2011	8.0	1707	3.3	25.3	255	7	partially reducing	0.47		n.d.	0.04	0.02	1.20	4.32
DC-W-11	27.09.2011	8.1	1702	2.9	24.9	379	24	partially reducing	< 0.02		n.d.	0.05	< 0.005	1.46	1.30
DR-W-1	29.09.2011	7.5	1395	2.7	24.0	128	150	partially reducing	< 0.02		n.d.	< 0.03	< 0.005	0.11	0.09
DR-W-2	29.09.2011	7.2	850	0.9	22.1	107	-51	reducing	0.64		n.d.	< 0.03	0.02	1.96	7.84
DR-W-3	29.09.2011	7.4	892	0.5	22.8	67	-32	reducing	0.57		n.d.	< 0.03	0.04	1.29	6.40
DR-W-6	06.10.2011	7.7	931	0.4	21.6	123	-73	reducing	0.67		n.d.	< 0.03	0.01	1.35	4.24
DR-W-7	12.10.2011	7.9	2092	8.0	17.3	2	313	partially reducing	0.30		n.d.	0.17	0.03	3.48	< 0.01
DR-W-8	06.10.2011	7.3	1656	1.4	25.2	15	1	partially reducing	0.27		n.d.	0.11	0.01	0.07	0.02
DR-W-9	06.10.2011	7.7	981	1.4	21.0	95	-16	reducing	0.24		n.d.	< 0.03	0.01	0.46	5.12
DW-W-1	06.10.2011	6.8	1605	1.6	26.6	39	-107	reducing	1.32		n.d.	0.17	< 0.005	3.60	49.92

n.d. - not determined; *repeated measurement under neutral pH conditions (laboratories of the chair for hydrogeology, TU Freiberg): ** because these values are less reliable Fe species were calculated with PhreeqC on the basis of ICP-MS results

Table A 8: Cations and anions of water samples analysed with ion chromatography (laboratories of the chair for hydrogeology, TU Freiberg)

Sample ID	Li^+	Na^+	NH_4^+	K^+	Mn^{2+}	Ca^{2+}	Mg^{2+}	F^-	Cl^-	Br^-	NO_3^-	PO_4	SO_4^{2-}	SO_3^{2-}	$S_2O_3^{2-}$	$**S_nO_6^{2-}$	$[SCN]^-$
	mg/L	mg/L	mg/L	mg/L	mg/L	mg/L	mg/L	mg/L	mg/L	mg/L	mg/L	mg/L	mg/L	mg/L	mg/L	mg/L	mg/L
DC-W-1	0.009	11.91		1.88		276	62.7	0.81	11.41	0.068	0.197	0.024	797	0.014	0.021	0.062	0.00
DC-W-2	0.013	13.80		1.79		302	74.4	1.10	15.69	0.066	0.056	0.019	889	0.010	0.145	0.096	0.00
DC-W-3	0.017	12.63	2.79	3.72	0.160	533	81.1	1.32	12.37	0.075	0.203	0.321	1783	0.000	0.162	0.147	0.00
DC-W-4	0.044	16.31	5.57	11.60	0.550	551	94.6	1.32	16.53	0.029	0.037	4.001	4840	0.015	0.070	-0.056	0.00
DC-W-5	0.013	14.02		1.75		278	74.3	0.98	15.48	0.084	0.025	0.027	863	0.008	1.171	0.850	0.00
DC-W-6	0.058	29.44	63.71	33.47	0.810	593	122.6	1.15	28.22	0.000	0.000	6.011	13210	0.059	0.060	0.019	0.00
DC-W-7	0.011	14.20	0.07	1.88		299	74.6	1.03	16.11	0.075	0.047	0.018	828	0.008	0.050	0.075	0.00
DC-W-8	0.011	14.07		1.85		301	76.3	1.09	15.94	0.082	0.048	0.015	888	0.000	0.071	0.085	0.00
DC-W-9	0.007	10.80		1.55		292	64.1	0.88	11.52	0.060	0.226	0.013	790	0.009	0.006	0.002	0.00
DC-W-10	0.015	14.18		1.91		306	70.7	1.06	15.76	0.061	0.080	0.014	855	0.000	1.719	0.710	0.00
DC-W-11	0.012	14.08		1.68		306	74.3	1.09	15.83	0.069	0.084	0.014	830	0.008	3.036	0.703	0.00
DR-W-1	0.007	10.50		1.42		240	62.9	1.06	10.95	0.062	0.090	0.009	627	0.012	n.d.	n.d.	0.00
DR-W-2	0.005	8.79		1.01		127	37.5	0.63	10.02	0.057	0.053	0.002	264	0.030	n.d.	n.d.	0.00
DR-W-3	0.008	9.05		0.97		132	39.1	0.66	10.39	0.051	0.033	0.003	285	0.000	n.d.	n.d.	0.00
DR-W-6	0.007	10.17		1.19		141	41.3	0.67	11.76	0.048	0.160	0.003	289	0.000	n.d.	n.d.	0.00
DR-W-7	0.019	136.53		2.05		297	38.3	0.19	230.42	0.282	0.141	0.011	657	0.000	n.d.	n.d.	0.00
DR-W-8	0.008	14.11	0.04	1.88		311	75.8	1.07	15.70	0.074	0.134	0.015	868	0.005	n.d.	n.d.	0.00
DR-W-9	0.007	10.89		1.18		150	42.3	0.69	13.12	0.059	0.074	0.001	317	0.309	n.d.	n.d.	0.00
DW-W-1	0.011	11.19	0.05	2.10		266	81.0	1.48	11.52	0.064	0.095	0.007	717	0.396	n.d.	n.d.	0.00

n.d. – not determined; **calculation: conc.($S_2O_3^{2-}{}_{cyanolysed(+\ KCN\ stabilisation)}$) – conc.($S_2O_3^{2-}{}_{uncyanolysed}$); *repeated measurement also showed wrong results: SnO_6^{2-} = -0.062 mg/L (0.006 — 0.068 = - 0.062)

Table A 9: ICP-MS results of water samples, in alphabetical order (laboratories of the chair for hydrogeology, TU Freiberg)

Element		**Ag**	**Al**	**As**	**B**	**Ba**	**Be**	**Bi**	**Br**	**Ca**	**Cd**	**Ce**	**Co**	**Cr**	**Cs**	**Cu**	**Dy**
Mode			2V	2V							2V		2V	2V		2V	
Unit		µg/L	**mg/L**	µg/L	µg/L	µg/L	µg/L	µg/L	µg/L	**mg/L**	µg/L	µg/L	µg/L	µg/L	µg/L	µg/L	µg/L
Detection limit	1:1	0.005	0.001	0.200	1.0	0.1	0.01	0.002	2.0	0.0	0.01	0.001	0.01	0.1	0.001	1.0	0.001
Detection limit	1:5	0.025	0.005	1.000	5.0	0.3	0.05	0.010	10.0	0.1	0.05	0.005	0.05	0.5	0.005	5.0	0.005
Detection limit	1:10	0.050	0.010	2.000	10.0	0.5	0.10	0.020	20.0	0.2	0.10	0.010	0.10	1.0	0.010	10.0	0.010
DC-W-1	1:1	0.005	0.01	0.536	70.1	27.7	< 0.01	0.034	67.2	309.8	0.09	4.60	0.16	< 0.1	0.034	< 1.0	0.008
DC-W-2	1:1	< 0.005	0.01	< 0.200	86.5	24.3	< 0.01	0.016	86.3	319.9	< 0.01	0.59	0.02	< 0.1	0.041	< 1.0	0.007
DC-W-3	1:1	< 0.005	5.53	0.605	72.7	30.3	0.19	0.010	74.6	533.8	0.07	8.20	1.49	14.6	0.172	< 1.0	0.653
DC-W-4	1:5	< 0.025	40.01	1.594	118.3	31.8	1.09	0.027	99.5	564.7	0.55	31.63	11.58	120.4	1.281	< 5.0	2.883
DC-W-5	1:1	< 0.005	0.14	< 0.200	85.3	23.1	< 0.01	0.004	84.7	316.7	< 0.01	2.34	0.06	0.3	0.035	< 1.0	0.015
DC-W-6	1:10	< 0.050	32.61	3.113	177.7	30.1	1.05	0.038	160.0	576.1	1.22	11.83	11.56	98.2	3.491	10.7	1.700
DC-W-7	1:1	< 0.005	0.00	< 0.200	91.3	22.9	< 0.01	0.002	81.6	315.4	< 0.01	0.04	0.02	< 0.1	0.034	< 1.0	0.006
DC-W-8	1:1	< 0.005	0.01	< 0.200	93.3	23.2	< 0.01	0.001	82.0	322.4	< 0.01	0.05	0.02	< 0.1	0.033	< 1.0	0.007
DC-W-9	1:1	< 0.005	0.01	0.564	73.7	25.9	< 0.01	< 0.002	64.3	300.6	0.01	0.03	0.15	< 0.1	0.013	< 1.0	0.005
DC-W-10	1:1	< 0.005	0.03	< 0.200	91.5	23.5	< 0.01	< 0.002	85.3	321.7	< 0.01	0.08	0.04	< 0.1	0.026	< 1.0	0.008
DC-W-11	1:1	< 0.005	0.04	< 0.200	88.4	23.2	< 0.01	< 0.002	82.3	314.1	< 0.01	0.06	0.05	0.1	0.030	< 1.0	0.008
DR-W-1	1:1	< 0.005	0.13	0.661	71.0	32.0	< 0.01	< 0.002	67.4	238.7	< 0.01	0.13	0.06	< 0.1	0.030	< 1.0	0.012
DR-W-2	1:1	< 0.005	0.03	< 0.200	48.5	48.8	< 0.01	< 0.002	55.9	127.5	< 0.01	0.03	0.02	< 0.1	0.009	< 1.0	0.003
DR-W-3	1:1	< 0.005	0.03	< 0.200	49.6	46.8	< 0.01	< 0.002	57.6	132.2	< 0.01	0.03	0.03	< 0.1	0.009	< 1.0	0.003
DR-W-6	1:1	< 0.005	0.03	< 0.200	51.5	45.4	< 0.01	< 0.002	59.4	139.6	< 0.01	0.03	0.01	< 0.1	0.009	< 1.0	0.003
DR-W-7	1:1	< 0.005	0.01	0.790	116.3	49.2	< 0.01	< 0.002	325.4	308.2	< 0.01	0.01	0.08	< 0.1	0.007	< 1.0	0.001
DR-W-8	1:1	< 0.005	0.04	0.534	90.5	29.7	< 0.01	< 0.002	84.0	320.4	< 0.01	0.21	0.15	0.1	0.009	< 1.0	0.019
DR-W-9	1:1	0.043	0.03	0.227	53.8	44.8	< 0.01	0.006	62.1	146.5	< 0.01	0.02	0.02	< 0.1	0.008	< 1.0	0.002
DW-W-1	1:1	< 0.005	0.00	< 0.200	76.3	20.9	< 0.01	< 0.002	66.9	274.1	< 0.01	0.02	0.02	0.2	0.001	< 1.0	0.001

Table A 10: ICP-MS (continuation I)

Element		Er	Eu	Fe	Ga	Gd	Ho	I	In	K	La	Li	Lu	Mg	Mn	Mo	Nd
Mode				3V						2V				2V	2V		
Unit		µg/L	µg/L	**mg/L**	µg/L	µg/L	µg/L	µg/L	µg/L	**mg/L**	µg/L	µg/L	µg/L	**mg/L**	µg/L	µg/L	µg/L
Detection limit	1:1	0.001	0.001	0.001	0.010	0.001	0.001	0.05	0.001	0.02	0.001	0.10	0.001	0.001	0.05	0.01	0.001
Detection limit	1:5	0.005	0.005	0.005	0.050	0.005	0.005	0.25	0.005	0.10	0.005	0.50	0.005	0.005	0.25	0.05	0.005
Detection limit	1:10	0.010	0.010	0.010	0.100	0.010	0.010	0.50	0.010	0.20	0.010	1.00	0.010	0.010	0.50	0.10	0.010
DC-W-1	1:1	0.005	0.009	0.03	0.048	0.036	0.002	9.20	0.022	3.04	10.250	8.61	0.001	61.0	19.4	12.25	0.040
DC-W-2	1:1	0.004	0.008	0.01	0.028	0.012	0.002	9.36	0.008	6.38	1.232	9.71	< 0.001	72.7	9.7	0.26	0.035
DC-W-3	1:1	0.349	0.217	7.41	0.216	0.970	0.131	8.65	0.007	6.18	5.424	11.84	0.034	67.3	109.0	3.33	3.995
DC-W-4	1:5	1.548	0.947	43.14	8.835	3.954	0.565	15.02	0.024	15.85	18.990	39.63	0.187	85.1	555.3	0.94	16.210
DC-W-5	1:1	0.008	0.011	0.16	0.042	0.033	0.003	9.08	0.003	24.43	4.746	9.71	0.001	70.4	12.2	0.37	0.091
DC-W-6	1:10	1.078	0.389	33.40	7.390	1.863	0.364	18.40	0.038	32.18	6.522	48.34	0.150	108.1	609.7	1.07	5.881
DC-W-7	1:1	0.003	0.008	0.01	0.021	0.006	0.001	9.59	< 0.001	1.99	0.024	10.02	< 0.001	73.3	9.4	0.65	0.022
DC-W-8	1:1	0.004	0.009	0.01	0.020	0.009	0.001	9.61	< 0.001	1.98	0.027	10.36	< 0.001	75.0	9.6	0.59	0.027
DC-W-9	1:1	0.003	0.009	0.02	0.024	0.006	0.001	7.62	< 0.001	1.74	0.020	8.80	< 0.001	61.0	19.3	11.32	0.019
DC-W-10	1:1	0.005	0.009	0.03	0.024	0.010	0.002	9.74	< 0.001	1.98	0.039	10.29	0.001	74.3	12.4	0.82	0.037
DC-W-11	1:1	0.005	0.009	0.03	0.026	0.009	0.002	9.63	< 0.001	2.14	0.035	9.84	< 0.001	72.3	21.6	1.11	0.035
DR-W-1	1:1	0.007	0.013	0.09	0.072	0.019	0.002	8.08	0.001	1.47	0.076	7.84	0.001	60.8	13.7	5.64	0.068
DR-W-2	1:1	0.002	0.014	0.01	0.026	0.005	0.001	7.40	< 0.001	1.00	0.018	5.77	< 0.001	35.8	4.2	0.28	0.018
DR-W-3	1:1	0.002	0.014	0.02	0.025	0.005	0.001	7.36	< 0.001	1.07	0.015	5.86	< 0.001	36.3	5.6	0.35	0.014
DR-W-6	1:1	0.002	0.014	0.02	0.028	0.005	0.001	7.37	< 0.001	1.00	0.015	6.06	< 0.001	38.2	5.8	0.61	0.016
DR-W-7	1:1	0.001	0.015	0.01	< 0.010	0.003	< 0.001	3.34	0.001	2.26	0.004	18.38	< 0.001	35.7	5.4	1.61	0.007
DR-W-8	1:1	0.010	0.015	0.15	0.020	0.028	0.004	10.08	< 0.001	2.11	0.106	10.06	0.001	74.2	31.4	3.86	0.107
DR-W-9	1:1	0.001	0.014	0.02	0.028	0.003	0.001	7.53	< 0.001	1.08	0.008	6.33	< 0.001	39.7	6.5	0.60	0.009
DW-W-1	1:1	0.001	0.006	0.27	0.012	0.001	< 0.001	7.76	< 0.001	2.03	0.005	9.29	< 0.001	80.4	51.4	0.07	0.007

Table A 11: ICP-MS results (continuation II)

Element		Ni	P	Pb	Pr	Rb	S	Sb	Sc	Se	Si	Sm	Sn	Sr	Tb	Te
Mode		2V	2V				2V		2V	1V	2V					
Unit		µg/L	µg/L	µg/L	µg/L	µg/L	**mg/L**	µg/L	µg/L	µg/L	**mg/L**	µg/L	µg/L	**mg/L**	µg/L	µg/L
Detection limit	1:1	0.10	10.00	0.01	0.001	0.005	0.5	0.010	0.10	0.5	0.10	0.001	0.05	0.00002	0.001	0.010
Detection limit	1:5	0.50	50.00	0.05	0.005	0.025	2.5	0.050	0.50	2.5	0.50	0.005	0.25	0.00010	0.005	0.050
Detection limit	1:10	1.00	100.00	0.10	0.010	0.050	5.0	0.100	1.00	5.0	1.00	0.010	0.50	0.00020	0.010	0.100
DC-W-1	1:1	1.65	28.96	0.49	0.010	1.81	304.7	0.217	0.22	< 0.5	8.34	0.009	< 0.05	4.33	0.002	< 0.010
DC-W-2	1:1	0.24	17.30	< 0.01	0.008	2.01	351.2	< 0.010	0.25	< 0.5	8.58	0.009	< 0.05	5.20	0.001	< 0.010
DC-W-3	1:1	25.18	347.10	0.27	0.973	5.51	610.3	0.095	0.47	< 0.5	14.80	0.873	0.11	4.64	0.121	< 0.010
DC-W-4	1:5	101.30	2489.00	6.07	3.919	40.40	1468.0	0.832	1.42	< 2.5	59.01	3.841	< 0.25	4.39	0.534	< 0.050
DC-W-5	1:1	0.76	39.29	0.02	0.022	2.35	333.9	< 0.010	0.26	< 0.5	9.07	0.019	< 0.05	4.82	0.003	< 0.010
DC-W-6	1:10	107.70	5393.00	5.79	1.462	61.23	3805.0	0.539	2.68	< 5.0	50.43	1.428	< 0.50	4.22	0.292	< 0.100
DC-W-7	1:1	0.21	24.67	< 0.01	0.005	1.84	437.9	< 0.010	0.27	< 0.5	9.14	0.005	< 0.05	4.94	0.001	< 0.010
DC-W-8	1:1	0.22	17.28	< 0.01	0.006	1.88	436.4	< 0.010	0.28	< 0.5	9.33	0.006	< 0.05	5.06	0.001	< 0.010
DC-W-9	1:1	1.49	16.78	< 0.01	0.004	1.72	313.4	0.367	0.23	< 0.5	8.97	0.005	< 0.05	4.09	0.001	< 0.010
DC-W-10	1:1	0.38	21.02	< 0.01	0.008	1.88	340.4	< 0.010	0.29	< 0.5	9.47	0.008	< 0.05	4.99	0.001	< 0.010
DC-W-11	1:1	0.74	23.25	< 0.01	0.008	1.94	330.8	0.134	0.26	< 0.5	9.31	0.008	< 0.05	4.84	0.001	< 0.010
DR-W-1	1:1	0.37	23.40	< 0.01	0.016	1.47	249.3	0.049	0.26	< 0.5	8.66	0.016	< 0.05	3.72	0.002	< 0.010
DR-W-2	1:1	0.15	< 10.00	< 0.01	0.004	0.75	242.8	0.011	0.15	< 0.5	6.81	0.004	< 0.05	2.69	0.001	< 0.010
DR-W-3	1:1	0.24	14.64	< 0.01	0.003	0.80	169.3	0.059	0.15	< 0.5	6.82	0.004	< 0.05	2.72	< 0.001	< 0.010
DR-W-6	1:1	0.10	13.62	< 0.01	0.003	0.80	129.5	< 0.010	0.16	< 0.5	6.99	0.004	< 0.05	2.79	< 0.001	< 0.010
DR-W-7	1:1	0.69	21.34	< 0.01	0.001	0.56	266.8	0.797	0.29	< 0.5	9.95	0.002	< 0.05	4.37	< 0.001	0.019
DR-W-8	1:1	0.51	33.07	< 0.01	0.024	1.71	355.5	0.305	0.30	< 0.5	10.00	0.024	< 0.05	4.88	0.003	< 0.010
DR-W-9	1:1	0.15	14.61	< 0.01	0.002	0.85	142.6	< 0.010	0.15	< 0.5	7.24	0.002	< 0.05	2.90	< 0.001	< 0.010
DW-W-1	1:1	0.16	22.87	< 0.01	0.001	1.77	473.1	< 0.010	0.25	< 0.5	11.34	0.002	< 0.05	4.56	< 0.001	< 0.010

Table A 12: ICP-MS results (continuation III)

Element		Th	Tl	Tm	U	V	Y	Yb	Zn
Mode						2V			2V
Unit		µg/L	µg/L	µg/L	µg/L	µg/L	µg/L	µg/L	µg/L
Detection limit	1:1	0.001	0.001	0.001	0.001	0.10	0.001	0.001	1.00
Detection limit	1:5	0.005	0.005	0.005	0.005	0.50	0.005	0.005	5.00
Detection limit	1:10	0.010	0.010	0.010	0.010	1.00	0.010	0.010	10.00
DC-W-1	1:1	0.001	0.196	0.001	4.841	1.65	0.11	0.004	22.72
DC-W-2	1:1	< 0.001	0.041	< 0.001	1.908	0.65	0.10	0.003	22.50
DC-W-3	1:1	0.014	0.081	0.041	3.088	7.42	4.61	0.241	68.56
DC-W-4	1:5	0.251	0.112	0.199	1.188	63.60	16.03	1.285	173.90
DC-W-5	1:1	0.001	0.076	0.001	2.110	0.93	0.14	0.006	17.91
DC-W-6	1:10	0.700	0.129	0.149	1.117	83.42	11.82	0.969	292.70
DC-W-7	1:1	< 0.001	0.002	< 0.001	1.821	0.61	0.09	0.003	48.80
DC-W-8	1:1	< 0.001	0.002	0.001	1.873	0.72	0.10	0.003	44.56
DC-W-9	1:1	< 0.001	0.004	< 0.001	4.660	1.51	0.08	0.003	81.91
DC-W-10	1:1	< 0.001	0.002	< 0.001	2.082	0.92	0.10	0.004	27.69
DC-W-11	1:1	0.001	0.002	0.001	1.962	1.02	0.09	0.003	17.62
DR-W-1	1:1	0.002	0.002	0.001	1.379	0.90	0.11	0.005	48.44
DR-W-2	1:1	< 0.001	< 0.001	< 0.001	0.514	0.60	0.04	0.002	27.95
DR-W-3	1:1	< 0.001	< 0.001	< 0.001	0.552	0.56	0.04	0.001	21.59
DR-W-6	1:1	< 0.001	< 0.001	< 0.001	0.610	0.51	0.04	0.001	19.26
DR-W-7	1:1	< 0.001	0.003	< 0.001	0.868	1.54	0.03	0.001	137.10
DR-W-8	1:1	0.004	0.002	0.001	1.801	0.73	0.17	0.008	31.22
DR-W-9	1:1	< 0.001	0.001	< 0.001	0.643	0.50	0.03	0.001	16.99
DW-W-1	1:1	< 0.001	< 0.001	< 0.001	0.261	< 0.1	0.03	< 0.001	58.98

Table A 13: RFA results of rock samples (laboratories of the chair for hydrogeology, TU Freiberg)

Sample ID	Ca	S	Mg	Si	Fe	Ag	Al	As	Ba	Bi	Br	Cd	Ce	Cl	Co	Cr	Cs
	g/kg	g/kg	g/kg	g/kg	g/kg	g/kg	g/kg	g/kg	g/kg	g/kg	g/kg	g/kg	g/kg	g/kg	g/kg	g/kg	g/kg
DS-PL-1	393	0.069	1.182	0.5281	0.0795	0.0155	<0.02	<0.0005	<0.002	<0.001	0.0014	<0.002	<0.002	0.0247	<0.003	<0.001	<0.004
DS-PL-3	359.9	0.8164	6.414	22.29	4.111	0.00018	6.902	0.0034	0.1285	<0.001	0.0016	<0.002	0.113	0.1215	<0.003	<0.001	<0.004
DS-PG-2b	292.8	209.3	19.18	2.806	0.5171	<0.002	<0.02	<0.0003	<0.002	<0.001	0.0012	<0.002	<0.002	0.2191	<0.003	<0.001	<0.004
DS-PG-4	247.1	178.2	17.47	3.913	0.7975	0.0085	<0.02	<0.0005	0.0403	<0.001	0.0005	<0.002	<0.002	0.2436	<0.003	<0.001	<0.004
DS-PL-5	368.5	0.5715	7.101	12.88	1.118	<0.002	3.14	<0.0004	0.2865	<0.001	0.0217	<0.002	<0.002	0.1003	<0.003	<0.001	<0.004
DC-SG-1	242.7	180.8	18.98	1.638	<0.001	<0.002	<0.02	<0.0005	0.0339	<0.001	0.0012	<0.002	<0.002	0.2177	<0.003	<0.001	<0.004
DC-SG-9a	239.6	178.6	18.06	2.768	<0.001	<0.0029	<0.02	<0.0005	0.0398	<0.001	0.0009	<0.002	<0.002	0.2435	<0.003	<0.001	<0.004
DC-SG-9c	293.6	212.8	17.59	5.134	<0.001	0.0106	<0.02	<0.0005	0.0245	<0.001	0.0009	<0.002	<0.002	0.2154	<0.003	<0.001	<0.004
DC-SG- 9b	283.4	219.3	19.05	1.962	0.0031	0.0088	<0.02	<0.0005	<0.002	<0.001	0.0013	<0.002	<0.002	0.1724	<0.003	<0.001	<0.004
DC-SG-9e	295.3	220.2	19.76	3.234	<0.001	0.0071	<0.02	<0.0005	0.0452	<0.001	0.0013	<0.002	<0.002	0.144	<0.003	<0.001	<0.004
DC-SG-14b	242.6	176.2	16.25	2.472	<0.001	<0.002	<0.02	<0.0005	0.0476	<0.001	0.0011	<0.002	<0.002	0.1699	<0.003	<0.001	<0.004
DC-SG-14c	240.5	180.8	18.44	2.182	<0.001	0.0146	<0.02	<0.0005	0.0343	<0.001	0.001	<0.002	<0.002	0.1676	<0.003	<0.001	<0.004
DC-SG-13a	121.4	154.4	7.35	245.6	0.3234	<0.002	<0.02	<0.0005	0.4716	<0.001	0.001	<0.002	<0.002	0.1341	<0.003	0.2078	<0.004
DC-SG-13b	213.2	178.1	11.97	120.2	0.1764	<0.002	<0.02	<0.0005	0.1767	<0.001	0.0011	<0.002	<0.002	0.141	<0.003	0.0991	<0.004
DC-SG-13c	288.7	209.8	16.91	25.16	0.9004	0.0095	<0.02	<0.0005	0.0449	<0.001	0.0008	<0.002	<0.002	0.1459	<0.003	<0.001	<0.004
DC-SG-15	244.5	182.7	18.02	4.796	<0.001	0.0056	<0.02	<0.0005	<0.002	<0.001	0.0011	<0.002	<0.002	0.2219	<0.003	<0.001	<0.004
DC-PL-15	393.1	1.765	1.341	1.476	0.4318	0.0038	0.3404	<0.0005	0.0368	<0.001	0.0009	<0.002	<0.002	0.0235	<0.003	<0.001	<0.004
DC-PL-16	389.2	4.967	1.535	2.196	8.361	<0.002	0.756	0.0035	<0.002	<0.001	0.0013	<0.002	<0.002	0.0539	<0.003	0.0053	<0.004
DR-C-9	84.02	0.7075	24.35	258.9	40.71	<0.002	73.98	0.0051	0.1728	<0.001	0.0007	<0.002	<0.002	0.062	0.0143	0.0617	<0.004

Table A 14: RFA results of rock samples (continuation I)

Sample ID	Cu	Ga	Ge	Hf	Hg	I	K	La	Mn	Mo	Nb	Ni	P	Pb	Rb	Sb
	g/kg	g/kg	g/kg	g/kg	g/kg	g/kg	g/kg	g/kg	g/kg	g/kg	g/kg	g/kg	g/kg	g/kg	g/kg	g/kg
DS-PL-1	<0.0004	0.0024	<0.0005	<0.001	<0.001	0.0102	<0.01	0.0263	0.0395	0.0134	<0.001	<0.0005	<0.003	0.0034	0.001	0.0115
DS-PL-3	0.0054	0.0035	<0.0005	<0.001	<0.001	0.0162	1.99	0.0618	0.1565	0.0107	<0.001	<0.0005	0.0687	0.0039	0.0094	0.0121
DS-PG-2b	<0.0011	<0.0005	<0.0005	<0.0016	<0.001	0.0231	0.63	<0.002	0.0068	0.0107	<0.001	0.0065	<0.03	0.0045	0.0024	0.0177
DS-PG-4	<0.0001	0.0011	<0.0005	<0.001	<0.001	<0.003	0.902	<0.002	0.0108	0.0113	<0.001	0.0025	<0.03	0.0019	0.0021	0.0112
DS-PL-5	0.0025	0.0017	<0.0005	<0.001	<0.001	0.0161	0.783	0.0965	0.2152	0.0113	<0.001	<0.0005	0.0984	0.0027	0.0037	0.0153
DC-SG-1	<0.0005	0.0011	<0.0003	<0.001	<0.001	0.0113	0.407	<0.002	<0.001	0.0125	<0.001	0.0026	<0.03	0.0016	0.001	0.0062
DC-SG-9a	<0.0005	0.0012	<0.0005	<0.001	<0.001	0.0133	0.557	<0.002	<0.001	0.0092	<0.001	0.0028	<0.03	0.001	0.0009	0.0139
DC-SG-9c	<0.0005	<0.0005	<0.0005	<0.001	<0.0006	0.0228	0.303	<0.002	<0.0005	0.0123	<0.001	0.0027	<0.03	0.0032	0.0014	0.0165
DC-SG- 9b	<0.0005	<0.0005	<0.0005	<0.0015	<0.001	0.0188	0.506	<0.002	<0.001	0.0117	<0.001	0.0043	<0.03	0.0035	0.0016	0.0158
DC-SG-9e	<0.0009	0.0021	<0.0005	<0.001	<0.001	0.0218	0.524	<0.002	<0.0015	0.0119	<0.001	0.0028	<0.03	0.0035	0.0012	0.0193
DC-SG-14b	<0.0002	0.0013	<0.0005	<0.001	<0.001	0.0131	0.51	<0.002	<0.0015	0.0141	<0.001	0.0036	<0.03	0.003	0.0011	0.0125
DC-SG-14c	<0.0005	<0.0005	<0.0005	<0.0013	<0.001	0.0103	0.552	<0.002	<0.001	0.0144	<0.001	0.004	<0.03	0.0021	0.0008	0.0049
DC-SG-13a	0.0025	0.0016	<0.0005	0.0059	<0.001	0.0032	0.263	<0.002	0.0134	0.0088	0.0096	0.0125	<0.03	0.0126	0.0014	0.0078
DC-SG-13b	<0.0013	0.0014	<0.0005	0.0012	<0.001	0.0137	0.372	0.0816	<0.001	0.0108	0.0025	0.0055	<0.03	0.0059	0.001	0.0139
DC-SG-13c	<0.0005	<0.0009	<0.0005	<0.001	<0.001	0.019	0.353	0.0592	0.0095	0.0116	<0.001	0.0033	<0.03	0.0027	0.0013	0.0147
DC-SG-15	<0.0005	0.0013	<0.0005	<0.001	<0.001	0.0179	0.39	<0.002	<0.0019	0.0135	<0.001	0.0015	<0.03	0.0024	0.001	0.011
DC-PL-15	<0.0012	0.0014	<0.0005	<0.001	<0.001	0.0186	<0.01	<0.002	0.0553	0.0119	<0.001	<0.0005	0.0272	0.0035	0.0013	0.0157
DC-PL-16	<0.0005	0.0014	<0.0005	<0.001	<0.001	0.0209	<0.01	<0.002	0.098	0.0466	<0.001	0.0319	0.0582	0.0027	0.0016	0.0162
DR-C-9	0.0122	0.0178	0.0008	0.0023	<0.001	0.0067	23.17	0.0779	0.5583	0.0075	0.0089	0.0558	0.7608	0.0072	0.098	<0.003

Table A 15: RFA results of rock samples (continuation II)

Sample ID	Se	Sn	Sr	Ta	Te	Th	Ti	Tl	U	V	W	Y	Zn	Zr
	g/kg	g/kg	g/kg	g/kg	g/kg	g/kg	g/kg	g/kg	g/kg	g/kg	g/kg	g/kg	g/kg	g/kg
DS-PL-1	<0.0005	0.0075	0.1337	0.064	0.0086	0.0029	<0.002	<0.001	<0.001	<0.031	0.0012	0.001	0.007	<0.001
DS-PL-3	<0.0005	0.0087	0.3681	0.0609	0.0082	0.0017	0.474	<0.0004	<0.001	<0.018	0.0009	0.0028	0.0215	0.0103
DS-PG-2b	<0.0005	0.0168	1.005	0.0779	0.0164	0.0021	0.08	0.0016	<0.0007	<0.035	<0.0012	0.0016	0.0118	<0.001
DS-PG-4	<0.0005	0.0034	1.1	0.0722	0.0036	<0.0004	0.0555	0.0005	<0.001	<0.021	<0.001	0.0009	0.0075	<0.001
DS-PL-5	<0.0005	0.0143	0.7159	0.0654	0.0159	0.002	0.273	<0.0002	<0.001	0.0995	<0.001	0.0026	0.0098	<0.0103
DC-SG-1	<0.0005	0.006	0.0515	0.0622	0.0118	0.0033	<0.002	0.0009	<0.001	<0.023	<0.001	0.0008	0.0068	<0.001
DC-SG-9a	<0.0005	0.0089	0.0614	0.0634	0.0118	0.0031	<0.002	0.0008	<0.001	<0.021	0.0015	<0.0005	0.0066	<0.001
DC-SG-9c	<0.0005	0.0129	0.0714	0.0716	0.017	0.0034	<0.002	0.0015	<0.001	<0.027	0.0021	0.0009	0.008	<0.001
DC-SG- 9b	<0.0005	0.012	0.1405	0.0714	0.015	0.0036	0.0251	0.0018	<0.001	<0.043	0.0025	0.0019	0.008	<0.001
DC-SG-9e	<0.0005	0.0173	0.0829	0.0648	0.0195	0.0033	0.0334	0.0016	<0.001	<0.030	<0.001	0.0011	0.0083	0.00003
DC-SG-14b	<0.0005	0.0093	0.0431	0.0628	0.0038	0.0027	0.0279	0.0013	<0.001	<0.020	0.0011	0.0008	0.0066	<0.001
DC-SG-14c	<0.0005	0.0042	0.0386	0.0656	0.007	0.0027	0.022	0.0012	<0.001	<0.022	0.0023	0.0009	0.0067	<0.0002
DC-SG-13a	<0.0005	0.0053	0.1093	0.0629	0.0063	0.0042	3.667	0.0011	0.0007	<0.0066	0.0036	0.0095	0.0089	0.2022
DC-SG-13b	<0.0005	0.0109	0.1019	0.0632	0.0098	0.0034	1.454	0.001	<0.001	<0.014	0.0012	0.0046	0.0103	0.0593
DC-SG-13c	<0.0005	0.0109	0.1173	0.0691	0.0099	0.0027	0.266	0.0008	<0.001	<0.024	<0.001	0.0025	0.0073	0.007
DC-SG-15	<0.0005	0.0029	0.3544	0.0703	0.0094	0.0025	<0.0035	0.0013	<0.001	<0.029	0.0011	0.0009	0.0067	<0.001
DC-PL-15	<0.0005	0.0145	0.1309	0.0667	0.0123	0.0025	<0.002	0.0011	<0.001	<0.024	0.001	0.0015	0.007	<0.001
DC-PL-16	0.0097	0.0125	0.1554	0.063	0.0173	0.0019	<0.018	<0.001	<0.001	<0.031	<0.0013	0.0018	0.0236	<0.001
DR-C-9	<0.0005	0.0011	0.2318	0.0621	0.0038	0.0089	5.173	<0.0004	<0.0005	0.095	0.0008	0.0205	0.089	0.1348

Table A 16: ICP-MS results of precipitations on water surfaces (results have to be taken with caution since analytical correctness cannot be ensured due to very little sample sizes); after analysing results were counted back from mg/L to mg/g (laboratories of the chair for hydrogeology, TU Freiberg)

Sample ID	**Ag**	**Al**	**As**	**B**	**Ba**	**Be**	**Bi**	**Br**	**Ca**	**Cd**	**Co**	**Cr**
Mode		2V	2V							2V	2V	2V
Unit	mg/g	mg/g	mg/g	mg/g	mg/g	mg/g	mg/g	mg/g	mg/g	mg/g	mg/g	mg/g
Detection limit (1:2)	0.00002	0.004	0.0008	0.004	0.0002	0.00004	0.00001	0.008	0.08	0.00004	0.00004	0.0004
DC-P-16 (1:2)	0.00002	4.36	< 0.0008	0.183	0.049	0.00006	< 0.00001	8.214	31.1	0.0006	0.0015	0.012
DC-P-2 (1:2)	0.00004	0.34	0.0015	0.189	0.062	< 0.00004	< 0.00001	0.168	154.1	0.0009	0.0002	0.001

Sample ID	**Cu**	**Fe**	**Ga**	**In**	**K**	**Li**	**Mg**	**Mn**	**Mo**	**Na**	**Ni**	**P**
Mode	2V	3V			2V		2V	2V		2V	2V	2V
Unit	mg/g	mg/g	mg/g	mg/g	mg/g	mg/g	mg/g	mg/g	mg/g	mg/g	mg/g	mg/g
Detection limit (1:2)	0.004	0.004	0.00004	0.000004	0.08	0.0004	0.004	0.0002	0.00004	0.02	0.0004	0.04
DC-P-16 (1:2)	0.058	4.00	0.00052	0.00001	5.40	0.0028	2.93	0.078	0.0005	1.56	0.05	0.70
DC-P-2 (1:2)	0.016	0.14	0.00005	< 0.000004	0.93	0.0006	1.38	0.041	0.0022	1.77	0.02	0.08

Sample ID	**Pb**	**Rb**	**S**	**Se**	**Si**	**Sr**	**Te**	**Tl**	**U**	**V**	**Zn**
Mode			2V	1V	2V					2V	2V
Unit	mg/g	mg/g	mg/g	mg/g	mg/g	mg/g	mg/g	mg/g	mg/g	mg/g	mg/g
Detection limit (1:2)	0.00004	0.00002	2.0	0.002	0.4	0.00008	0.00004	0.000004	0.000004	0.0004	0.004
DC-P-16 (1:2)	0.011	0.003	40.9	0.003	1.36	0.09	< 0.00004	0.00001	0.0004	0.009	0.29
DC-P-2 (1:2)	0.003	0.001	4.7	0.003	1.63	0.88	< 0.00004	0.00001	0.0004	0.002	0.13

Table A 17: Modelling with PhreeqC: List of input parameters for calculations based on llnl.dat and for calculations based on PhreeqC.dat

Database	Input parameters
llnl.dat	pH, pe, temp, Na, Ca, K, N(-3) as NH_4^+, Mg, Mn, Fe, Cl, N(+5) as NO_3^-, N(+3) as NO_2^-, S(6) as SO_4^{2-}, S(+4) as SO_3^{2-}, S(-2), S(+2) as $S_2O_3^{2-}$, P as PO_4, C(4) as C, C(-4) as CH_4, C(-3) as C_2H_6, C(-2) as C_2H_4, F, Al, Si as SO_2, Li, Be, B, Sr, Co, Ni, Cu, Zn, Cr, As, Br, Mo, Cd, Ba, Pb, U
phreeqc.dat	pH, pe, Na, Ca, K, Mg, Mn, Fe, Cl, N(+5) as NO_3^-, N(+3) as NO_2^-, S(6) as SO_4^{2-}, S(-2), P as PO_4, C(4) as C, C(-4) as CH_4, F, Al, Si as SO_2, Li, B, Sr, Cu, Zn, Br, Cd, Ba, Pb

Table A 18: Cluster analyses: List of input parameters for clustering of water samples (grey labelled variables were excluded from cluster analysis)

n	Input parameter
49/(36)	in-situ parameter (pH, E_H, EC, T, O_2), N species (NH_4^+, NO_3^-, NO_2^-), S species (SO_4^{2-}, SO_3^{2-}, S^{2-}), C species (HCO_3^-, CO_2, $CaHCO_3^+$, $MgHCO_3^+$, $CaCO_3^0$, CO_3^{2-}, $MgCO_3$), Fe species (Fe^{2+}, $FeHCO_3^+$, $FeCO_3^0$, $FeSO_4^0$, $Fe(OH)_3^0$), Na, Ca, K, Mg, Mn, PO_4, Cl, F, Al, SiO_2, Li, Be, B, Sr, Co, Ni, Cu, Zn, Cr, As, Br, Mo, Cd, Ba, Pb, U.

Table A 19: Agglomeration Schedule of cluster analysis (Ward' method, squared Euclidian distances, 0-1 standardisation)

Agglomeration Schedule						
Stage i	Cluster Combined			Stage Cluster First Appears		
	Cluster 1	Cluster 2	Coefficients $\hat{a}_i$	Cluster 1	Cluster 2	Next Stage
1	7	8	0	0	0	5
2	13	14	0	0	0	9
3	10	11	0.01	0	0	8
4	1	9	0.01	0	0	13
5	2	7	0.02	0	1	12
6	12	17	0.03	0	0	10
7	15	18	0.04	0	0	9
8	5	10	0.06	0	3	10
9	13	15	0.1	2	7	15
10	5	12	0.14	8	6	12
11	4	6	0.21	0	0	18
12	2	5	0.31	5	10	14
13	1	3	0.42	4	0	16
14	2	19	0.58	12	0	16
15	13	16	0.77	9	0	17
16	1	2	0.97	13	14	17
17	1	13	1.28	16	15	18
18	1	4	2.35	17	11	0

Table A 20: Cluster Memberships according to different levels of clustering (bold number represent the selected classification)

	Cluster Membership						
Case	**8 Cluster**	**7 Cluster**	**6 Cluster**	**5 Cluster**	**4 Cluster**	**3 Cluster**	**2 Cluster**
DC-W-1	**1**	1	1	1	1	1	1
DC-W-2	**2**	2	2	2	2	1	1
DC-W-3	**3**	3	1	1	1	1	1
DC-W-4	**4**	4	3	3	3	2	2
DC-W-5	**5**	2	2	2	2	1	1
DC-W-6	**4**	4	3	3	3	2	2
DC-W-7	**2**	2	2	2	2	1	1
DC-W-8	**2**	2	2	2	2	1	1
DC-W-9	**1**	1	1	1	1	1	1
DC-W-10	**5**	2	2	2	2	1	1
DC-W-11	**5**	2	2	2	2	1	1
DR-W-1	**5**	2	2	2	2	1	1
DR-W-2	**6**	5	4	4	4	3	1
DR-W-3	**6**	5	4	4	4	3	1
DR-W-6	**6**	5	4	4	4	3	1
DR-W-7	**7**	6	5	5	4	3	1
DR-W-8	**5**	2	2	2	2	1	1
DR-W-9	**6**	5	4	4	4	3	1
DW-W-1	**8**	7	6	2	2	1	1

Table A 21: Calculation of errors and conclusions from the charge balance error and the comparison of recorded to modelled conductivity

Sample ID	EC_{Rec}	EC_{model}	EC_{RD}	Error	Error*2	Ionic strength	Electrical balance	Conclusion
	µS/cm	µS/cm	%	%	%	mol/kg	mol/kg	
DC-W-1	1583	1514	2.23	-1.35	-2.69	0.0286	-0.0004	deficiency of cations
DC-W-2	1730	1652	2.31	-0.6	-1.19	0.0312	-0.0002	deficiency of cations
DC-W-3	2840	2590	4.6	-3.15	-6.3	0.0504	-0.0016	deficiency of cations
DC-W-4	13340	14559	4.37	-1.46	-2.92	0.0968	-0.0018	surplus of anions
DC-W-5	1710	1623	2.61	-4.42	-8.85	0.0302	-0.0014	deficiency of cations
DC-W-6	42700	43596	1.04	-4.54	-9.09	0.204	-0.0143	surplus of anions
DC-W-7	1725	1604	3.63	2.9	5.8	0.0303	0.0009	deficiency of anions
DC-W-8	1740	1671	2.02	-1.74	-3.48	0.0315	-0.0006	deficiency of cations
DC-W-9	1589	1531	1.86	1.51	3.02	0.0291	0.0005	deficiency of anions
DC-W-10	1707	1657	1.49	-1.72	-3.45	0.0311	-0.0006	deficiency of cations
DC-W-11	1702	1630	2.16	1.13	2.25	0.0308	0.0004	deficiency of anions
DR-W-1	1395	1359	1.31	1.88	3.76	0.0252	0.0005	deficiency of anions
DR-W-2	850	875	1.45	-1.9	-3.8	0.015	-0.0003	surplus of anions
DR-W-3	892	895	0.17	-0.87	-1.75	0.0154	-0.0002	surplus of anions
DR-W-6	931	926	0.27	1.22	2.44	0.0161	0.0002	deficiency of anions
DR-W-7	2092	2067	0.6	1.21	2.43	0.0329	0.0005	deficiency of anions
DR-W-8	1656	1652	0.12	1.94	3.87	0.0314	0.0007	deficiency of anions
DR-W-9	981	976	0.26	0.28	0.55	0.017	0.0001	deficiency of anions
DW-W-1	1605	1570	1.1	0.45	0.9	0.0291	0.0001	deficiency of anions

Table A 22: Saturation indices of selected mineral phases for all water samples calculated with PhreeqC (llnl.dat)

Cluster ID	Sample ID	Calcite $CaCO_3^0$	Aragonite $CaCO_3^0$	Dolomite $CaMg(CO_3)_2^0$	Magnesite $MgCO_3^0$	Siderite $FeCO_3^0$	Anhydrite $CaSO_4^0$	Gypsum $CaSO_4^0 *H_2O$	Sulphur S^0	Pyrite FeS_2^0	Sphalerite ZnS^0	Quartz SiO_2^0
I-1	DC-W-1	0.34	0.19	1.37	-0.61	-2.04	-0.69	-0.49	1.72	-4.57	0.54	0.21
	DC-W-9	0.36	0.21	1.40	-0.60	-2.61	-0.68	-0.48	2.38	-11.65	-2.64	0.24
I-2	DC-W-2	0.10	-0.05	0.93	-0.79	-2.74	-0.61	-0.44	0.44	4.23	5.46	0.16
	DC-W-7	-0.26	-0.41	0.22	-1.14	-3.18	-0.63	-0.46	-1.95	4.00	5.32	0.19
	DC-W-8	-0.05	-0.19	0.65	-0.92	-2.98	-0.61	-0.44	0.26	4.39	5.68	0.20
I-3	DC-W-3	-7.23	-7.38	-13.97	-8.38	-7.22	-0.27	-0.05	-5.13	5.63	0.61	0.49
I-4	DC-W-4	-10.93	-11.08	-21.32	-12.03	-10.17	-0.24	-0.02	3.01	3.55	-2.66	1.10
	DC-W-6	-12.04	-12.18	-23.43	-13.04	-11.42	-0.21	0.01	-0.25	-0.42	-5.28	1.03
I-5	DC-W-5	0.81	0.66	2.39	-0.05	-0.81	-0.66	-0.48	1.37	1.09	3.68	0.20
	DC-W-10	1.16	1.02	3.03	0.25	-1.35	-0.63	-0.45	1.38	-0.67	3.65	0.21
	DC-W-11	1.19	1.05	3.12	0.30	-1.27	-0.64	-0.46	1.39	-1.69	2.91	0.21
	DR-W-1	0.62	0.48	2.01	-0.24	-1.34	-0.81	-0.62	2.02	-6.57	-0.20	0.21
	DR-W-8	0.38	0.24	1.50	-0.51	-1.26	-0.62	-0.44	0.87	1.11	3.44	0.24
I-8	DW-W-1	0.06	-0.09	0.95	-0.72	-1.34	-0.73	-0.57	0.80	8.40	7.32	0.27
II-6	DR-W-2	0.14	0.00	1.11	-0.67	-2.27	-1.32	-1.11	1.08	3.67	5.49	0.14
	DR-W-3	0.30	0.15	1.43	-0.51	-2.06	-1.28	-1.07	1.18	2.47	4.84	0.13
	DR-W-6	0.61	0.46	2.04	-0.22	-1.81	-1.27	-1.05	0.87	3.82	5.88	0.16
	DR-W-9	0.71	0.57	2.23	-0.13	-1.70	-1.22	-1.00	1.28	1.02	4.29	0.19
II-7	DR-W-7	0.91	0.76	2.25	-0.33	-5.27	-0.80	-0.55	2.92	-19.24	-4.34	0.40

Table A 23: Saturation indices of selected mineral phases for all water samples calculated with PhreeqC (llnl.dat) (continuation I); chemical formula of clay minerals are given below the table

Cluster ID	Sample ID	Halite	Kaolinite	Illite	Montmorillonite-Ca	Gibbsite		Boehmite	Diaspore	Goethite	Hematite	Magnetite
		NaCl				$Al(OH)_3^0$	$Fe(OH)_3^0$	$AlOOH^0$	$AlOOH^0$	$FeOOH^0$	$Fe_2O_3^0$	$Fe_3O_4^0$
I-1	DC-W-1	-8.49	3.68	3.13	3.23	1.28	-1.91	1.46	1.86	3.23	7.44	4.70
	DC-W-9	-8.53	4.05	3.52	3.60	1.44	-0.32	1.62	2.02	4.82	10.61	7.28
I-2	DC-W-2	-8.30	3.87	2.98	3.06	1.42	-6.29	1.61	2.02	-1.19	-1.40	-5.09
	DC-W-7	-8.27	3.21	1.87	2.21	1.06	-8.38	1.26	1.66	-3.29	-5.58	-10.06
	DC-W-8	-8.28	3.59	2.49	2.71	1.24	-7.03	1.44	1.84	-1.93	-2.88	-7.07
I-3	DC-W-3	-8.47	-4.49	-10.23	-6.93	-3.08	-14.76	-2.91	-2.50	-9.60	-18.23	-26.51
I-4	DC-W-4	-8.28	-12.08	-19.89	-13.61	-7.48	-13.48	-7.32	-6.91	-8.31	-15.65	-26.77
	DC-W-6	-7.85	-15.75	-24.49	-17.34	-9.25	-15.46	-9.08	-8.67	-10.30	-19.63	-31.96
I-5	DC-W-5	-8.29	5.20	5.32	4.93	2.04	-1.68	2.24	2.64	3.42	7.83	6.73
	DC-W-10	-8.28	3.28	3.46	3.64	1.07	-1.60	1.26	1.66	3.50	7.99	6.58
	DC-W-11	-8.28	3.40	3.63	3.81	1.13	-1.12	1.33	1.73	3.99	8.97	7.71
	DR-W-1	-8.56	5.59	5.51	5.06	2.24	-0.13	2.43	2.83	4.99	10.96	9.08
	DR-W-8	-8.29	4.99	4.67	4.44	1.90	-2.99	2.09	2.49	2.12	5.22	3.25
I-8	DW-W-1	-8.52	3.01	2.02	2.47	0.87	-5.86	1.07	1.48	-0.77	-0.55	-3.13
II-6	DR-W-2	-8.64	4.86	4.06	3.83	1.95	-5.29	2.12	2.53	-0.14	0.69	-2.60
	DR-W-3	-8.61	4.52	3.84	3.70	1.79	-4.40	1.97	2.37	0.74	2.45	-0.43
	DR-W-6	-8.51	4.30	3.98	3.85	1.65	-4.34	1.82	2.23	0.82	2.61	0.22
	DR-W-9	-8.43	4.21	3.99	3.92	1.58	-3.11	1.74	2.15	2.05	5.08	2.86
II-7	DR-W-7	-6.12	3.23	3.33	3.66	0.89	-0.78	1.03	1.44	4.43	9.83	4.24

kaolinit: $Al_4[(OH)_8|Si_4O_{10}]$; ; illit: $(K,H_3O)(Al,Mg,Fe)_2(Si,Al)_4O_{10}[(OH)_2,(H_2O)]$; montmorillonite: $(Na,Ca)_{0.33}(Al,Mg)_2(Si_4O_{10})(OH)_2 \cdot nH_2O$

Table A 24: Distribution of sulphur species modelled with PhreeqC (input: sum of determined S species as S). Species of concentrations < 1 mg/L are not listed

Sample ID	S(-2)	S(+6)	H_2S	SO_4^{2-}	$CaSO_4^0$	$MgSO_4^0$	$SrSO_4^0$	$NaSO_4^-$	KSO_4^-	$FeSO_4^0$	HSO_4^-	$AlSO_4^+$	$Al(SO_4)_2^-$
	mg/L	mg/L	mg/L	mg/L	mg/L	mg/L	mg/L	mg/L	mg/L	mg/L	mg/L	mg/L	mg/L
DC-W-1	0.00	268.85	0.00	592.20	189.56	98.61	2.35	1.29	0.16	0.01	0.00	0.00	0.00
DC-W-2	0.00	299.96	0.00	643.03	217.14	126.89	2.88	1.58	0.17	0.00	0.00	0.00	0.00
DC-W-3	603.62	0.00	642.71	0.00	0.00	0.00	0.00	0.00	0.00	0.00	0.00	0.00	0.00
DC-W-4	0.00	1641.92	0.00	1953.09	559.29	210.07	3.32	3.90	2.17	37.85	2349.09	34.78	35.05
DC-W-5	0.00	293.68	0.00	637.65	199.65	125.57	2.69	1.60	0.16	0.06	0.00	0.00	0.00
DC-W-6	0.33	4516.16	0.35	3100.24	593.19	276.97	3.09	8.40	7.32	28.94	9837.07	26.83	32.25
DC-W-7	0.00	279.59	0.00	594.25	205.14	122.26	2.61	1.51	0.16	0.00	0.01	0.00	0.00
DC-W-8	0.00	299.66	0.00	641.12	215.50	129.66	2.80	1.60	0.17	0.00	0.01	0.00	0.00
DC-W-9	0.00	266.48	0.00	580.40	195.81	99.22	2.17	1.14	0.13	0.00	0.00	0.00	0.00
DC-W-10	0.00	290.61	0.00	625.96	213.09	116.82	2.72	1.58	0.17	0.01	0.00	0.00	0.00
DC-W-11	0.00	281.69	0.00	602.08	206.52	119.16	2.57	1.52	0.15	0.01	0.00	0.00	0.00
DR-W-1	0.00	211.42	0.00	462.40	141.78	88.28	1.75	0.92	0.10	0.02	0.00	0.00	0.00
DR-W-2	0.00	91.67	0.00	215.07	46.70	33.03	0.82	0.41	0.04	0.00	0.00	0.00	0.00
DR-W-3	0.00	98.24	0.00	229.01	50.98	36.44	0.87	0.44	0.04	0.00	0.00	0.00	0.00
DR-W-6	0.00	98.77	0.00	228.80	52.80	37.03	0.88	0.50	0.05	0.00	0.00	0.00	0.00
DR-W-7	0.00	221.90	0.00	503.57	162.48	46.21	1.99	12.20	0.14	0.00	0.00	0.00	0.00
DR-W-8	0.00	292.87	0.00	623.61	217.01	124.81	2.64	1.56	0.17	0.06	0.00	0.00	0.00
DR-W-9	0.00	108.64	0.00	251.28	59.73	39.68	0.97	0.57	0.05	0.00	0.00	0.00	0.00
DW-W-1	0.00	258.82	0.00	549.93	173.61	128.01	2.32	1.12	0.17	0.09	0.01	0.00	0.00

Table A 25: Distribution of main C species modelled with PhreeqC on the basis of TIC values

Sample ID	HCO_3^-	CO_2	$CaHCO_3^+$	$MgHCO_3^+$	$CaCO_3^0$
	mg/L	mg/L	mg/L	mg/L	mg/L
DC-W-1	176.65	12.05	10.33	2.86	1.48
DC-W-2	188.29	26.77	11.70	3.45	0.86
DC-W-3	0.04	25.72	0.00	0.00	0.00
DC-W-4	0.00	18.72	0.00	0.00	0.00
DC-W-5	204.62	5.61	11.72	3.77	4.43
DC-W-6	0.00	17.47	0.00	0.00	0.00
DC-W-7	184.62	60.10	11.62	3.48	0.38
DC-W-8	213.81	48.09	13.22	4.01	0.62
DC-W-9	181.76	12.93	11.24	3.02	1.55
DC-W-10	221.72	3.18	13.87	3.89	9.98
DC-W-11	209.44	2.63	13.19	3.92	10.74
DR-W-1	216.55	9.04	11.61	3.77	2.85
DR-W-2	256.95	24.85	8.71	3.32	0.93
DR-W-3	242.61	16.05	8.45	3.22	1.34
DR-W-6	251.05	8.64	9.20	3.51	2.71
DR-W-7	188.48	3.55	11.95	1.98	5.21
DR-W-8	189.84	14.30	12.21	3.59	1.67
DR-W-9	255.51	7.19	9.80	3.58	3.45
DW-W-1	263.30	53.97	15.08	5.61	0.79

Table A 26: Distribution of Fe species modelled with PhreeqC on the basis of ICP-MS values

Sample ID	Fe	Fe(2)	Fe(3)	Fe^{2+}	$FeHCO_3^+$	$FeCO_3^0$	$FeSO_4^0$	$Fe(OH)_3^0$
	mg/L	mg/L	mg/L	mg/L	mg/L	mg/L	mg/L	mg/L
DC-W-1	0.03	0.03	0.00	0.01	0.02	0.00	0.01	0.00
DC-W-2	0.01	0.01	0.00	0.00	0.01	0.00	0.00	0.00
DC-W-3	7.42	7.42	0.00	5.15	0.00	0.00	6.18	0.00
DC-W-4	43.39	43.39	0.00	29.68	0.00	0.00	37.29	0.00
DC-W-5	0.16	0.16	0.00	0.07	0.13	0.03	0.05	0.00
DC-W-6	33.89	33.89	0.00	23.35	0.00	0.00	28.65	0.00
DC-W-7	0.01	0.01	0.00	0.00	0.01	0.00	0.00	0.00
DC-W-8	0.01	0.01	0.00	0.00	0.01	0.00	0.00	0.00
DC-W-9	0.02	0.01	0.02	0.00	0.01	0.00	0.00	0.03
DC-W-10	0.03	0.02	0.00	0.01	0.02	0.01	0.01	0.00
DC-W-11	0.03	0.03	0.00	0.01	0.02	0.01	0.01	0.00
DR-W-1	0.09	0.07	0.02	0.03	0.06	0.01	0.02	0.04
DR-W-2	0.01	0.01	0.00	0.01	0.02	0.00	0.00	0.00
DR-W-3	0.02	0.02	0.00	0.01	0.02	0.00	0.00	0.00
DR-W-6	0.02	0.02	0.00	0.01	0.02	0.00	0.00	0.00
DR-W-7	0.01	0.00	0.01	0.00	0.00	0.00	0.00	0.02
DR-W-8	0.15	0.15	0.00	0.07	0.13	0.01	0.05	0.00
DR-W-9	0.02	0.02	0.00	0.01	0.02	0.00	0.00	0.00
DW-W-1	0.27	0.27	0.00	0.11	0.28	0.01	0.07	0.00

Table A 27: Comparison of IC anion measurements carried out at: 1 - *Kurdistan Institution for Strategic Studies & Scientific Research*, Sulaimani (Iraq) and 2 - chair of Hydrogeology, TU Freiberg (Germany); RD [%] = AD/mean%

			DC-W-1	DC-W-2	DC-W-3	DC-W-4	DC-W-5	DC-W-6	DC-W-8	DC-W-9	DC-W-10	DC-W-11	DR-W-1	DR-W-2	DR-W-3	DR-W-6	DR-W-7
F^-	1	mg/L	0.07	0.1	0.11	n.d.	0.12	0.11	0.1	0.09	0.11	0.1	0.1	0.1	0.09	0.09	0.01
	2	mg/L	0.81	1.1	1.32	1.32	0.98	1.15	1.09	0.88	1.06	1.09	1.06	0.63	0.66	0.67	0.19
	RD	*%*	*84.2*	*83.6*	*84.7*	*n.d.*	*78.2*	*82.5*	*83.1*	*81.4*	*81.2*	*83.2*	*82.8*	*72.7*	*76.0*	*76.5*	*90.0*
Cl^-	1	mg/L	9.05	14.2	10.2	9.6	16.6	15.5	14.48	10.1	15.3	15.8	11.2	11.1	11.9	13.6	238.8
	2	mg/L	11.41	15.69	12.37	16.53	15.48	28.22	15.94	11.52	15.76	15.83	10.95	10.02	10.39	11.76	230.42
	RD	*%*	*11.6*	*5.0*	*9.6*	*26.5*	*3.5*	*29.1*	*4.8*	*6.6*	*1.5*	*0.1*	*1.1*	*5.1*	*6.8*	*7.3*	*1.8*
NO_3^-	1	mg/L	0.12	n.d.	n.d.	n.d.	n.d.	n.d.	n.d.	0.05	n.d.	n.d.	n.d.	n.d.	n.d.	n.d.	n.d.
	2	mg/L	0.2	0.06	0.2	0.04	0.02	0	0.05	0.23	0.08	0.08	0.09	0.05	0.03	0.16	0.14
	RD	*%*	*24.2*	*n.d.*	*n.d.*	*n.d.*	*n.d.*	*n.d.*	*n.d.*	*63.7*	*n.d.*	*n.d.*	*n.d.*	*n.d.*	*n.d.*	*n.d.*	*n.d.*
PO_4	1	mg/L	n.d.	n.d.	n.d.	n.d.	n.d.	n.d.	n.d.	n.d.	n.d.	n.d.	491.8	n.d.	n.d.	n.d.	n.d.
	2	mg/L	0.02	0.02	0.32	4	0.03	6.01	0.01	0.01	0.01	0.01	0.01	0	0	0	0.01
	RD	*%*	*n.d.*	*n.d.*	*n.d.*	*n.d.*	*n.d.*	*n.d.*	*n.d.*	*n.d.*	*n.d.*	*n.d.*	*100*	*n.d.*	*n.d.*	*n.d.*	*n.d.*
SO_4^{2-}	1	mg/L	480.3	522.1	1180.3	3472.3	699.4	8249.3	636.3	596.4	660.2	668.4	491.8	137.6	267.7	192.4	143.5
	2	mg/L	796.7	888.5	1783.0	4840.0	862.8	13209.6	887.8	789.7	855.1	830.4	626.6	264.0	284.9	288.7	657.5
	RD	*%*	*24.8*	*26.0*	*20.3*	*16.5*	*10.5*	*23.1*	*16.5*	*14.0*	*12.9*	*10.8*	*12.1*	*31.5*	*3.1*	*20.0*	*64.2*

n.d. - not detected; RD – relative deviation, AD – absolute deviation from the mean value

Table A 28: Determination of water types under consideration of main anions and cations > 20%

		Cations [100%]						Anions [100%]				
Cluster ID	**Sample ID**	**Ca^{2+}**	**Mg^{2+}**	**Na^{+}**	**K^{+}**	**NH_4^{+}**	**Fe^{2+}**	**HCO_3^{-}**	**Cl^{-}**	**SO_4^{2-}**	**$HS^{-}/H_2S/ S^{2-}$**	**Water type (> 20%)**
I-1	DC-W-1	70.66	26.41	2.65	0.25	0.03	0.00	14.62	1.63	83.74	0.02	Ca-Mg-SO_4
	DC-W-9	71.57	25.90	2.31	0.19	0.03	0.00	15.09	1.65	83.27	0.00	Ca-Mg-SO_4
I-2	DC-W-2	68.56	27.89	2.73	0.21	0.61	0.00	14.00	2.01	83.95	0.03	Ca-Mg-SO_4
	DC-W-7	68.59	28.18	2.84	0.22	0.18	0.00	14.59	2.19	83.19	0.02	Ca-Mg-SO_4
	DC-W-8	68.28	28.54	2.78	0.22	0.19	0.00	15.61	2.00	82.35	0.03	Ca-Mg-SO_4
I-3	DC-W-3	77.64	19.49	1.61	0.28	0.45	0.54	0.00	0.93	98.52	0.56	*Ca-SO_4
I-4	DC-W-4	73.04	20.65	1.88	0.79	0.82	2.82	0.00	0.46	99.30	0.24	*** Ca-Mg-SO_4
	DC-W-6	64.09	21.84	2.77	1.85	7.64	1.81	0.00	0.29	99.71	0.00	*** Ca-Mg-SO_4
I-5	DC-W-5	67.17	29.61	2.96	0.22	0.03	0.01	15.14	1.97	81.11	1.78	Ca-Mg-SO_4
	DC-W-10	70.10	26.72	2.83	0.22	0.12	0.00	16.40	2.01	80.37	1.22	Ca-Mg-SO_4^{-}
	DC-W-11	69.24	27.78	2.78	0.20	0.00	0.00	16.15	2.10	81.36	0.38	Ca-Mg-SO_4
	DR-W-1	67.84	29.36	2.59	0.21	0.00	0.01	20.99	1.83	77.15	0.03	*Ca-Mg-HCO_3-SO_4
	DR-W-8	69.18	27.80	2.74	0.21	0.07	0.01	14.39	2.05	83.56	0.01	Ca-Mg-SO_4
I-8	DW-W-1	64.55	32.45	2.37	0.26	0.36	0.02	19.03	1.43	65.80	13.73	**Ca-Mg-SO_4
II-6	DR-W-2	64.29	31.22	3.87	0.26	0.36	0.00	40.18	2.70	52.45	4.67	Ca-Mg-HCO_3-SO_4
	DR-W-3	64.29	31.32	3.84	0.24	0.31	0.00	37.51	2.76	55.96	3.77	Ca-Mg-HCO_3-SO_4
	DR-W-6	64.23	31.11	4.05	0.28	0.34	0.00	38.38	3.09	56.06	2.47	Ca-Mg-HCO_3-SO_4
	DR-W-9	65.23	30.27	4.12	0.26	0.12	0.00	36.50	3.23	57.49	2.78	Ca-Mg-HCO_3-SO_4
II-7	DR-W-7	61.84	13.12	24.75	0.22	0.07	0.00	13.27	27.92	58.81	0.00	Ca-Na-Cl-SO_4

*tendency to Ca^{2+}-Mg^{2+}-SO_4^{2-} ** tendency to Ca^{2+}-Mg^{2+}-HCO_3-SO_4^{2-} ***tendency to Ca^{2+}-SO_4^{2-}, acidic sites (influence of H^{+} ions is not considered)

Table A 29: Short description, GPS data and altitude of surface karst features in the surrounding of Darzila cave

ID	GPS data	Altitude [m]	Description
DS-K-1	N35 08.931 E45 16.746	753	rillenkarren
DS-K-2	N35 08.993 E45 16.641	779	doline
DS-K-3	N35 09.039 E45 16.688	801	meandering karren
DS-K-4	N35 09.204 E45 16.870	846	rillenkarren
DS-K-5	N35 09.121 E45 16.885	824	etched surfaces
DS-K-6	N35 08.996 E45 16.931	783	etched surfaces
DS-K-7e	N35 08.796 E45 16.839	704	several pits in a dry valley
DS-K-8	N35 08.769 E45 16.838	694	roofed crevasse
DS-K-9	N35 08.755 E45 16.700	678	doline
DS-K-10	N35 08.488 E45 17.557	653	doline
DS-K-11	N35 08.479 E45 17.558	650	doline
DS-K-12	N35 08.480 E45 17.596	653	crevasse
DS-K13	N35 08.513 E45 17.807	665	doline
DS-K-14	N35 08.516 E45 17.847	668	doline (stench of sulphur, water)
DS-K-15	N35 08.538 E45 17.839	670	roofed crevasse
DS-K-16	N35 08.541 E45 17.862	671	crevasse (smell of sulphur, accessible)
DS-K-17	N35 08.531 E45 17.923	671	crevasse
DS-K-18	N35 08.535 E45 17.893	672	crevasse
DS-K-19	N35 08.510 E45 17.869	669	doline (stench of sulphur, water)
DS-K-20	N35 08.532 E45 17.838	669	cave
DS-K-21	N35 08.792 E45 17.736	730	big cave
DS-K-22	N35 08.871 E45 16.859	773	bitumen
DS-K-23	N35 08.957 E45 16.898	771	trittkarren

Table A 30: GPS data and altitude of Darzila cave, Darzila village and water and oil sampling points

ID	GPS data	Altitude [m]
Darzila cave	N35 08.779 E45 16.741	688
Darzila village	N35 08.474 E45 17.237	640
DR-W-1	N35 08.632 E45 17.375	664
DR-W-1b	N35 08.707 E45 17.426	680
DR-W-2	N35 08.544 E45 17.372	645
DR-W-2b	N35 08.538 E45 17.363	644
DR-W-3	N35 08.470 E45 17.297	637
DR-O-4	N35 08.439 E45 17.265	634
DR-O-5	N35 08.439 E45 17.239	633
DR-W-6	N35 08.424 E45 17.175	632
DR-W-7	N35 08.330 E45 17.105	637
DR-W-8	N35 08.548 E45 17.029	637
DR-W-8b	N35 08.549 E45 17.007	637
DR-W-9	N35 08.480 E45 16.900	631
DW-W-1	N35 08.794 E45 16.635	687

Table A 31: GPS data and altitude of rock sampling points

ID	GPS data	Altitude [m]	Geological Formation
DS-PG-2b	N35 09.001 E45 18.355	791	Lower Fars Formation
DS-PG-4	N35 26.649 E45 09.062	661	Lower Fars Formation
DS-PL-1	N35 08.803 E45 16.697	691	Pila Spi Formation
DS-PL-3	N35 27.035 E45 10.176	715	Oligocene
DS-PL-5	N35 08.558 E45 17.067	643	Oligocene

9.2. Appendix B – Figures

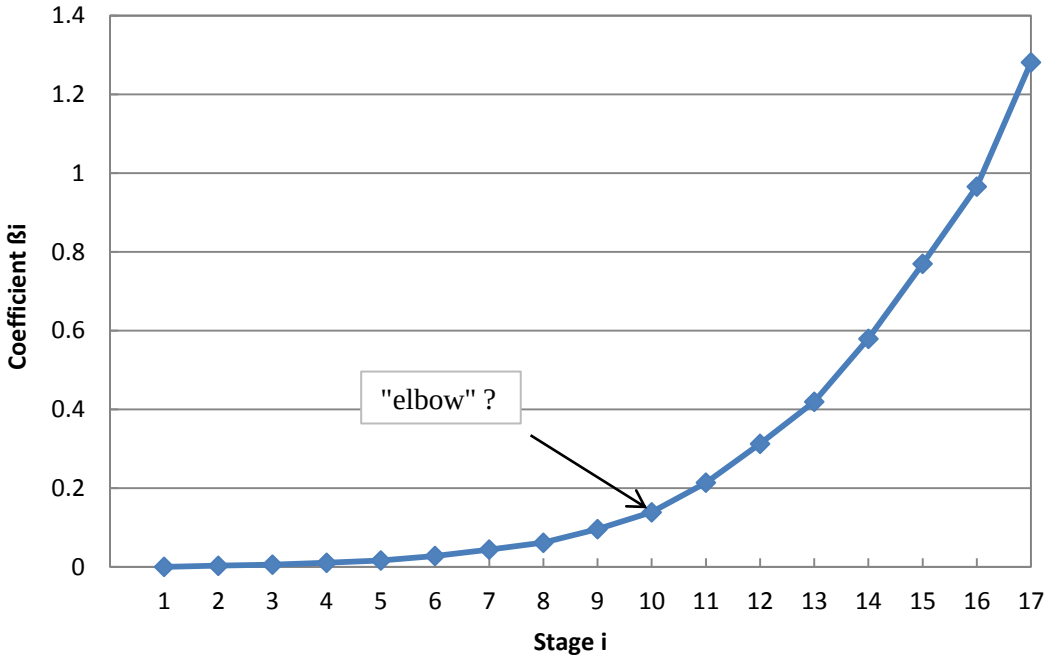

Figure B 1: Increase in heterogeneity (coefficients β_i) during the agglomeration process of clusters; the arrow tagged a sudden increase in heterogeneity giving an indication of the optimal number of clusters ($N_{cluster}$ = 19 – 10 = 9)

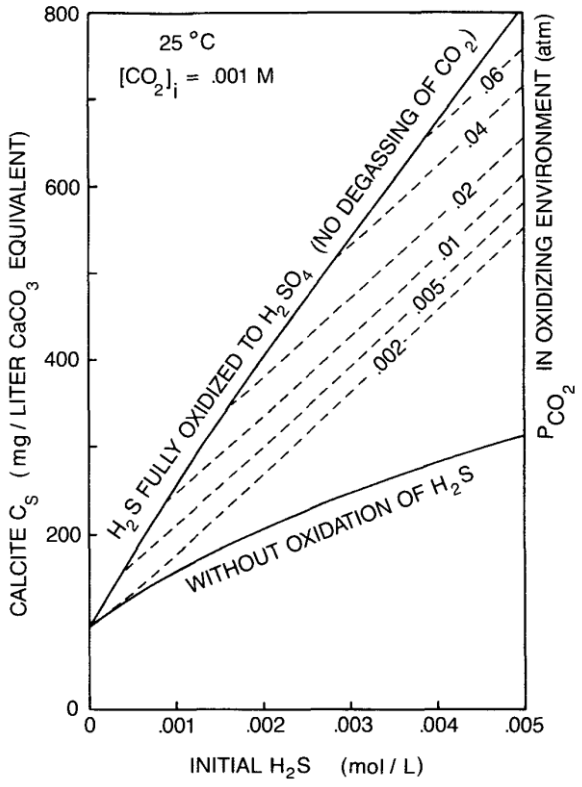

Figure B 2: Change in calcite solubility when H_2S oxidises to sulphuric acid (effects of other components are ignored) (Palmer 1991)

9.3. Appendix C – Data CD

➢ **Statistical analyses with SPSS Statistics 20**

- Data Sheet
- Results of Kolmogorov-Smirnov test
- Spearman correlation matrix
- Results of Cluster analysis
- Elbow criteria
- Results of Kruskal-Wallis test
- Check for homogeneity (F-value)
- Descriptive statistics according to clusters